ENCLOSURE 7

TENNESSEE VALLEY AUTHORITY
BROWNS FERRY NUCLEAR PLANT (BFN)
UNITS 1, 2, AND 3

TECHNICAL SPECIFICATIONS (TS) CHANGES TS-431 AND TS-418 -
EXTENDED POWER UPRATE (EPU) - STEAM DRYER EVALUATIONS

CDI REPORT NO. 07-05NP, "FINITE ELEMENT MODEL FOR STRESS ASSESSMENT OF BROWNS FERRY NUCLEAR UNIT 1 STEAM DRYER TO 250 HZ"

(NON-PROPRIETARY VERSION)

Attached is the **Non-Proprietary Version** of CDI Report No. 07-05, "Finite Element Model for Stress Assessment of Browns Ferry Nuclear Unit 1 Steam Dryer to 250 Hz."

This Document Does Not Contain Continuum Dynamics, Inc. Proprietary Information

CDI Report No. 07-05NP

Finite Element Model for Stress Assessment of Browns Ferry Nuclear Unit 1 Steam Dryer to 250 Hz

Revision 0

Prepared by

Continuum Dynamics, Inc.
34 Lexington Avenue
Ewing, NJ 08618

Prepared under Purchase Order No. 00053157 for

TVA / Browns Ferry Nuclear Plant
Nuclear Plant Road, P. O. Box 2000 PAB-2M
Decatur, AL 35609

Approved by

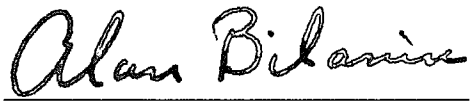

Alan J. Bilanin

Reviewed by

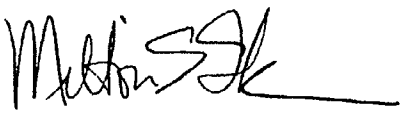

Milton E. Teske

July 2007

This report complies with Continuum Dynamics, Inc. Nuclear Quality Assurance Program currently in effect.

Executive Summary

The finite element model and analysis methodology, used to assess stresses induced by the flow of steam through the steam dryer at Brown Ferry Nuclear Unit 1 (BFN1), are described and applied to obtain stresses at CLTP conditions. The analysis is carried out in the frequency domain, which confers a number of useful computational advantages over a time-accurate transient analysis including the ability to assess the effects of frequency scalings in the loads without the need for additional finite element calculations. [[

(3)]]

The analysis begins by developing a series of unit stress solutions corresponding to the application of a unit pressure at a MSL at specified frequency, f. Each unit solution is obtained by first calculating the associated acoustic pressure field using a separate analysis that solves the damped Helmholtz equation within the steam dryer [1]. This pressure field is then applied to a finite element structural model of the steam dryer and the harmonic stress response at frequency, f, calculated using the commercial ANSYS 10.0 finite element analysis software. This stress response constitutes the unit solution and is stored as a file for subsequent processing. Once all unit solutions have been computed, the stress response for any combination of MSL pressure spectrums (obtained by Fast Fourier Transform of the pressure histories in the MSLs) is determined by a simple matrix multiplication of these spectrums with the unit solutions.

This report provides details of the ANSYS 10.0 finite element structural model of the BFN1 steam dryer and reviews pertinent modeling considerations. It also summarizes the framework underlying the development and application of unit solutions in the frequency domain and shows how these solutions are used to develop stress histories for general load conditions. Next, it reviews the assessment of these stresses for compliance with the ASME B&PV Code, Section III, subsection NG, for the load combination corresponding to normal operation (the Level A Service Condition). [[

(3)]]

Results obtained from application of the methodology to the BFN1 steam dryer show that at nominal CLTP operation the minimum stress ratio (SR) anywhere on the steam dryer is SR=1.20. The loads used to obtain this value account for all the end-to-end biases and uncertainties in the loads model [2]. In order to account for uncertainties in the finite element model, the stresses are also computed for loads that are shifted in the frequency domain by ±2.5%, ±5%, ±7.5% and ±10%. The minimum stress ratio encountered at any frequency shift is found to be SR=0.96 occurring at the -10% shift. Further inspection of the stresses shows that virtually all of the response results from a strong 218 Hz signal in the loading and stresses which are identified with dead-headed safety valve standpipes in the system. This signal can be removed by plugging these unused standpipes. In that case the minimum stress ratio associated with alternating stresses more than doubles to SR=2.0. Given that the biases and uncertainties in loads are already accounted for, this stress ratio is expected to qualify the dryer with considerable margin at EPU conditions. The stress ratio due to maximum stresses is dominated by static loads and remains virtually unchanged at SR=1.25 (with the 218 Hz signal included) and SR=1.26 (218 Hz signal removed).

Table of Contents

1. Introduction and Purpose

Plans to qualify the Browns Ferry nuclear plant for operation at Extended Power Uprate (EPU) operating condition require an assessment of the steam dryer stresses experienced under the increased loads. The steam dryer loads due to pressure fluctuations in the main steam lines (MSLs) are potentially damaging and the cyclic stresses from these loads can produce fatigue cracking if loads are sufficiently high. The industry has addressed this problem with physical modifications to the dryers, as well as a program to define steam dryer loads and their resulting stresses.

The purpose of the stress analysis discussed here is to calculate the maximum and alternating stresses generated during Current Licensed Thermal Power (CLTP) and determine the margins that exist when compared to stresses that comply with the ASME Code (ASME B&PV Code, Section III, subsection NG). This step establishes whether the modifications done prior to commercial operations are adequate for sustaining structural integrity and preventing future weld cracking under planned EPU operating conditions. The load combination considered here corresponds to normal operation (the Level A Service Condition) and includes fluctuating pressure loads developed from Browns Ferry Unit 2 (BFN2) main steam line data, and weight. The fluctuating pressure loads, induced by the flowing steam, are predicted using a separate acoustic circuit analysis of the steam dome and main steam lines [3]. Level B service conditions, which include seismic loads, are not included in this evaluation.

[[

[3]]] This approach also affords a number of additional computational advantages over transient simulations including: [[

[3]]] This last advantage is realized through the use of "unit" solutions representing the stress distribution resulting from the application of a unit fluctuating pressure at one of the MSLs at a particular frequency. [[

[3]]]

This report describes the overall methodology used to obtain the unit solutions in the frequency domain and how to assemble them into a stress response for a given combination of pressure signals in the MSLs. This is followed by details of the BFN1 steam dryer finite element

model including the elements used and overall resolution, treatment of connections between elements, the hydrodynamic model, the implementation of structural damping and key idealizations/assumptions inherent to the model. Post-processing procedures are also reviewed including the computation of maximum and alternating stress intensities, identification of high stress locations, adjustments to stress intensities at welds, and evaluation of stress ratios used to establish compliance with the ASME Code. The results in terms of stress intensity distributions and stress ratios are presented next, together with PSDs of the dominant stress components. The latter show that the load and structural response are dominated by a strong 218 Hz component that is due to dead-headed safety valve standpipes and is responsible for all of the lowest stress ratios. Results are also presented with the 218 Hz signal removed. In this case the lowest alternating stress ratio due to acoustic loads is 2.0.

2. Methodology

2.1 Overview

Based on previous analysis undertaken at Quad Cities Units 1 and 2, the steam dryer can experience strong acoustic loads due to the fluctuating pressures in the MSLs connected to the steam dome containing the dryer. C.D.I. has developed an acoustic circuit model (ACM) that, given a collection of strain gage measurements [4] of the fluctuating pressures in the MSLs, predicts the acoustic pressure field anywhere inside the steam dome and on the steam dryer [1-3]. The ACM is formulated in frequency space and contains two major components that are directly relevant to the ensuing stress analysis of concern here. [[

(3)]]

[[

[3]]]

[[

2.2 [[[3]]]

[3]]]

[[

[3]]]

2.3 Computational Considerations

Focusing on the structural computational aspects of the overall approach, there are a number of numerical and computational considerations requiring attention. The first concerns the transfer of the acoustic forces onto the structure, particularly the spatial and frequency resolutions. The ANSYS finite element program inputs general distributed pressure differences using a table format. This consists of regular 3D rectangular (i.e., block) $n_x \times n_y \times n_z$ mesh where n_α is the number of mesh points in the i-th Cartesian direction and the pressure difference is provided at each mesh point (see Section 3.10). These tables are generated separately using a program that reads the loads provided from the ACM software, distributes these loads onto the finite element mesh using a combination of interpolation procedures on the surface and simple diffusion schemes off the surface (off-surface loads are required by ANSYS to ensure proper interpolation of forces), and written to ASCII files for input to ANSYS. A separate load file is written at each frequency for the real and imaginary component of the complex force.

The acoustic field is stored at 5 Hz intervals from 0 to 250 Hz. While a 5 Hz resolution is sufficient to capture frequency dependence of the acoustic field (i.e., the pressure at a point varies gradually with frequency), it is too coarse for representing the structural response especially at low frequencies. For 1% critical structural damping, one can show that the frequency spacing needed to resolve a damped resonant peak at natural frequency, f_n, to within 5% accuracy is $\Delta f = 0.0064 \times f_n$. Thus for f_n=10 Hz where the lowest structural response modes occur, a frequency interval of 0.064 Hz or less is required. In our calculations we require that 5% maximum error be maintained over the range from f_n=5 Hz to 250 Hz resulting in a finest frequency interval of 0.0321 Hz at the low frequency end (this adequately resolves all structural modes up to 250 Hz). Since there are no structural modes between 0 to 5 Hz, a 0.5 Hz spacing is used over this range with minimal (less than 5%) error. The unit load, $\hat{\mathbf{f}}_n(\omega, \mathbf{R})$, at any frequency, ω_k, is obtained by linear interpolation of the acoustic solutions at the two nearest frequencies, ω_i and ω_{i+1}, spaced 5 Hz apart. Linear interpolation is sufficient since the pressure load varies slowly over the 5 Hz range (linear interpolation of the structural response would not be acceptable over this range since it varies much more rapidly over the same interval).

Solution Management

[[

[3]]]

Upon completion of each frequency calculation, ANSYS is instructed to export the stresses which are stored in text files. There is one file per MSL per frequency per real/imaginary

component, and each file contains the complete stress state over all nodes on the dryer. This format is convenient from a solution point of view. However, it makes it difficult to extract the stress response at a node since, in order to do so, thousands of files must be opened and searched through thousands of nodes until the node of interest is reached. [[

[3]]]

Structural Damping

In harmonic analysis one has a broader selection of damping models than in transient simulations. A damping factor, z, of 1% critical damping is used in the structural analysis. In transient simulations, this damping can only be enforced exactly at two frequencies (where the damping model is "pinned"). Between these two frequencies the damping factor can by considerably smaller, for example 0.5% or less depending on the pinning frequencies. Outside the pinning frequencies, damping is higher. With harmonic analysis it is straightforward to enforce very close to 1% damping over the entire frequency range. In this damping model, the damping matrix, **D**, is set to

$$\mathbf{D} = \frac{2z}{\omega}\mathbf{K} \tag{7}$$

where **K** is the stiffness matrix and ω the forcing frequency. One can show that with this model the damping factor varies between 0.995% and 1.005% which is a much smaller variation than using the pinned model required in transient simulation.

Load Frequency Rescaling

One way to evaluate the sensitivity of the stress results to approximations in the structural modeling and applied loads is to rescale the frequency content of the applied loads. In this procedure the nominal frequencies, ω_k, are shifted to $(1+\lambda)\omega_k$, where the frequency shift, λ, ranges between $\pm 10\%$, and the response recomputed for the shifted loads. The objective of the frequency shifting can be explained by way of example. Suppose that in the actual dryer a strong structural-acoustic coupling exists at a particular frequency, ω^*. This means that the following conditions hold simultaneously: (i) the acoustic signal contains a significant signal at ω^*; (ii) the structural model contains a resonant mode of natural frequency, ω_n, that is near ω^*; and (iii) the associated structural mode shape is strongly coupled to the acoustic load (i.e., integrating the product of the mode shape and the surface pressure over the steam dryer surface produces a significant modal force). Suppose now that because of discretization errors and modeling idealizations that the predicted resonance frequency differs from ω^* by a small amount (e.g., 1.5%). Then condition (ii) will be violated and the response amplitude therefore significantly diminished. By shifting the load frequencies one re-establishes condition (ii) when $(1+\lambda)\omega^*$ is near ω_n. The other two requirements also hold and a strong structural acoustic interaction is restored.

[[

[3]]]

Evaluation of Maximum and Alternating Stress Intensities

Once the unit solutions have been obtained, the most intensive computational steps in the generation of stress intensities are: (i) the FFTs to evaluate stress time histories from (5); and (ii) the calculation of alternating stress intensities. [[

[3]]]

The high computational penalty incurred in calculating the alternating stress intensities is due to the fact that this calculation involves comparing the stress tensors at every pair of points in the stress history. This comparison is necessary since in general the principal stress directions can vary during the response, thus for N samples in the stress history, there will be (N-1)N/2 such pairs or, for N=64K (the number required to accurately resolve the spectrum up to 250 Hz in 0.01 Hz intervals), 2.1×10^9 calculations per node each requiring the determination of the roots to a cubic polynomial. [[

[3]]]

3. Finite Element Model Description

A description of the ANSYS model of the Browns Ferry Unit 1 steam dryer follows.

3.1 Steam Dryer Geometry

A geometric representation of the Browns Ferry steam dryer was developed from available drawings (provided by TVA and included in the design record file, DRF-TVA-250B) within the Workbench module of ANSYS. The completed model is shown in Figure 1. This model includes the following modifications made to the Browns Ferry Unit 1 steam dryer on-site:

- The 0.5 inch thick old outer hoods were cut away and replaced with 1 inch thick outer hoods.
- Channel-shaped hood assemblies composed of 1 inch thick plates were added to the outer hoods.
- The vertical hood supports located underneath the hood were cut away following the replacement with the thicker outer hood and exterior hood reinforcement assemblies.
- The top tie rods were replaced with thicker new ones. The gussets on the top of the outer hoods supporting the steam dam plate were cut away to facilitate installation of the new tie bars and possibly alleviate local stresses.

The modified areas are shown in Figure 2.

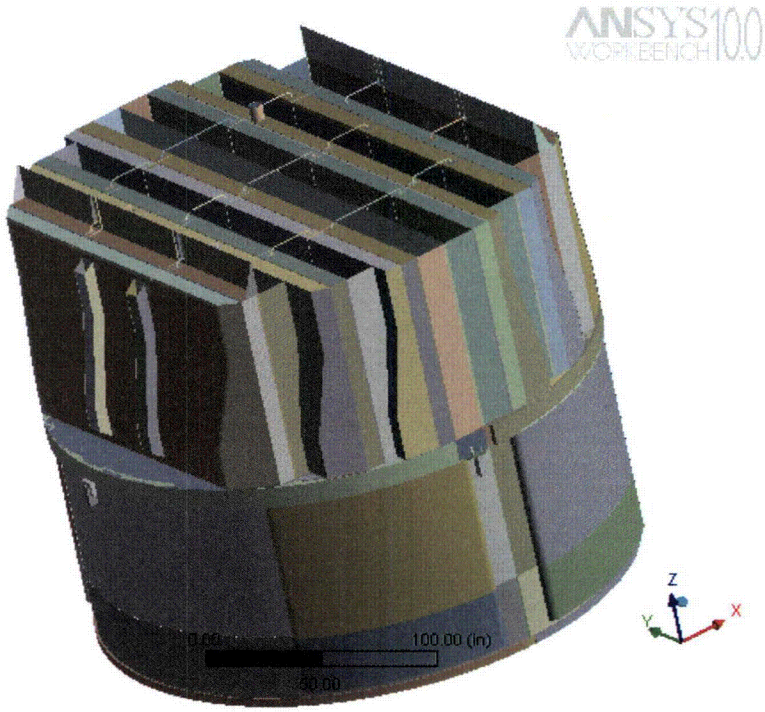

Figure 1. Overall geometry of the Browns Ferry Unit 1 steam dryer model.

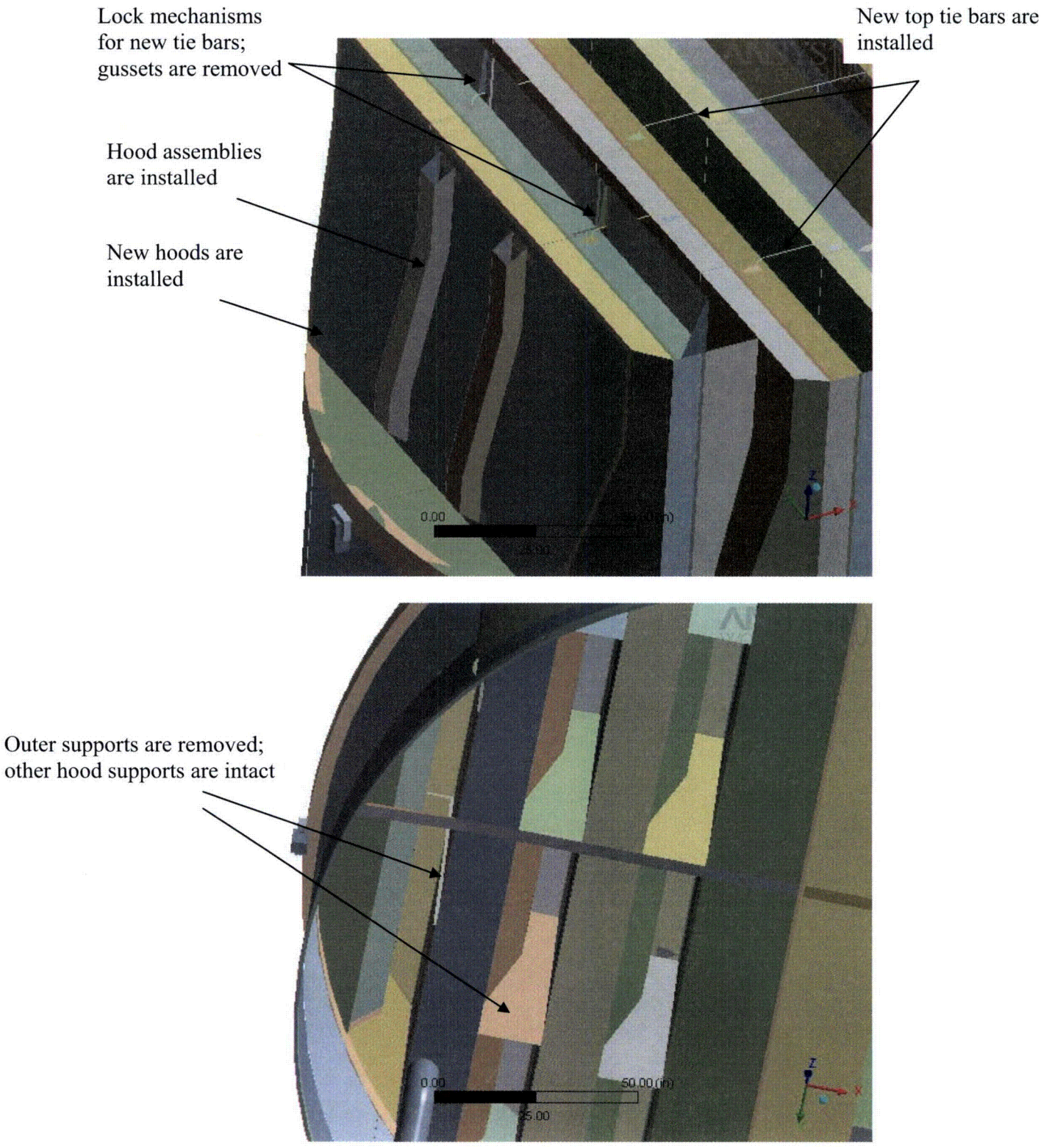

Figure 2. On-site modifications accounted for in the model and associated geometrical details.

3.2 Material Properties

The steam dryer is constructed from Type 304 stainless steel and has an operating temperature of 550°F. Properties used in the analysis are summarized below in Table 1.

Table 1. Material properties.

	Young's Modulus (10^6 psi)	Density (lbm/in^3)	Poisson's Ratio
structural steel	25.55	0.284	0.3
structural steel with added water inertia	25.55	1.055	0.3

The structural steel modulus is taken from Appendix A of the ASME Code for Type 304 Stainless Steel at an operating temperature 550°F. The effective properties of perforated plates and submerged parts are discussed in Sections 3.4 and 3.6. Note that the increased effective density for submerged components is only used in the harmonic analysis. When calculating the stress distribution due to the static dead weight load, the unmodified density of steel (0.284 lbm/in^3) is used throughout.

3.3 Model Simplifications

The following simplifications were made to achieve reasonable model size while maintaining good modeling fidelity for key structural properties:

- Perforated plates were approximated as continuous plates using modified elastic properties designed to match the static and modal behaviors of the perforated plates. The perforated plate structural modeling is summarized in Section 3.4 and Appendix C.

- The drying vanes were replaced by point masses attached to the corresponding trough bottom plates and vane bank top covers. The bounding perforated plates, vane bank end plates, and vane bank top covers were explicitly modeled (see Section 3.5).

- The added mass properties of the lower part of the skirt below the reactor water level were obtained using a separate hydrodynamic analysis (see Section 3.6).

- [[ ]]$^{(3)}$

- Four steam dryer support brackets that are located on the reactor vessel and spaced at 90° intervals were explicitly modeled. Fixed constraints (zero displacement) were imposed at the outer side of each bracket where it makes contact with the vessel wall. Nodal constraints (zero relative displacement) were introduced in the areas of contact between steam dryer and support brackets.

- Most welds were replaced by node-to-node connections; interconnected parts share common nodes along the welds. In other locations the constraint equations between nodal degrees of freedom were introduced as described in Section 3.9.

3.4 Perforated Plate Model

The perforated plates were modeled as solid plates with adjusted elastic and dynamic properties. Properties of the perforated plates were assigned according to the type and size of perforation. Based on [7], for an equilateral square pattern with given hole size and spacing, the effective moduli of elasticity were found.

The adjusted properties for the perforated plates are shown in Table 2 as ratios to material properties of structural steel, provided in Table 1. Locations of perforated plates are classified by steam entry / exit vane bank side and vertical position.

Tests were carried out to verify that this representation of perforated plates by continuous ones with modified elastic properties preserves the modal properties of the structure. These tests are summarized in Appendix C and compare the predicted first modal frequency for a cantilevered perforated plate against an experimentally measured value. The prediction was obtained for a 40% open area plate (the maximum open area ratio of the perforated plates at BFN1, as seen in Table 2) using the analytical formula for a cantilevered plate and the modified Young's modulus and Poisson's ratio given by O'Donnell [7]. The measured and predicted frequencies are in close agreement, differing by less than 3%.

[[

$^{(3)}$]]

[[

(3)]]

Figure 3. [[

(3)]]

Table 2. Material properties of perforated plates.

[[

(3)]]

3.5 Vane Bank Model

The vane bank assemblies consist of many vertical angled plates that are computationally expensive to model explicitly, since a prohibitive number of elements would be required. These parts have significant weight which is transmitted through the surrounding structure, so it is important to capture their gross inertial properties. Here the vane banks are modeled as a collection of point masses located at the center of mass for each vane bank section (Figure 4). The following masses were used for the vane bank sections, based on data found on provided drawings:

inner banks, 1575 lbm, 4 sections per bank;

middle banks, 1450 lbm, total 4 sections per bank; and
outer banks, 1515 lbm, 3 sections per bank.

These masses were applied to the base plates and vane top covers using the standard ANSYS point mass modeling option, element MASS21. ANSYS automatically distributes the point mass inertial loads to the nodes of the selected structure. The distribution algorithm minimizes the sum of the squares of the nodal inertial forces, while ensuring that the net forces and moments are conserved. Vane banks are not exposed to main steam lines directly, but rather shielded by the hoods.

The collective stiffness of the vane banks is expected to be small compared to the surrounding support structure and is neglected in the model. In the static case it is reasonable to expect that this constitutes a conservative approach, since neglecting the stiffness of the vane banks implies that the entire weight is transmitted through the adjacent vane bank walls and supports. In the dynamic case the vane banks exhibit only a weak response since (i) they have large inertia so that the characteristic acoustically-induced forces divided by the vane masses and inertias yield small amplitude motions, velocities and accelerations; and (ii) they are shielded from acoustic loads by the hoods, which transfer dynamic loads to the rest of the structure. Thus, compared to the hoods, less motion is anticipated on the vane banks so that approximating their inertial properties with equivalent point masses is justified. Nevertheless, the bounding parts, such as perforated plates, side panels, and top covers, are retained in the model. Errors associated with the point mass representation of the vane banks are compensated for by frequency shifting of the applied loads.

3.6 Water Inertia Effect on Submerged Panels

Water inertia was modeled by an increase in density of the submerged structure to account for the added hydrodynamic mass. This added mass was found by a separate hydrodynamic analysis (included in DRF-TVA-250B supporting this report) to be 0.1928 lbm/in^2 on the submerged skirt area. This is modeled by effectively increasing the material density for the submerged portions of the skirt. Since the skirt is 0.25 inches thick, the added mass is equivalent to a density increase of 0.771 lbm/in^3. This added water mass was included in the ANSYS model by appropriately modifying the density of the submerged structural elements when computing harmonic response. For the static stresses, the unmodified density of steel is used throughout.

3.7 Structural Damping

Structural damping was defined as 1% of critical damping for all frequencies. This damping is consistent with guidance given on pg. 10 of NRC RG-1.20 [11].

3.8 Mesh Details and Element Types

Shell elements were employed to model the skirt, hoods, perforated plates, side and end plates, trough bottom plates, reinforcements, base plates and cover plates. Specifically, the four-node, Shell Element SHELL63, was selected to model these structural components. This element models bending and membrane stresses, but omits transverse shear. The use of shell elements is appropriate for most of the structure where the characteristic thickness is small compared to the other plate dimensions. For thicker structures, such as the upper and lower

support rings, solid brick elements were used to provide the full 3D stress. Tie bars were modeled with BEAM188 beam elements. The elements SURF154 are used to assure proper application of pressure loading to the structure. Mesh details and element types are shown in Table 3 and Table 4, respectively.

The mesh is generated automatically by ANSYS with adaptive refinement near edges. The maximum allowable mesh spacing is specified by the user. Here a 3 inch maximum allowable spacing is specified everywhere except in the following areas: drain pipes (2 inch maximum spacing); base plates (2.75 inches); perforated plates (2 inches); top tie rods (0.75 inches); and the curved portions of the drain channels (1.5 inches). Details of the finite element mesh are shown in Figure 5. Numerical experiments carried out using the ANSYS code applied to simple analytically tractable plate structures with dimensions and mesh spacings similar to the ones used for the steam dryer, confirm that the natural frequencies are accurately recovered (less than 1% errors for the first modes). These errors are compensated for by the use of frequency shifting.

3.9 Connections Between Structural Components

Most connections between parts are modeled as node-to-node connections. This is the correct manner (i.e., within the finite element framework) of joining elements away from discontinuities. At joints between shells, this approach omits the additional stiffness provided by the extra weld material. Also, locally 3D effects are more pronounced. The latter effect is accounted for using weld factors. The deviation in stiffness due to weld material is negligible, since weld dimensions are on the order of the shell thickness. The consequences upon modal frequencies and amplitude are, to first order, proportional to t/L where t is the thickness and L a characteristic shell length. The errors committed by ignoring additional weld stiffness are thus small and readily compensated for by performing frequency shifts.

When joining shell and solid elements, however, the problem arises of properly constraining the rotations, since shell element nodes contain both displacement and rotational degrees of freedom at every node whereas solid elements model only the translations. A node-to-node connection would effectively appear to the shell element as a simply supported, rather than (the correct) cantilevered restraint and significantly alter the dynamic response of the shell structure.

To address this problem, constraint equations are used to properly connect adjacent shell- and solid-element modeled structures. Basically, all such constraints express the deflection (and rotation for shell elements) of a node, $\mathbf{R}_1$, on one structural component in terms of the deflections/rotations of the corresponding point, $\mathbf{P}_2$, on the other connected component. Specifically, the element containing $\mathbf{P}_2$ is identified and the deformations at $\mathbf{P}_2$ determined by interpolation between the element nodes. The following types of shell-solid element connections are used in the steam dryer model including the following:

1. Connections of shell faces to solid faces (Figure 6a). While only displacement degrees of freedom are explicitly constrained, this approach also implicitly constrains the rotational degrees of freedom when multiple shell nodes on a sufficiently dense grid are connected to the same solid face.
2. Connections of shell edges to solids (e.g., connection of the bottom of closure plates with the upper ring). Since solid elements do not have rotational degrees of freedom, the

coupling approach consisted of having the shell penetrate into the solid by one shell thickness and then constraining both the embedded shell element nodes (inside the solid) and the ones located on the surface of the solid structure (see Figure 6b). Numerical tests involving simple structures showed that this approach and penetration depth reproduce both the deflections and stresses of the same structure modeled using only solid elements or ANSYS' bonded contact technology. Continuity of rotations and displacements is achieved.

The use of constraint conditions rather than the bonded contacts advocated by ANSYS for connecting independently meshed structural components confers better accuracy and useful numerical advantages to the structural analysis of the steam dryer including better conditioned and smaller matrices. The smaller size results from the fact that equations and degrees of freedom are eliminated rather than augmented (in Lagrange multiplier-based methods) by additional degrees of freedom. Also, the implementation of contact elements relies on the use of very high stiffness elements (in penalty function-based implementations) or results in indefinite matrices (Lagrange multiplier implementations) with poorer convergence behavior compared to positive definite matrices.

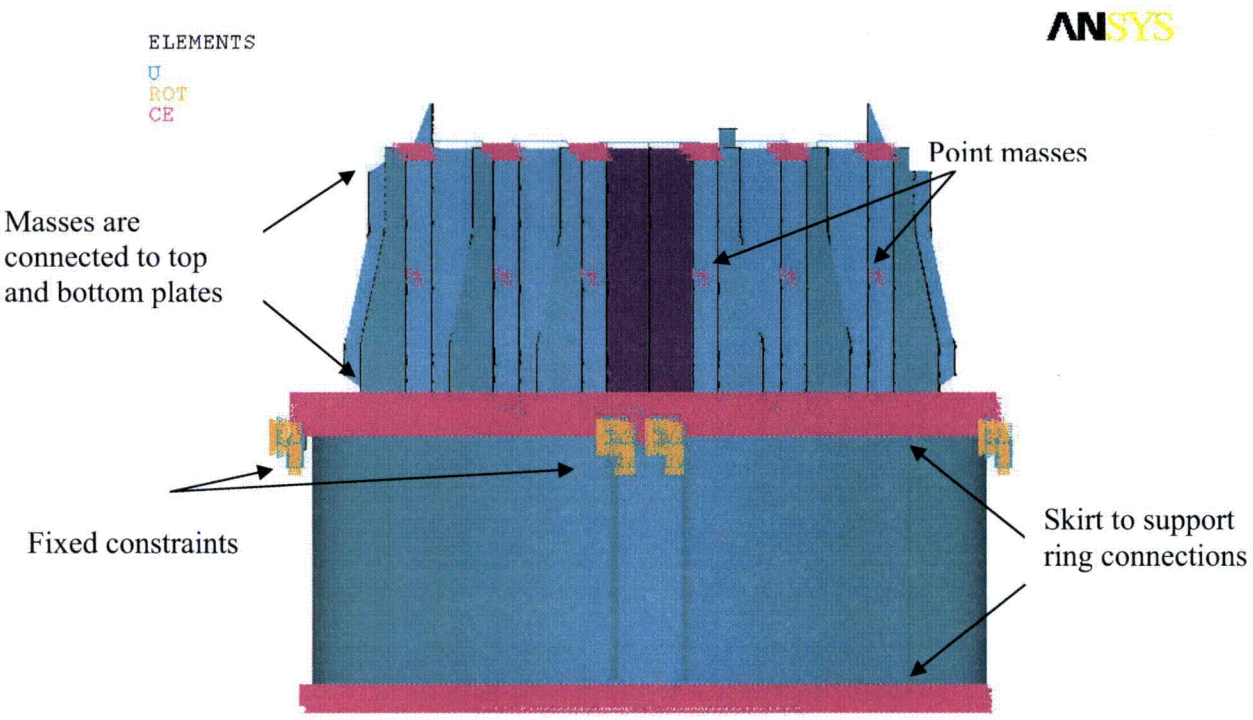

Figure 4. Point masses representing the vanes. The pink shading represents where constraint equations between nodes are applied.

Table 3. FE Model Summary.

Description	Quantity
Total Nodes[1]	95,984
Total Elements	117,661

1. Not including additional damper nodes and elements.

Table 4. Listing of Element Types.

Generic Element Type Name	Element Name	ANSYS Name
20-Node Quadratic Hexahedron	SOLID186	20-Node Hexahedral Structural Solid
10-Node Quadratic Tetrahedron	SOLID187	10-Node Tetrahedral Structural Solid
4-Node Elastic Shell	SHELL63	4-Node Elastic Shell
Mass Element	MASS21	Structural Mass
Pressure Surface Definition	SURF154	3D Structural Surface Effect
Beam element	BEAM188	3-D Finite Strain Beam
Damper element	COMBIN14	Spring-Damper

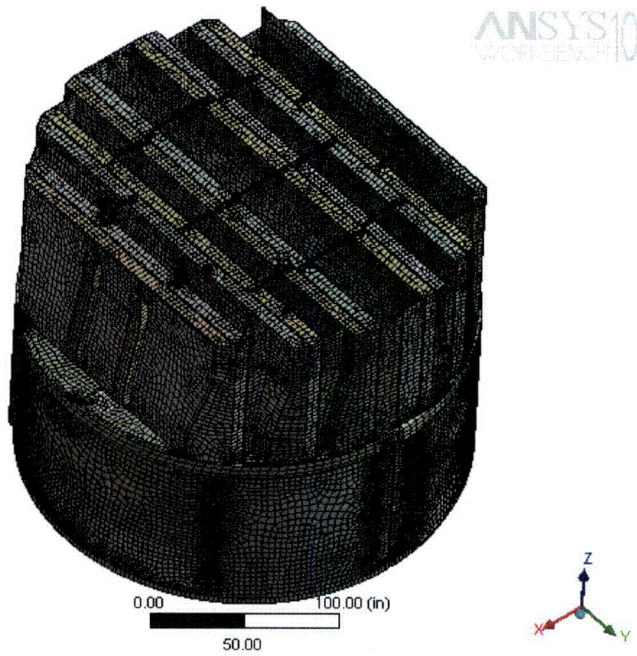

Figure 5a. Mesh overview.

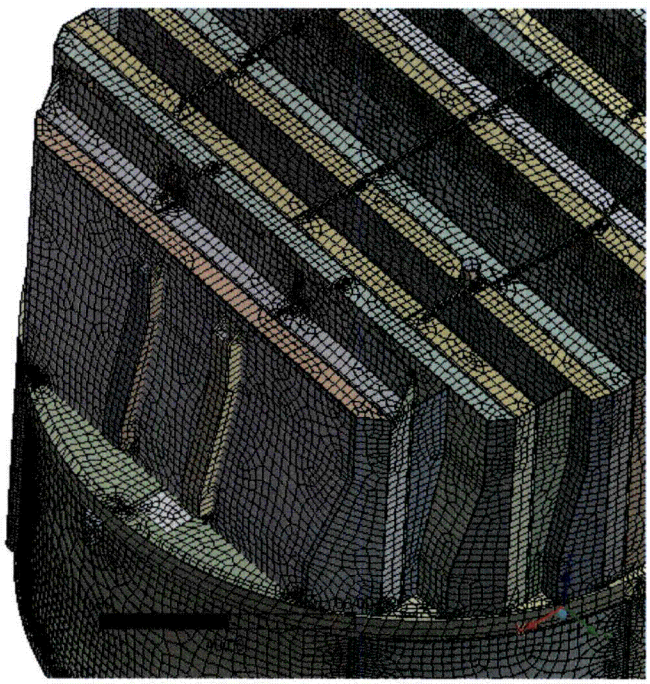

Figure 5b. Close-up of mesh showing hoods and hood assemblies.

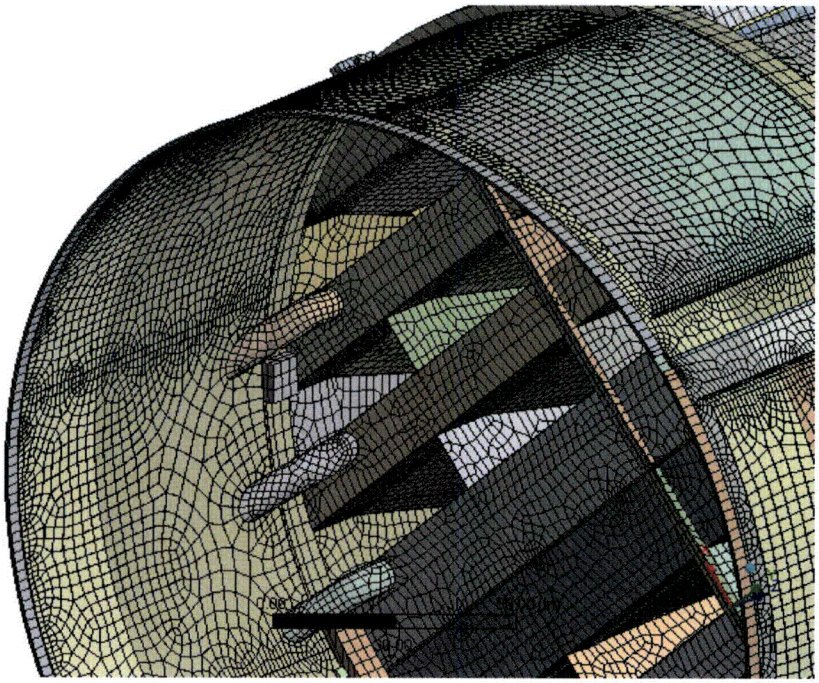

Figure 5c. Close-up of mesh showing drain pipes and hood supports.

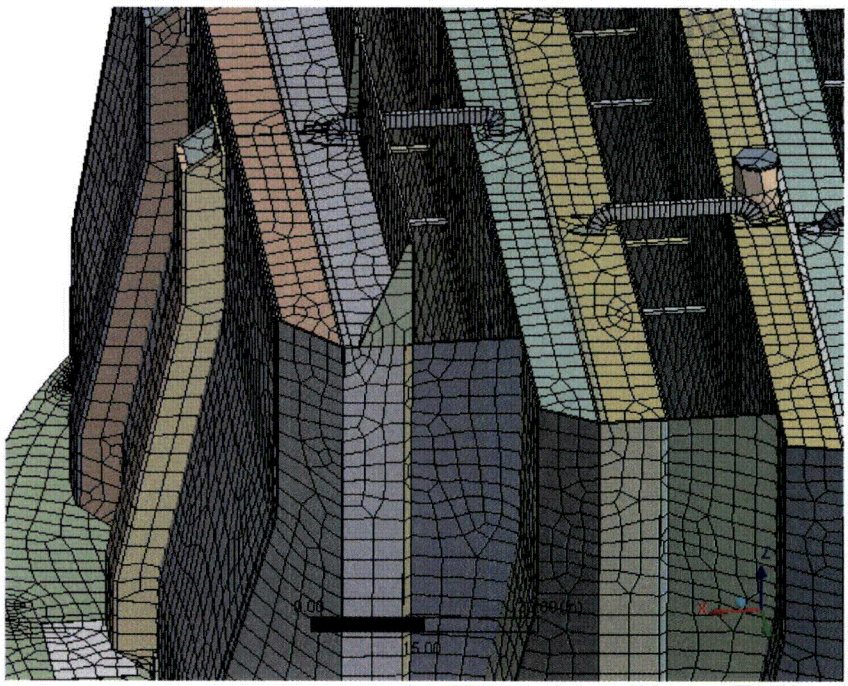

Figure 5d. Close-up of mesh showing node-to-node connections between various plates.

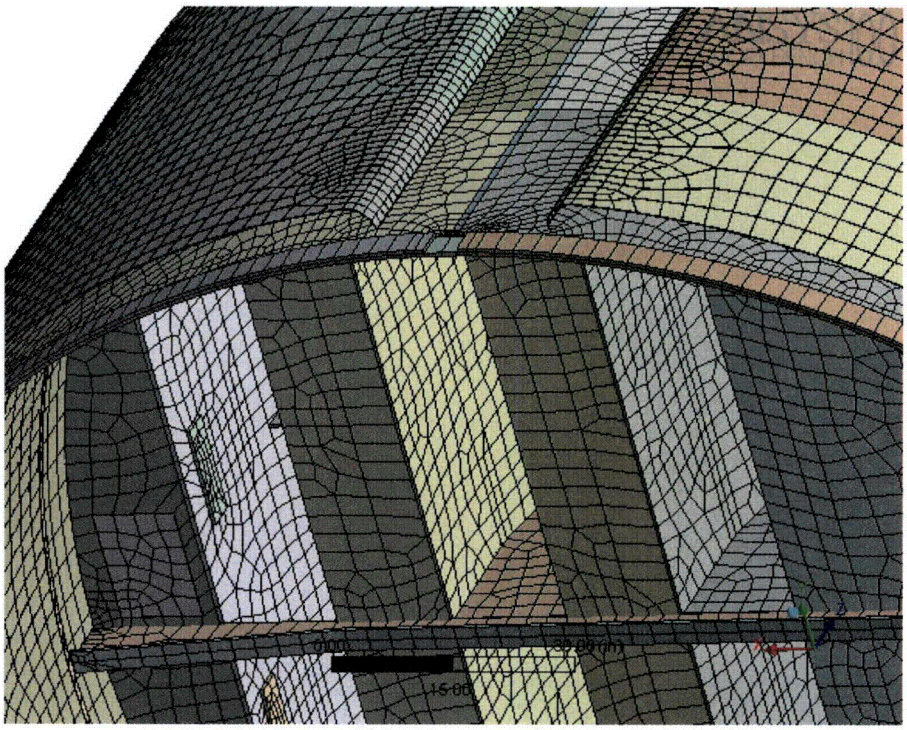

Figure 5e. Close-up of mesh showing node-to-node connections between the skirt and drain channels; supporting beams and base plates; hood supports and hoods.

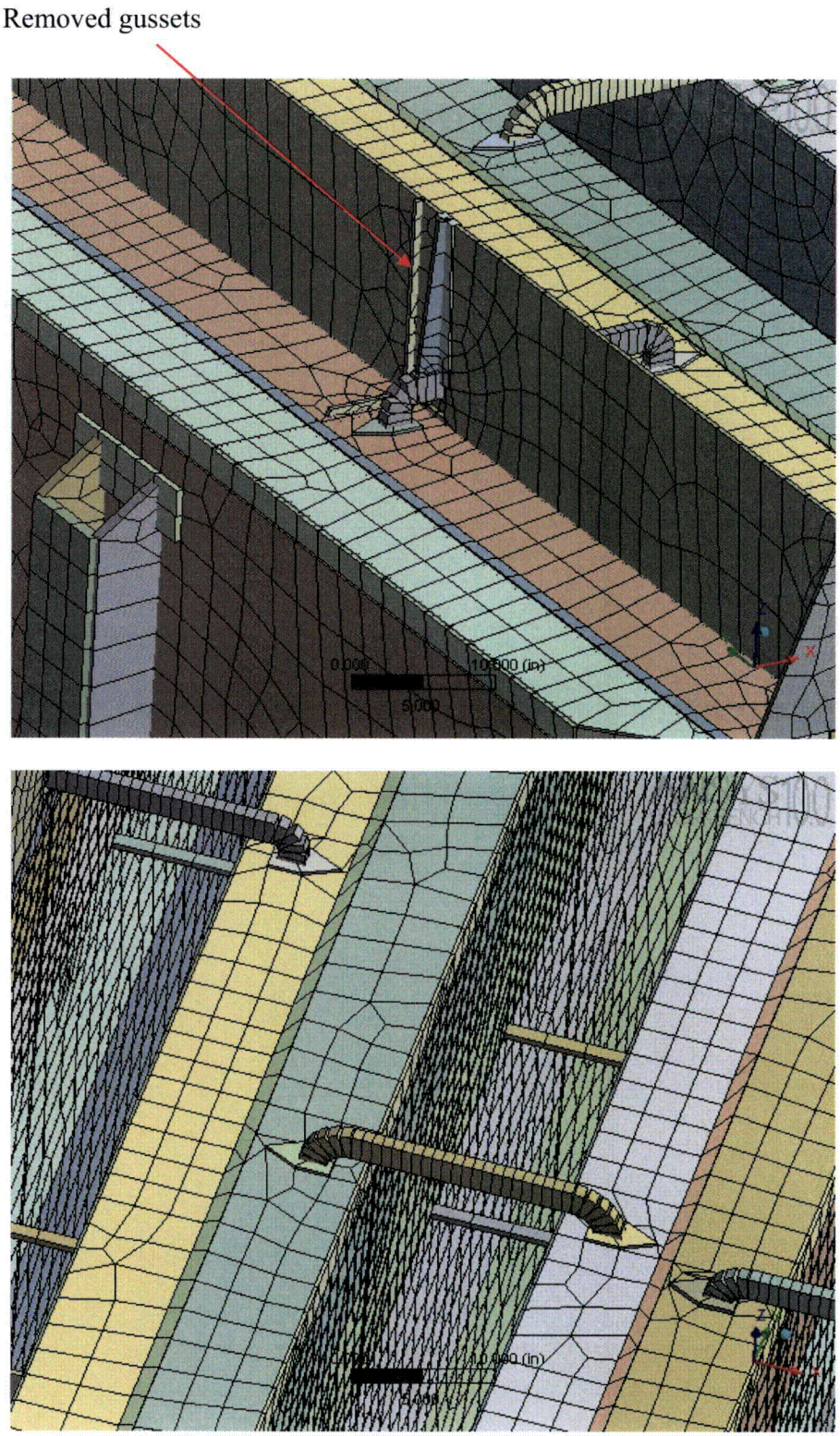

Figure 5f. Close-up view of tie bars connecting vane cover plates and adjacent to the steam dam.

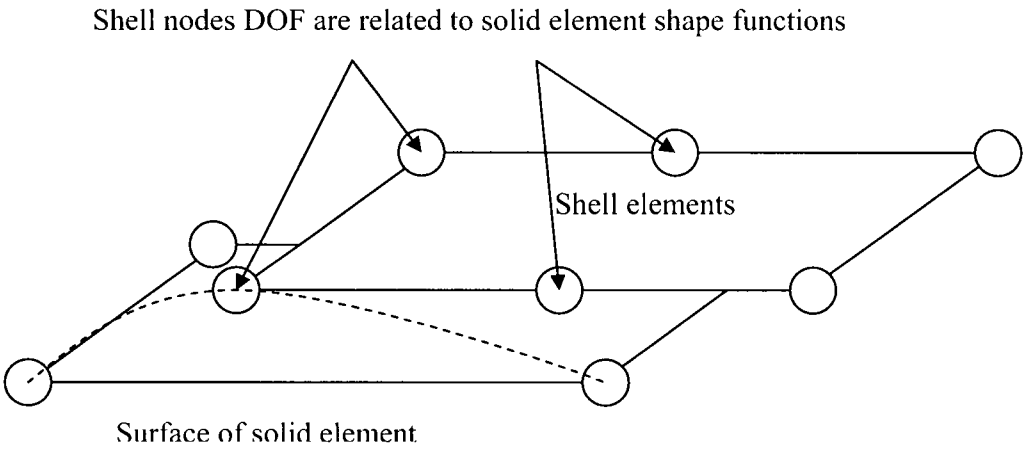

Figure 6a. Face-to-face shell to solid connection.

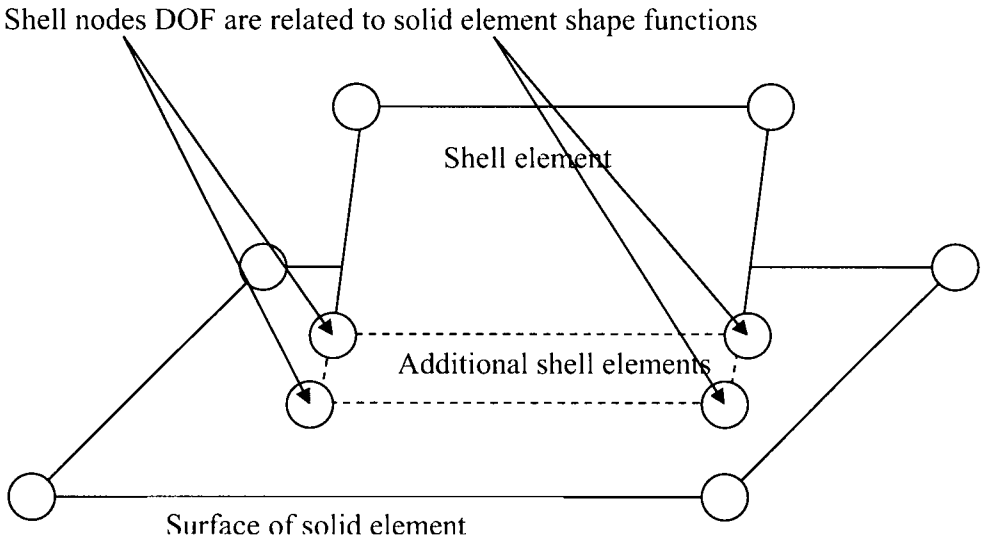

Figure 6b. Shell edge-to-solid face connection.

3.10 Pressure Loading

The harmonic loads are produced by the pressures acting on the exposed surfaces of the steam dryer. At every frequency and for each MSL, the pressure distribution corresponding to a unit pressure at the MSL inlet is represented on a three-inch grid lattice grid (i.e., a mesh whose lines are aligned with the x-, y- and z-directions) that is superimposed over the steam dryer surface. This grid is compatible with the "TableLoads" format used by ANSYS to "paint" general pressure distributions upon structural surfaces. The pressures are obtained from the Helmholtz solver routine in the acoustic analysis [1].

In general, the lattice nodes do not lie on the surface, so that to obtain the pressure differences at the surface, it is necessary to interpolate the pressure differences stored at the lattice nodes. This is done using simple linear interpolation between the eight forming nodes of the lattice cell containing the surface point of interest. Inspection of the resulting pressures at selected nodes shows that these pressures vary in a well-behaved manner between the nodes with prescribed pressures. Graphical depictions of the resulting pressures and comparisons between the peak pressures in the original nodal histories and those in the final surface load distributions produced in ANSYS, all confirm that the load data are interpolated accurately and transferred correctly to ANSYS.

The harmonic pressure loads are only applied to surfaces above the water level, as indicated in Figure 7. In addition to the pressure load, the static loading induced by the weight of the steam dryer is analyzed separately. The resulting static and harmonic stresses are linearly combined to obtain total values which are then processed to calculate maximum and alternating stress intensities for assessment in Section 5.

[[

[3]]] This is useful since revisions in the loads model do not necessitate recalculation of the unit stresses.

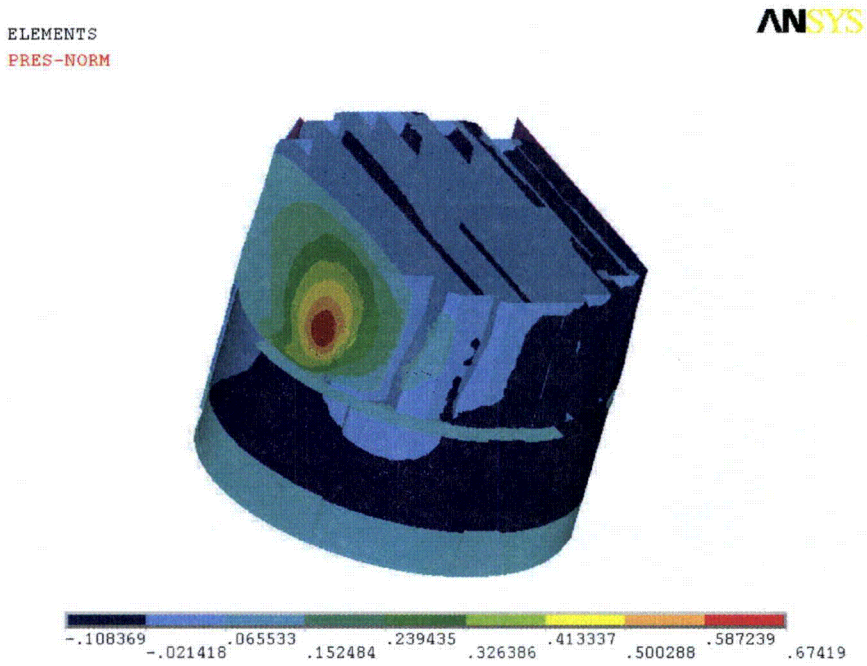

Frequency no. 372: 50.2 Hz

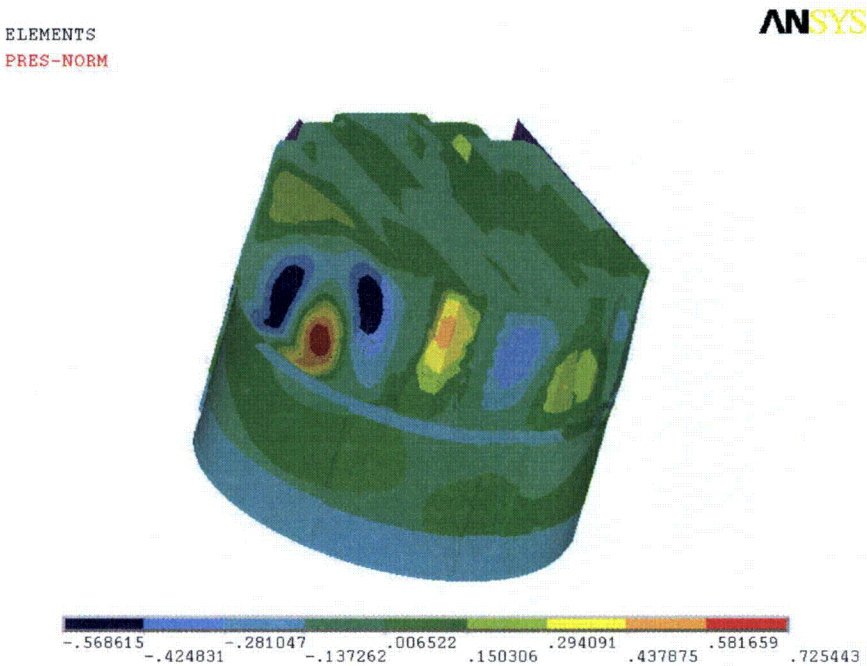

Frequency no. 589: 200.89 Hz

Figure 7. Real part of unit pressure loading MSL C (in psid) on the steam dryer at different frequencies. No loading is applied to the submerged light blue surface, solid support rings and dividing plates above the outer hoods.

4. Structural Analysis

The solution is decomposed into static and harmonic parts, where the static solution produces the stress field induced by the supported structure subjected to its own weight and the harmonic solution accounts for the harmonic stress field due to the unit pressure of given frequency in one of the main steam lines. All solutions are linearly combined, with amplitudes provided by signal measurements in each steam line, to obtain the final displacement and stress time histories. This decomposition facilitates the prescription of the added mass model accounting for hydrodynamic interaction and allows one to compare the stress contributions arising from static and harmonic loads separately. Proper evaluation of the maximum membrane and membrane+bending stresses requires that the static loads due to weight be accounted for. Hence both static and harmonic analyses are carried out.

4.1 Static Analysis

The results of the static analysis are shown in Figure 8. The locations with highest stress include the upper support ring areas near support brackets with stress intensity 6,759 psi; outer hood above upper support ring with stress intensity 6,808 psi; top of closure plates with stress intensity 4,521 psi. Close up views of these locations are shown in Figure 9.

4.2 Harmonic Analysis

The harmonic pressure loads were applied to the structural model at all surface nodes described in Section 3.10. Typical stress intensity distributions over the structure are shown in Figure 10. Stresses were calculated for each frequency, and results from static and harmonic calculations were combined.

To evaluate maximum stresses, the stress harmonics including the static component are transformed into a time history using FFT, and the maximum and alternating stress intensities for the response, evaluated. According to ASME B&PV Code, Section III, Subsection NG-3216.2 the following procedure was established to calculate alternating stresses. For every node, the stress difference tensors, $\boldsymbol{\sigma}'_{nm} = \boldsymbol{\sigma}_n - \boldsymbol{\sigma}_m$, are considered for all possible pairs of the stresses σ_n and σ_m at different time levels, t_n and t_m. Note that all possible pairs require consideration, since there are no "obvious" extrema in the stress responses. However, in order to contain computational cost, extensive screening of the pairs takes place (see Section 2.3), so that pairs known to produce alternating stress intensities less than 1,500 psi are rejected. For each remaining stress difference tensor, the principal stresses S_1, S_2, S_3 are computed and the maximum absolute value among principal stress differences, $S_{nm} = \max\{|S_1 - S_2|, |S_1 - S_3|, |S_2 - S_3|\}$, obtained. The alternating stress at the node is then one-half the maximum value of S_{nm} taken over all combinations (n,m), i.e., $S_{alt} = \frac{1}{2}\max_{n,m}\{S_{nm}\}$. This alternating stress is compared against allowable values, depending on the node location with respect to welds.

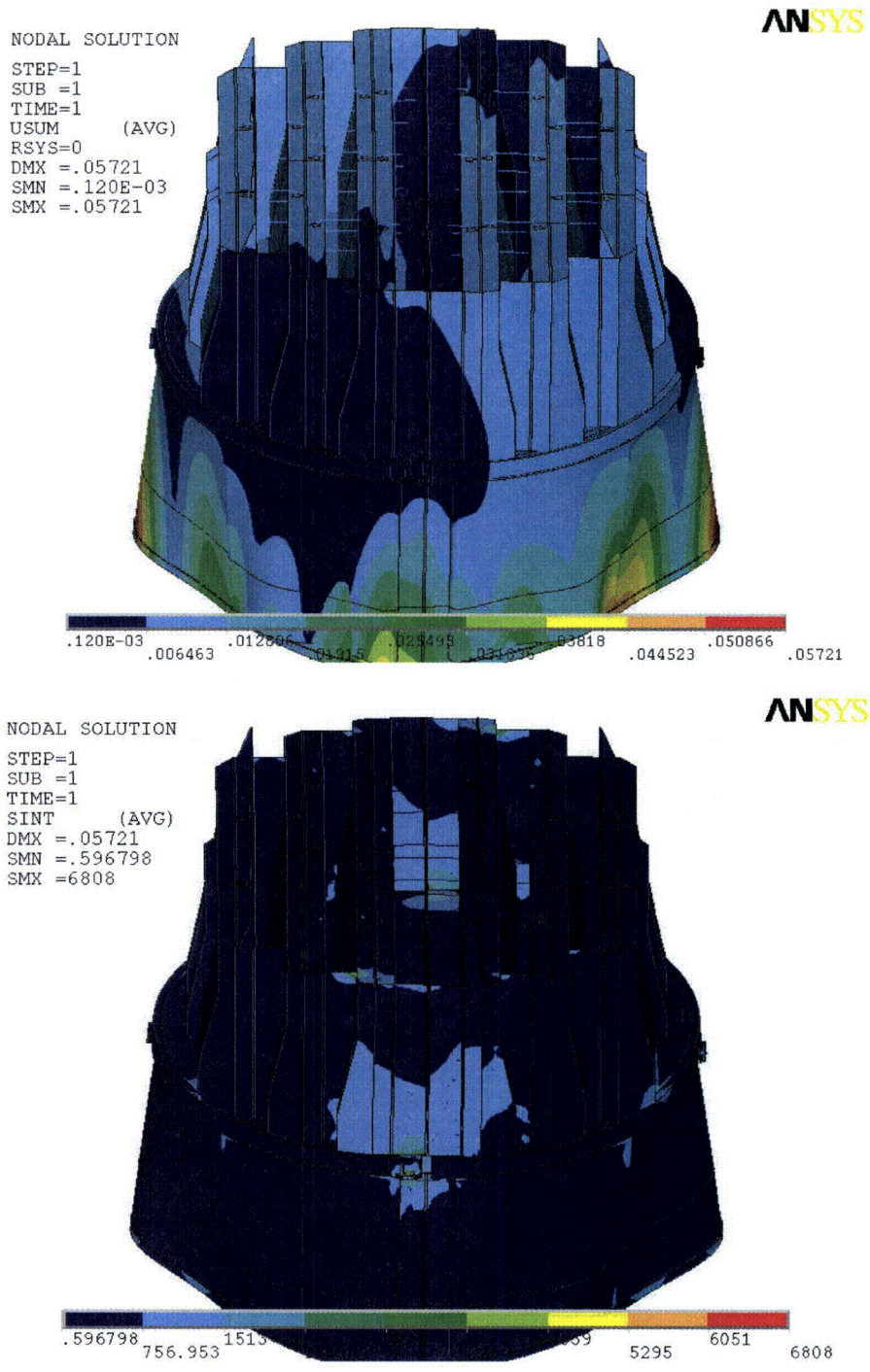

Figure 8. Overview of static calculations showing displacements (top, in inches) and stress intensities (bottom, in psi). Maximum displacement (DMX) is 0.057 inches; maximum stress intensity (SMX) is 6,808 psi. Note that displacements are amplified for visualization.

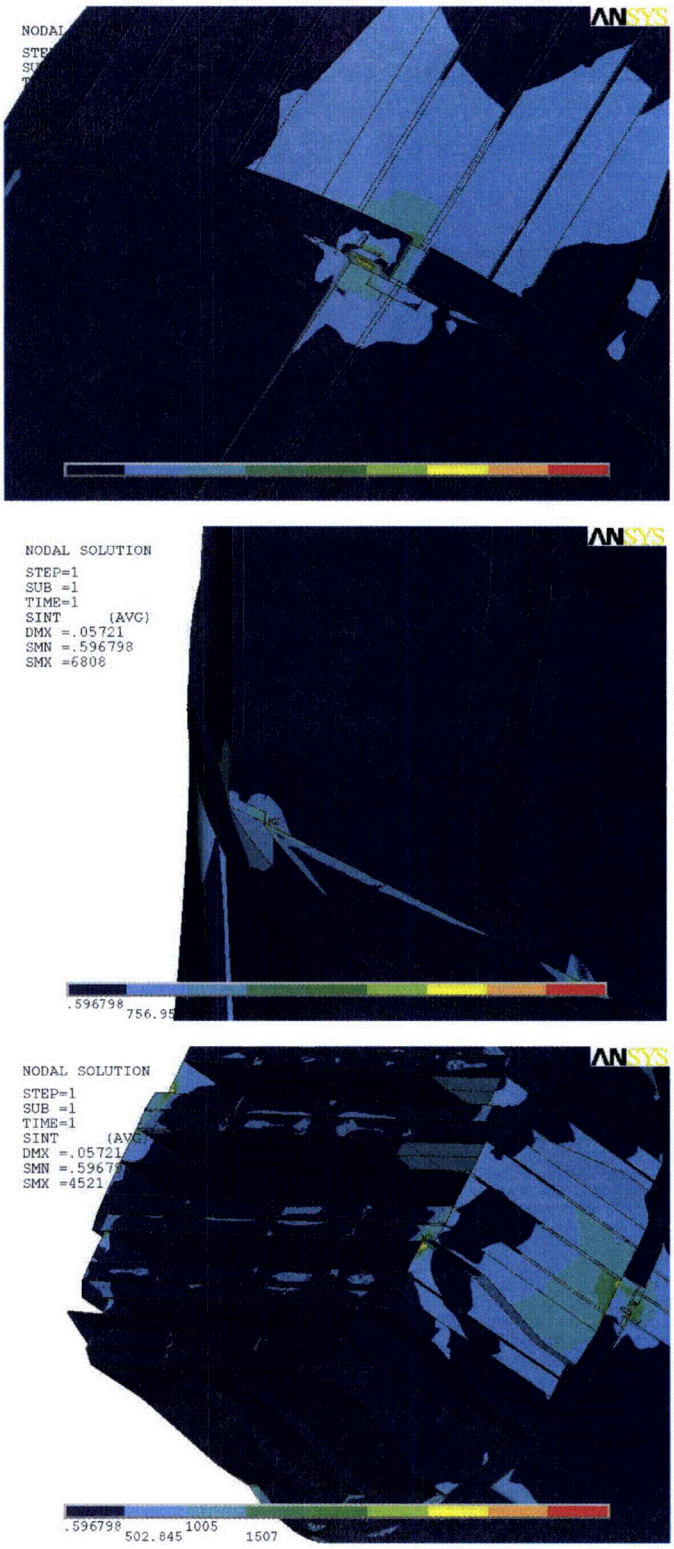

Figure 9. Close-up of high static stress intensity (in psi) locations near support brackets, at outer hood, and at closure plates.

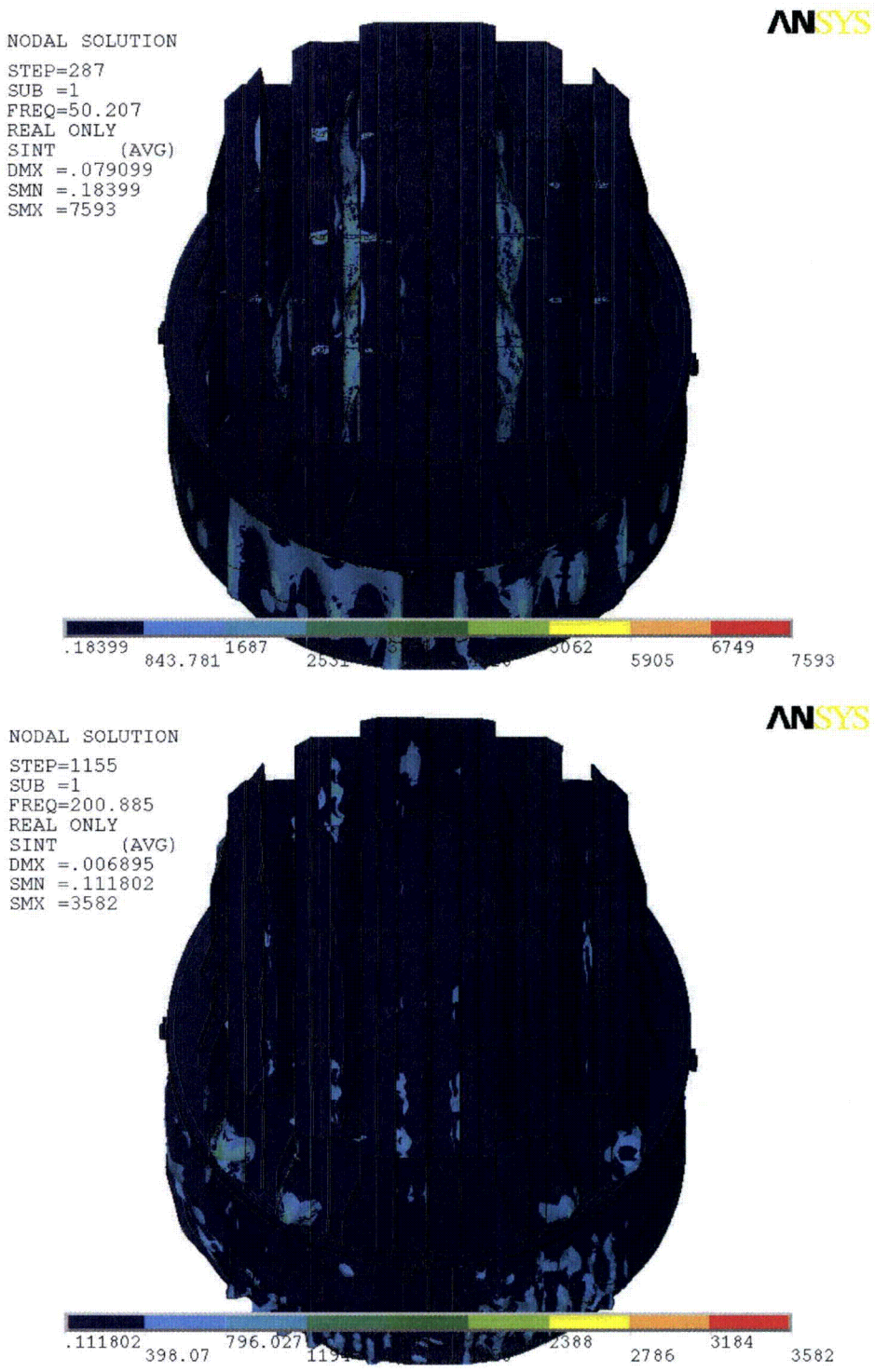

Figure 10. Overview of harmonic calculations showing real part of stress intensities (in psi) along with displacements. Unit loading MSL C for frequencies 50.2 Hz (top) and 200.9 Hz (bottom).

4.3 Post-Processing

The static and transient stresses computed at every node with ANSYS were exported into files for subsequent post-processing. These files were then read into separate customized software to compute the maximum and alternating stresses at every node. The maximum stress was defined for each node as the largest stress intensity occurring during the time history. Alternating stresses were calculated according to the ASME standard described above. For shell elements the maximum stresses were calculated separately at the mid-plane, where only membrane stress is present, and at top/bottom of the shell, where bending stresses are also present.

For nodes that are shared between several structural components or lie on junctions, the maximum and alternating stress intensities are calculated as follows. First, the nodal stress tensor is computed separately for each individual component by averaging over all finite elements meeting at the node and belonging to the same structural component. The time histories of these stress tensors are then processed to deduce the maximum and alternating stress intensities for each structural component. Finally, for nodes shared across multiple components, the highest of the component-wise maximum and alternating stresses is recorded as the "nodal" stress. This approach prevents averaging of stresses across components and thus yields conservative estimates for nodal stresses at the weld locations where several components are joined together.

The maximum stresses are compared against allowable values which depend upon the stress type (membrane, membrane+bending, alternating – Pm, Pm+Pb, S_{alt}) and location (at a weld or away from welds). These allowables are specified in the following section. For solid elements the most conservative allowable for membrane stress, Pm, is used, although bending stresses are nearly always present also. The structure is then assessed in terms of stress ratios formed by dividing allowables by the computed stresses at every node. Stress ratios less than unity imply that the associated maximum and/or alternating stress intensities exceed the allowable levels. Post-processing tools calculate the stress ratios, identifying the nodes with low stress ratios and generating files formatted for input to the 3D graphics program, TecPlot, which provides more general and sophisticated plotting options than currently available in ANSYS.

4.4 Computation of Stress Ratios for Structural Assessment

The ASME B&PV Code, Section III, subsection NG provides different allowable stresses for different load combinations and plant conditions. The stress levels of interest in this analysis are for the normal operating condition, which is the Level A service condition. The load combination for this condition is:

Normal Operating Load Combination = Weight + Pressure + Thermal

The weight and fluctuating pressure contributions have been calculated in this analysis and are included in the stress results. The static pressure differences and thermal expansion stresses are small, since the entire steam dryer is suspended inside the reactor vessel and all surfaces are exposed to the same conditions. Seismic loads only occur in Level B and C cases, and are not considered in this analysis.

Allowable Stress Intensities

The ASME B&PV Code, Section III, subsection NG shows the following (Table 5) for the maximum allowable stress intensity (Sm) and alternating stress intensity (Sa) for the Level A service condition. The allowable stress intensity values for type 304 stainless steel at operating temperature 550°F are taken from Table I-1.2 and Fig. I-9.2.2 of Appendix I of Section III, in the ASME B&PV Code. The calculation for different stress categories is performed in accordance with Fig. NG-3221-1 of Division I, Section III, subsection NG.

Table 5. Maximum Allowable Stress Intensity and Alternating Stress Intensity for all areas other than welds. The notation Pm represents membrane stress; Pb represents stress due to bending; Q represents secondary stresses (from thermal effects and gross structural discontinuities, for example); and F represents additional stress increments (due to local structural discontinuities, for example).

Type	Notation	Service Limit	Allowable Value (psi)
Maximum Stress Allowables:			
General Membrane	Pm	Sm	18,300
Membrane + Bending	Pm + Pb	1.5 Sm	27,450
Primary + Secondary	Pm + Pb + Q	3.0 Sm	54,900
Alternating Stress Allowable:			
Peak = Primary + Secondary + F	S_{alt}	Sa	13,600

When evaluating welds, either the calculated or allowable stress was adjusted, to account for stress concentration factor and weld quality. Specifically:

- For maximum allowable stress intensity, the allowable value is decreased by multiplying its value in Table 5 by 0.55.

- For alternating stress intensity, the calculated weld stress intensity is multiplied by a weld stress intensity (fatigue) factor of 1.8, before comparison to the Sa value given above.

The weld factors of 0.55 and 1.8 were selected based on the observable quality of the shop welds and liquid penetrant NDE testing of all welds (excluding tack and intermittent welds, which were subject to 5X visual inspection) during fabrication. These factors are consistent with fatigue strength reduction factors recommended by the Welding Research Council, [12], and stress concentration factors at welds, provided in [13] and [14]. In addition, critical welds are subject to periodical visual inspections in accordance with the requirements of GE SIL 644 SIL and BWR VIP-139 [15]. Therefore, for weld stress intensities, the allowable values are shown in Table 6.

These factors (0.55 and 1.8) also conservatively presume that the structure is joined using fillet welds unless specified otherwise. Since fillet welds correspond to larger stress concentration factors than other types of welds, this assumption is a conservative one.

Table 6. Weld Stress Intensities.

Type	Notation	Service Limit	Allowable Value (psi)
Maximum Stress Allowables:			
General Membrane	Pm	0.55 Sm	10,065
Membrane + Bending	Pm + Pb	0.825 Sm	15,098
Primary + Secondary	Pm + Pb + Q	1.65 Sm	30,195
Alternating Stress Allowables:			
Peak = Primary + Secondary + F	S_{alt}	Sa	13,600

Comparison of Calculated and Allowable Stress Intensities

The classification of stresses into general membrane or membrane + bending types was made according to the exact location, where the stress intensity was calculated; namely, general membrane, Pm, for middle surface of shell element, and membrane + bending, Pm + Pb, for other locations. For solid elements the most conservative, general membrane, Pm, allowable is used.

The structural assessment is carried out by computing stress ratios between the computed maximum and alternating stress intensities, and the allowable levels. Locations where any of the stresses exceed allowable levels will have stress ratios less than unity. Since computation of stress ratios and related quantities within ANSYS is time-consuming and awkward, a separate FORTRAN code was developed to compute the necessary maximum and alternating stress intensities, Pm, Pm+Pb, and S_{alt}, and then compare it to allowables. Specifically, the following quantities were computed at every node:

1. The maximum membrane stress intensity, Pm (evaluated at the mid-thickness location for shells),
2. The maximum membrane+bending stress intensity, Pm+Pb, (taken as the largest of the maximum stress intensity values at the bottom, top, and mid thickness locations, for shells),
3. The alternating stress, S_{alt}, (the maximum value over the three thickness locations is taken).
4. The stress ratio due to a maximum stress intensity assuming the node lies at a non-weld location (note that this is the minimum ratio obtained considering both membrane stresses and membrane+bending stresses):
   SR-P(nw) = min{ Sm/Pm, 1.5 * Sm/(Pm+Pb) }.
5. The alternating stress ratio assuming the node lies at a non-weld location,
   SR-a(nw) = Sa / (1.1 * S_{alt}),
6. The same as 4, but assuming the node lies on a weld,
   SR-P(w)=SR-P(nw) * f_{sw} * 0.55
7. The same as 5, but assuming the node lies on a weld,
   SR-a(w)=SR-a(nw) * f_{sw} / 1.8.

where f_{sw}=1 at all welds (when justified, f_{sw} can be adjusted to reflect different weld types). Note that in steps 4 and 6, the minimum of the stress ratios based on Pm and Pm+Pb, is taken. The allowables listed in Table 5, Sm=18,300 psi and Sa=13,600 psi. The factors, 0.55 and 1.8, are the weld factors discussed above. The factor of 1.1 accounts for the differences in Young's moduli for the steel used in the steam dryer and the values assumed in alternating stress allowable. According to NG-3222.4 in subsection NG of Section III of the ASME Code, the effect of elastic modulus upon alternating stresses is taken into account by multiplying alternating stress S_{alt} at all locations by the ratio, E/E_{model}=1.1, where:

$E = 28.3\ 10^6$ psi, as shown on Fig. I-9.2.2. ASME BP&V Code
$E_{model} = 25.55\ 10^6$ psi (Table 1)

The nodes with stress ratios lower than 4 are plotted in TecPlot (a 3D graphics plotting program widely used in engineering communities [16]) to establish whether they lie on a weld or not. The appropriate maximum and alternating stress ratios, SR-P and SR-a, are thus determined and a final listing of nodes having the smallest stress ratios is generated. These nodes are tabulated and depicted in the Results Sections.

5. Results

5.1 General Stress Distribution and High Stress Locations

The maximum stress intensities obtained by post-processing the ANSYS stress histories for CLTP at nominal frequency and with frequency shift operating conditions are listed in Table 7. Contour plots of the stress intensities over the steam dryer structure are shown on Figure 11 (nominal frequency), Figure 12 (maximum stress over all nine frequency shifts including nominal), Figure 13 (-10% frequency shift), and Figure 14 (+10% frequency shift). The figures are oriented to emphasize the high stress regions. Note that these stress intensities *do not* account for weld factors but include end-to-end bias and uncertainty. Further, it should be noted that since the allowable stresses vary with location, stress intensities do not necessarily correspond to regions of primary structural concern. Instead, structural evaluation is more accurately made in terms of the stress ratios which compare the computed stresses to allowable levels with due account made for stress type and weld factors. Comparisons on the basis of stress ratios are made in Section 5.2.

The tabulated stresses are obtained by computing the relevant stress intensities at every node and then sorting the nodes according to stress levels. The highest stress node is noted and all neighboring nodes within 10 inches of the highest stress node and its symmetric images (i.e., reflections across the x=0 and y=0 planes) are "blanked" (i.e., excluded from the search for subsequent high stress locations). Of the remaining nodes, the next highest stress node is identified and its neighbors (closer than 10 inches) blanked. The third highest stress node is similarly located and the search continued in this fashion until all nodes are either blanked or have stresses less than half the highest value on the structure or stress ratios lower than 4. The blanking of neighboring nodes is intended to prevent extracting peak stress nodes from essentially the same location on the structure.

The maximum stress intensities in most areas are low (less than 500 psi, or 5% of the most conservative critical stress). For the membrane stresses (Pm) the high stress regions tend to occur at: (i) the restraint locations for the upper support ring and (ii) the upper edges of the closure plates. The first location experiences high stresses since the entire weight of the structure is transmitted through relatively small pads to the external structure. The stress is dominated by the static component since the stress intensities at this location do not vary significantly with frequency shift and alternating stress intensities remain below 1500 psi at all shifts. The closure plates experience high stresses since they restrain any motion of the adjacent vane banks. The associated stresses also contain a larger contribution from acoustic loading as is evident in the last column in Table 7 recording the alternating stress intensities.

The membrane + bending stress (Pm+Pb) distributions are quite different and show evidence of significant modal response in all cases. Modal excitations are most pronounced for the nominal frequency (Figure 12b) and ±10% frequency shifts (Figure 14b) where vibrations are most evident on the skirt and drain channels and the inner closure plates at the ends of the large middle plate spanning the dryer. This plate also exhibits vibration motions along its top edge (see Figure 14b). For nominal and negative frequency shifts the hood supports also exhibit a strong response as is seen, for example, in Figure 12c. Stress concentrations are observed at several locations coinciding with welds including: (i) where the closure plates connect to the

hoods or vane bank end plates; (ii) along the skirt/drain channel welds; (iii) the junctions between the upper tie bars and top cover plates of the vane banks; and (iv) the hood support/cover or base plate joints.

The alternating stress, S_{alt}, distributions are qualitatively similar to those for Pm+Pb, but are much more localized. This is true for all frequency shifts and is due to the presence of a single 218 Hz dominant frequency in the load spectrum (see discussion in Section 5.3). The alternating stress intensity contour plots essentially record the modes excited by this signal, which here are seen to be confined to the skirt and drain channels, inner closure plates, the large middle plate, the end plates of the vane banks and the hood supports. The strong response of these components is not surprising, since they essentially comprise plates that are thin (and therefore easily excited) and of large dimension so that they support a significant number of response modes over the applied load frequency range. Since the submerged skirt and hood supports are not subjected to pressure loads the responses are due to modal excitation and transmission of dynamic loads from elsewhere in the structure.

Shifting the frequencies has a relatively weak effect on the maximum membrane (Pm) and membrane+bending (Pm+Pb) stresses due to the presence of a large static component. The variations with frequency shift in the alternating stresses on the other hand are more pronounced with a variation in maximum stress intensity of approximately 2,000 psi. Examining Table 7b shows that high stresses are obtained with both negative and positive frequency shifts. Because of the presence of a dominant 218 Hz signal in the load, the effect of frequency shifting is to simply excite a different collection of modes at each shift. Thus at the -10% shift, the modes at 196 Hz are most strongly excited which, from Figure 13c and d are seen to occur on the vane bank endplates and hood supports. The +10% shift excites modes near 240 Hz which now occur on the drain channels and inner closure plates. For the +10% shift the hood supports show only a weak response.

Table 7a. Locations with highest predicted stress intensities for CLTP conditions with no frequency shift.

Stress Category	Location		Location (in)				Stress Intensities (psi)		
		Weld	x	y	z	node	Pm	Pm+Pb	S_{alt}
Pm	upper support ring/support	Yes	-5.8	-122.4	-6.5	7705	8046	8046	<1500
"	inner hood/top cover plate/middle closure plate	Yes	-31.5	-108.4	88.9	76022	6292	6677	2376
"	outer hood/hood support	Yes	-93.5	-28.7	86.9	89700	5299	5443	4117
"	T-cross-section stiffener	No	-99.3	0.0	0.0	74585	4971	5047	<1500
"	middle hood/top cover plate/outer closure plate	Yes	62.5	-85.0	88.9	87593	4534	5264	2989
Pm+Pb	submerged drain channel/skirt	Yes	-91.0	76.7	-100.5	77550	2071	8648	4584
"	outer hood/cover plate	Yes	-102.0	60.2	0.0	91589	1131	8531	1707
"	upper support ring/support	Yes	-5.8	-122.4	-6.5	7705	8046	8046	<1500
"	inner hood/top cover plate/middle closure plate	Yes	-31.5	-108.4	88.9	76022	6292	6677	2376
"	middle hood/outer base plate/hood support	Yes	-70.8	-54.6	0.0	91667	4514	6337	5729
S_{alt}	middle hood/outer base plate/hood support	Yes	-70.8	-54.6	0.0	91667	4514	6337	5729
"	submerged drain channel/skirt	Yes	91.0	-76.7	-100.5	84412	2145	8533	4718
"	lock gusset	No	78.3	31.4	91.6	75630	3593	4525	4484
"	outer hood/hood support	Yes	-93.5	-28.7	86.9	89700	5299	5443	4117
"	middle base plate/hood support/vane bank	Yes	-55.0	-54.6	0.0	86676	1066	3895	3814

Node numbers are retained for further reference.
Spatial coordinates are in a reference frame whose origin is located at the intersection of the steam dryer centerline and the plane containing the base and cover plates (this plane also contains the top of the upper support ring and the bottom edges of the hoods). The y-axis is parallel to the hoods, the x-axis is normal to the hoods pointing from MSL C/D to MSL A/B, and the z-axis is vertical, positive up.

Table 7b. Locations with highest predicted stress intensities taken over all frequency shifts CLTP conditions.

Stress Category	Location	Weld	% Freq. Shift	Location (in)				Stress Intensities (psi)		
				x	y	z	node	Pm	Pm+Pb	S_{alt}
Pm	upper support ring/support	Yes	+5	5.8	122.4	-6.5	7532	8047	8047	<1500
"	inner hood/top cover plate/middle closure plate	Yes	0	-31.5	-108.4	88.9	76022	6292	7431	3151
"	outer hood/hood support	Yes	-2.5	-93.5	-28.7	86.9	89700	5496	5808	4545
"	inner hood/middle base plate/hood support	Yes	-7.5	-39.8	59.8	0.0	91796	5307	7405	5113
"	middle hood/top cover plate/outer closure plate	Yes	-7.5	-62.5	85.0	88.9	78847	5041	5480	3397
Pm+Pb	submerged drain channel/skirt	Yes	-5	91.0	76.7	-100.5	85938	2832	10488	6518
"	top perforated plate/inner closure plate/inner side panel	Yes	+7.5	15.0	118.9	88.9	89175	2064	8937	6694
"	outer hood/cover plate	Yes	+7.5	-102.0	60.2	0.0	91589	1191	8868	2084
"	upper support ring/support	Yes	+5	5.8	122.4	-6.5	7532	8047	8047	<1500
"	submerged drain channel/skirt	Yes	-7.5	-11.5	118.4	-100.5	76751	1962	7979	5317
S_{alt}	middle hood/outer base plate/hood support	Yes	-10	70.8	54.6	0.0	87364	4385	7643	7143
"	inner hood/middle base plate/hood support	Yes	+7.5	39.8	59.8	0.0	91846	3700	7851	7027
"	top perforated plate/inner closure plate/inner side panel	Yes	+7.5	15.0	118.9	88.9	89175	2064	8937	6694
"	submerged drain channel/skirt	Yes	-5	-91.0	-76.7	-100.5	86016	2809	10059	6628
"	middle base plate/hood support/vane bank	Yes	-10	55.0	54.6	0.0	93714	1007	6410	6321

See Table 7a for coordinates description.

Table 7c. Locations with highest predicted stress intensities for CLTP conditions with -10% frequency shift.

Stress Category	Location		Location (in)				Stress Intensities (psi)		
		Weld	x	y	z	node	Pm	Pm+Pb	S_{alt}
Pm	upper support ring/support	Yes	5.8	122.4	-6.5	7532	7888	7888	<1500
"	inner hood/top cover plate/middle closure plate	Yes	31.5	108.4	88.9	87571	6183	6399	2010
"	T-cross-section stiffener	No	-99.3	0.0	0.0	74585	4921	4959	<1500
"	inner hood/middle base plate/hood support	Yes	-39.8	59.8	0.0	91796	4792	5184	3180
"	middle hood/top cover plate/outer closure plate	Yes	62.5	-85.0	88.9	87593	4597	5039	2769
Pm+Pb	submerged drain channel/skirt	Yes	-91.0	-76.7	-100.5	86016	2180	8368	4747
"	outer hood/cover plate	Yes	-102.0	60.2	0.0	91589	1061	8241	<1500
"	upper support ring/support	Yes	5.8	122.4	-6.5	7532	7888	7888	<1500
"	middle hood/outer base plate/hood support	Yes	-70.8	54.6	0.0	87549	3930	7801	6699
"	middle base plate/hood support/vane bank	Yes	55.0	54.6	0.0	93714	671	6410	6321
S_{alt}	middle hood/outer base plate/hood support	Yes	70.8	54.6	0.0	87364	3654	7643	7143
"	middle base plate/hood support/vane bank	Yes	55.0	54.6	0.0	93714	671	6410	6321
"	middle side panel/vane bank	Yes	55.0	108.4	12.1	88569	774	5029	4869
"	submerged drain channel/skirt	Yes	-91.0	-76.7	-100.5	86016	2180	8368	4747
"	middle end wall	No	62.5	103.7	19.2	58609	519	4664	4594

See Table 7a for coordinates description.

Table 7d. Locations with highest predicted stress intensities for CLTP conditions with +10% frequency shift.

Stress Category	Location		Location (in)				Stress Intensities (psi)		
		Weld	x	y	z	node	Pm	Pm+Pb	S_{alt}
Pm	upper support ring/support	Yes	5.8	122.4	-6.5	7532	7910	7910	<1500
"	inner hood/top cover plate/middle closure plate	Yes	31.5	108.4	88.9	87571	5956	6876	2575
"	T-cross-section stiffener	No	-99.3	0.0	0.0	74585	5040	5103	<1500
"	inner hood/middle base plate/hood support	Yes	39.8	-59.8	0.0	91831	4577	4749	2726
"	outer hood/hood support	Yes	93.5	-28.7	86.9	88530	4169	4596	2985
Pm+Pb	outer hood/cover plate	Yes	-102.0	60.2	0.0	91589	1157	8444	1750
"	upper support ring/support	Yes	5.8	122.4	-6.5	7532	7910	7910	0
"	submerged drain channel/skirt	Yes	91.0	-76.7	-100.5	84412	1854	7207	3402
"	inner hood/top cover plate/middle closure plate	Yes	-31.5	-108.4	88.9	76022	5845	7183	2979
"	inner side panel/top cover plate/inner closure plate	Yes	-15.0	-118.9	88.9	77828	1986	6723	4396
S_{alt}	lock gusset	No	-78.3	-31.4	91.6	75607	3438	5201	5166
"	inner side panel/top cover plate/inner closure plate	Yes	-15.0	-118.9	88.9	77828	1986	6723	4396
"	tie bar/top cover plate	Yes	48.0	3.0	88.9	92355	1087	4561	3755
"	tie bar/middle bank top cover plate	Yes	60.5	31.4	88.9	79136	531	4246	3739
"	outer hood/cover plate	Yes	102.0	-60.8	0.0	90532	3778	6614	3639

See Table 7a for coordinates description.

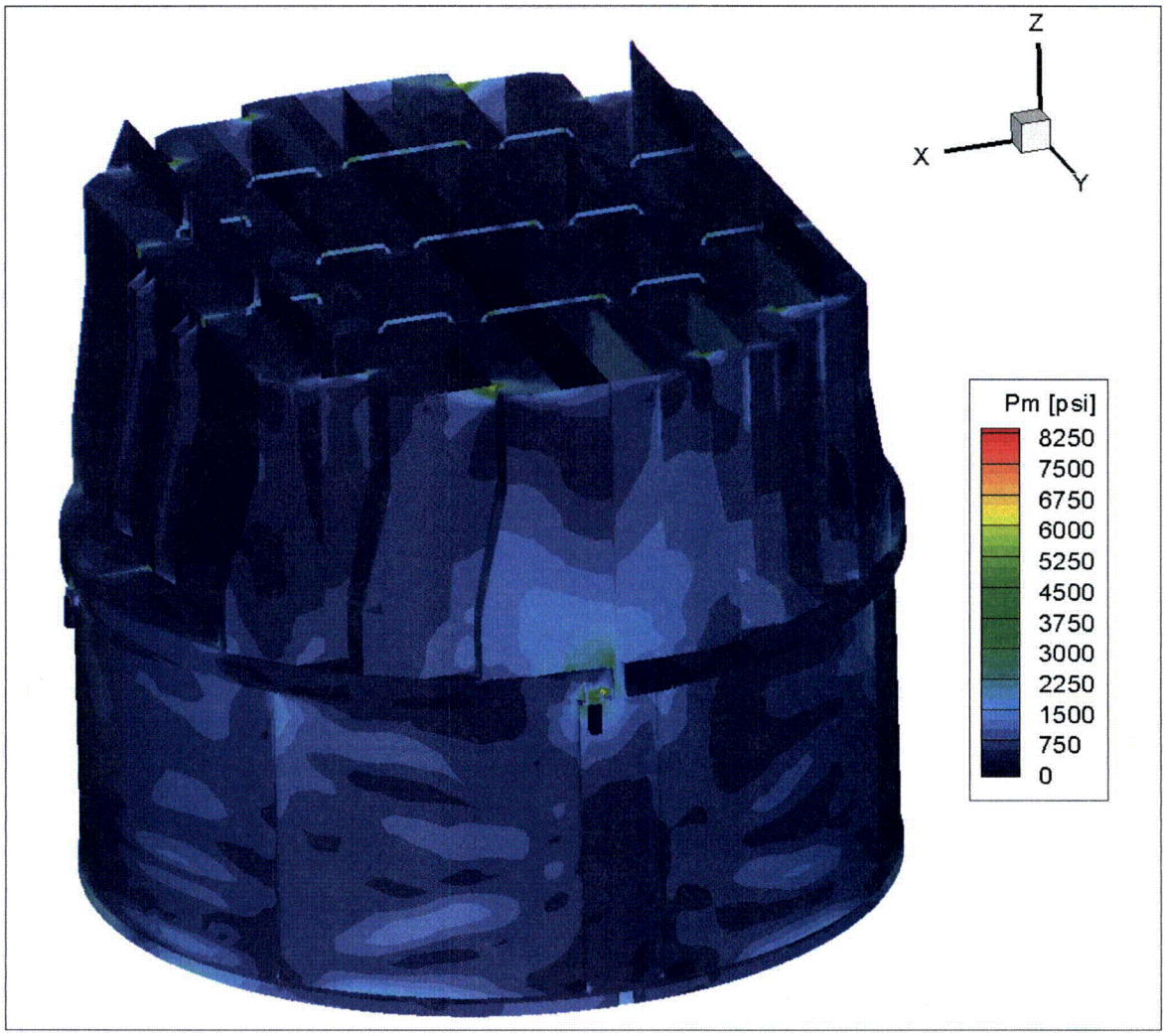

Figure 11a. Contour plot of maximum membrane stress intensity, Pm, for CLTP load. The maximum stress intensity is 8,046 psi.

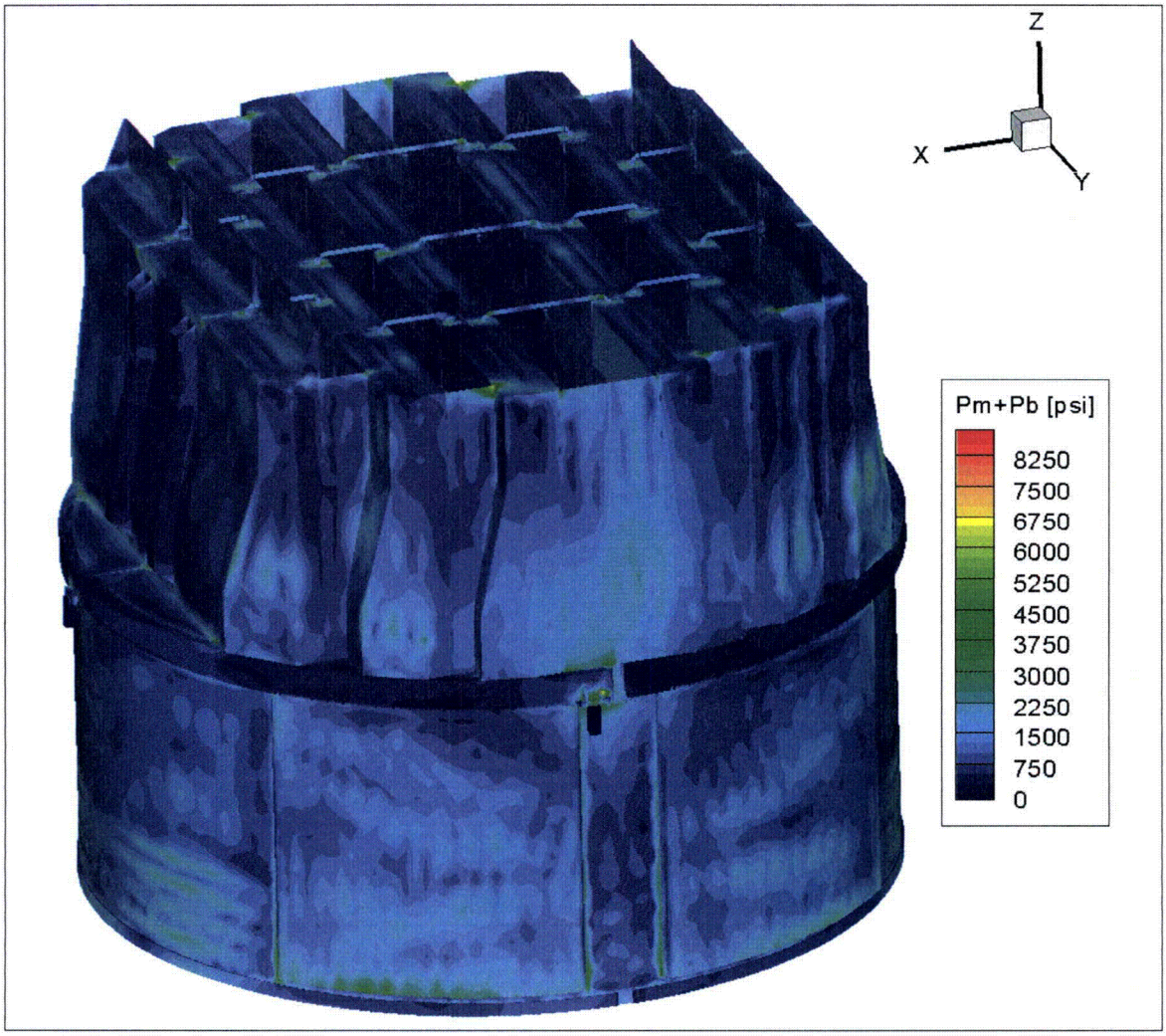

Figure 11b. Contour plot of maximum membrane+bending stress intensity, Pm+Pb, for CLTP load. The maximum stress intensity is 8,648 psi.

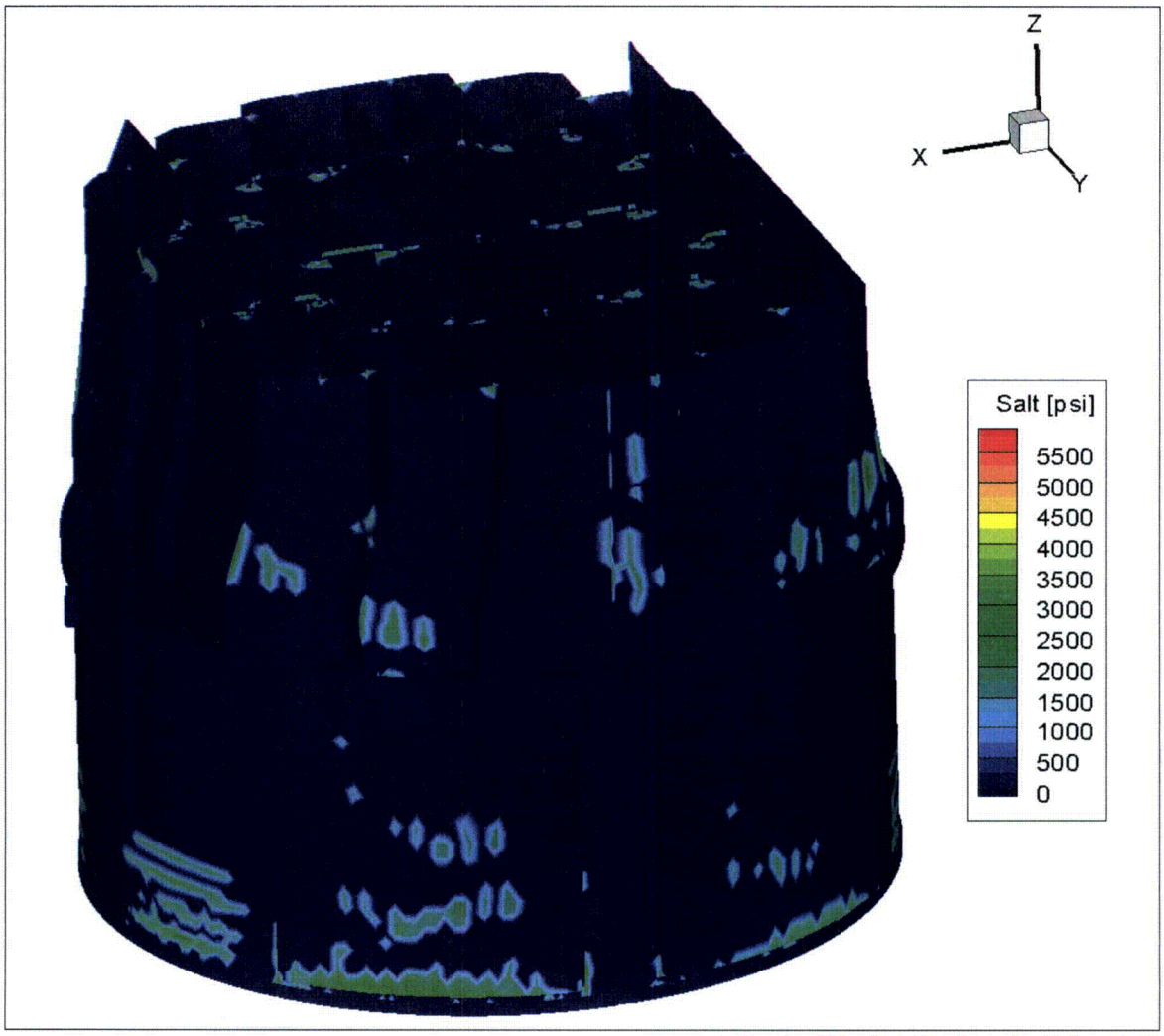

Figure 11c. Contour plot of alternating stress intensity, S_{alt}, for CLTP load. The maximum alternating stress intensity is 5,729 psi. First view.

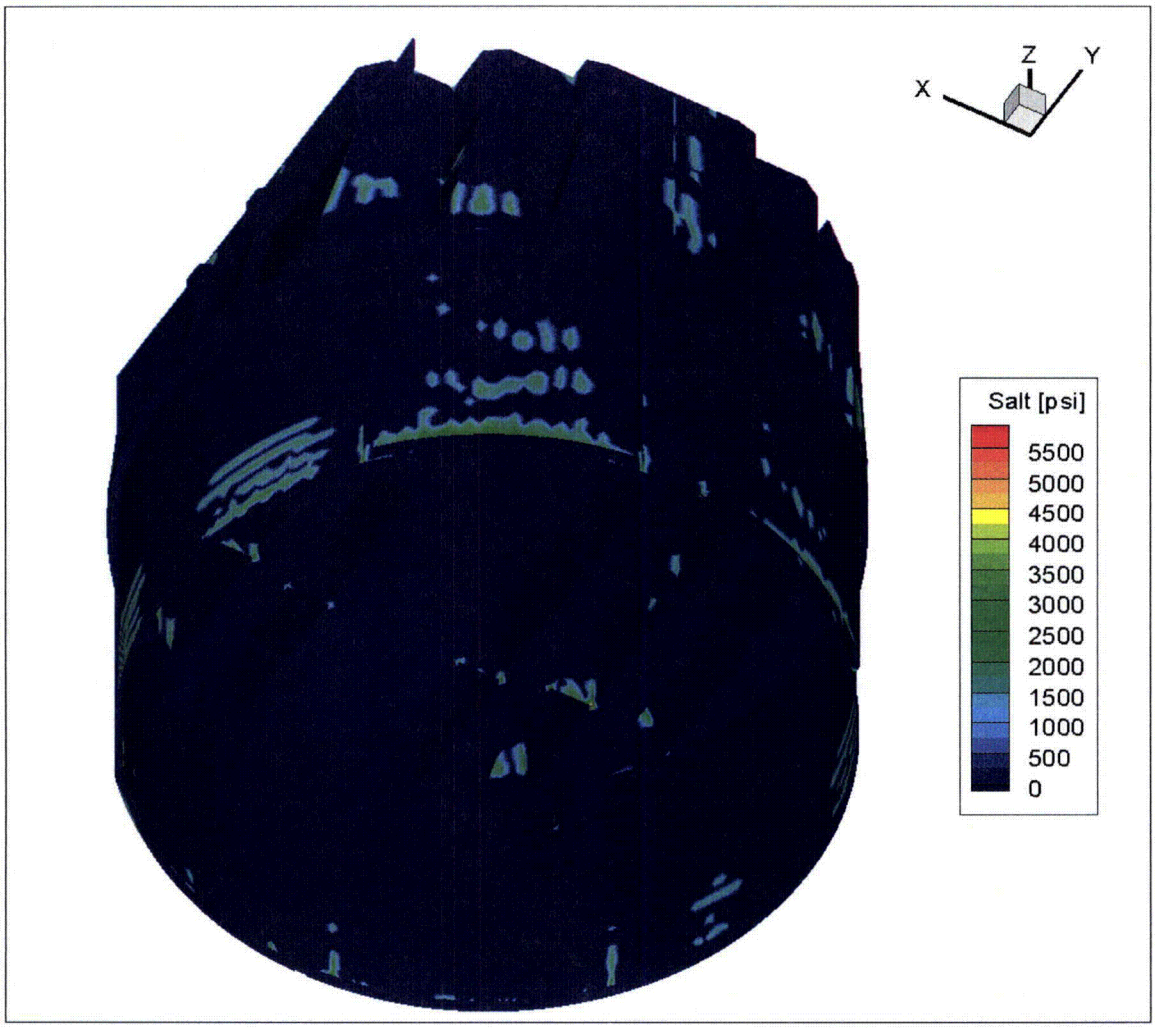

Figure 11d. Contour plot of alternating stress intensity, S_{alt}, for CLTP load. This second view from below shows the high alternating stress intensity at the base plate/middle hood/hood support junction.

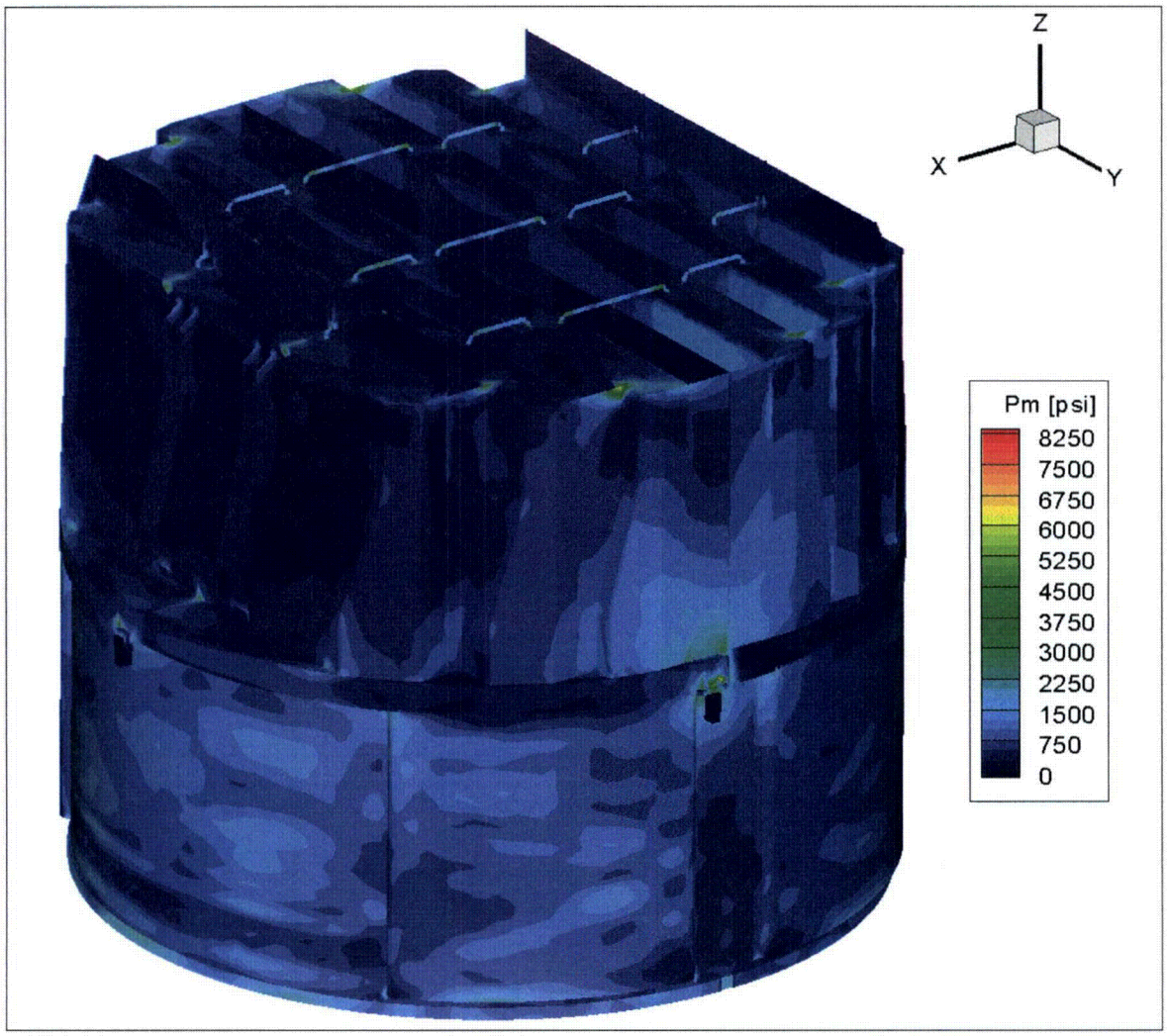

Figure 12a. Contour plot of maximum membrane stress intensity, Pm, for CLTP operation with frequency shifts. The recorded stress at a node is the maximum value taken over all frequency shifts. The maximum stress intensity is 8,047 psi.

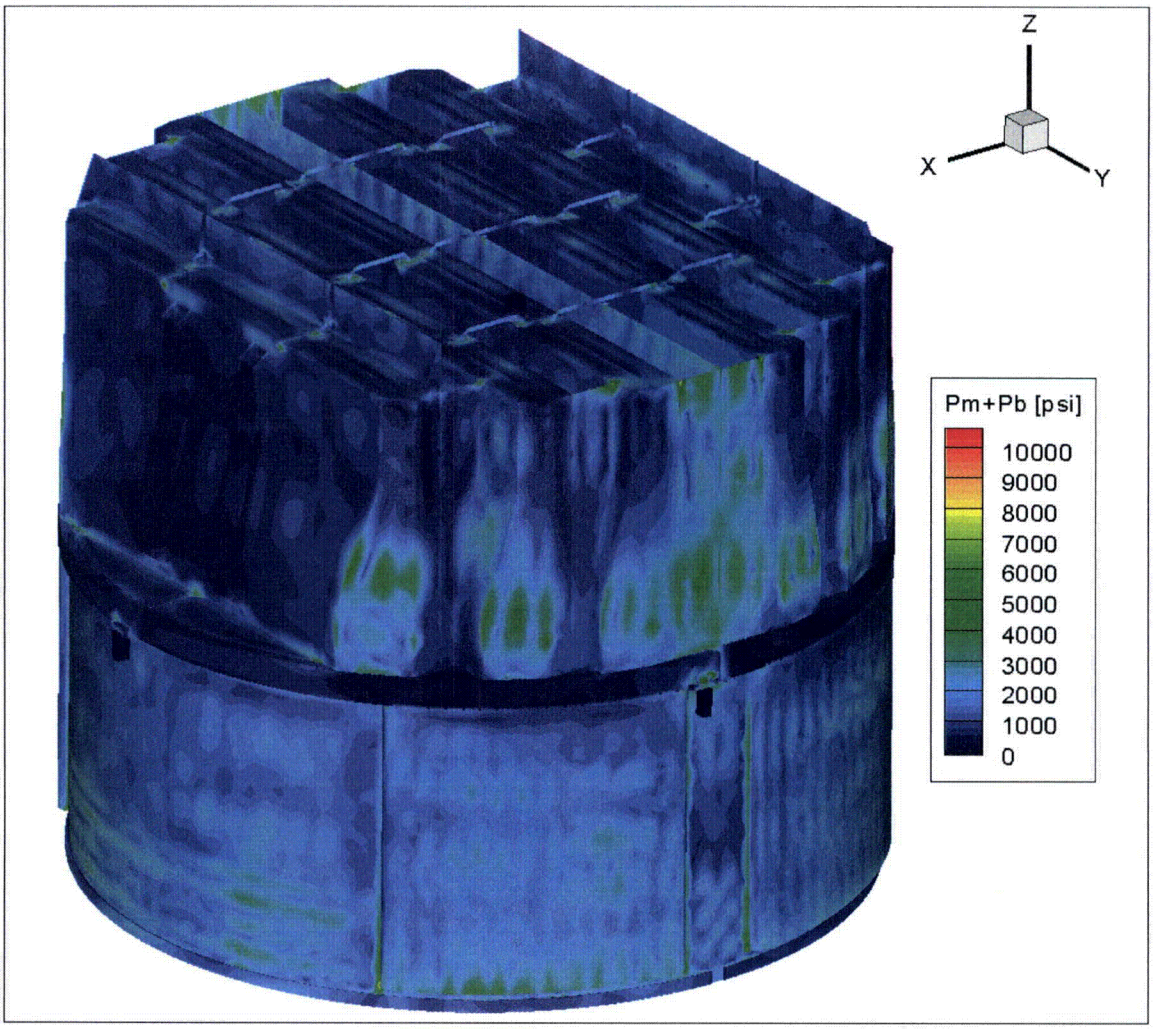

Figure 12b. Contour plot of maximum membrane+bending stress intensity, Pm+Pb, for CLTP operation with frequency shifts. The recorded stress at a node is the maximum value taken over all frequency shifts. The maximum stress intensity is 10,488 psi. First view.

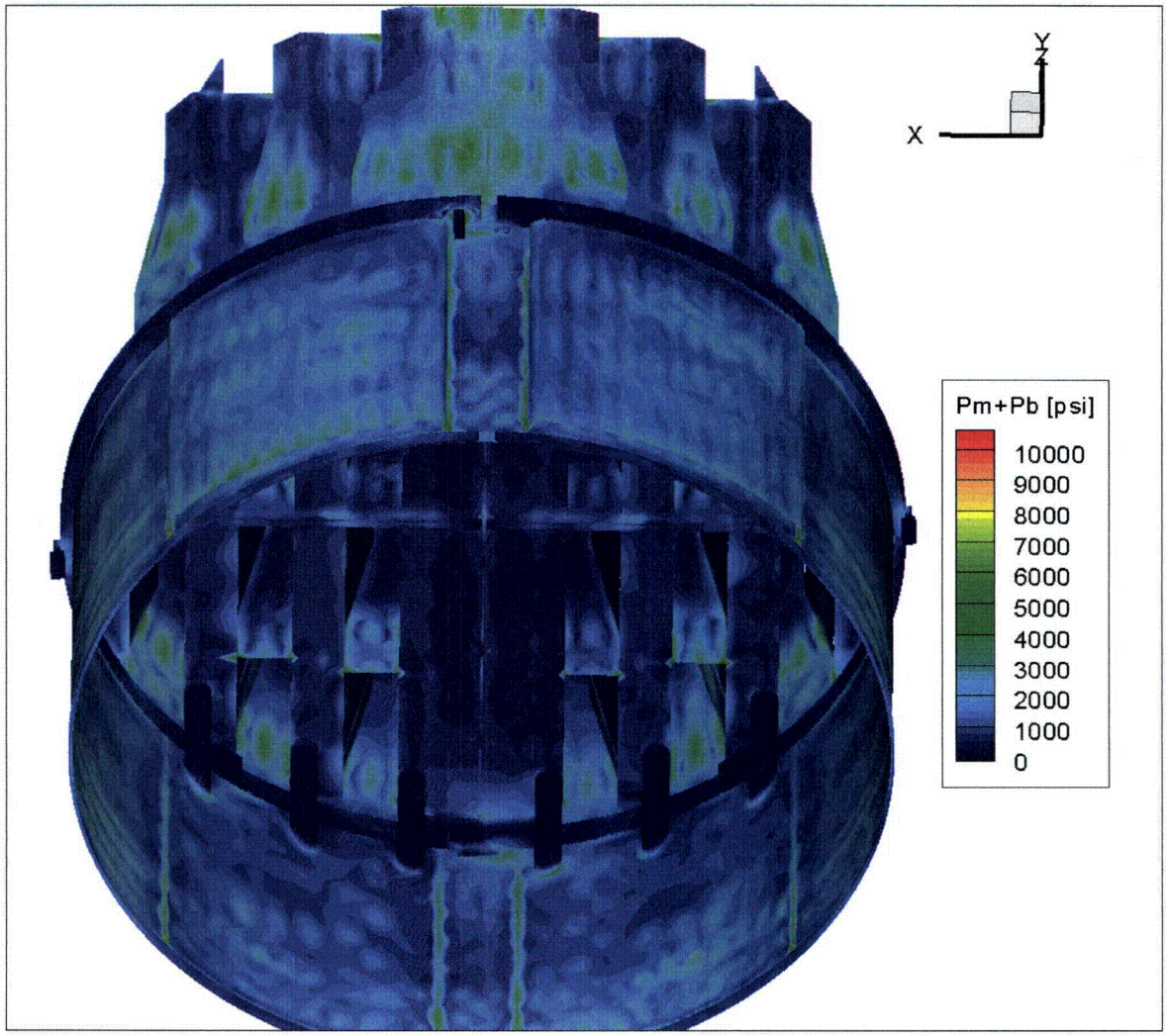

Figure 12c. Contour plot of maximum membrane+bending stress intensity, Pm+Pb, for CLTP operation with frequency shifts. This second view from beneath reveals high stress and modal response of interior hood supports.

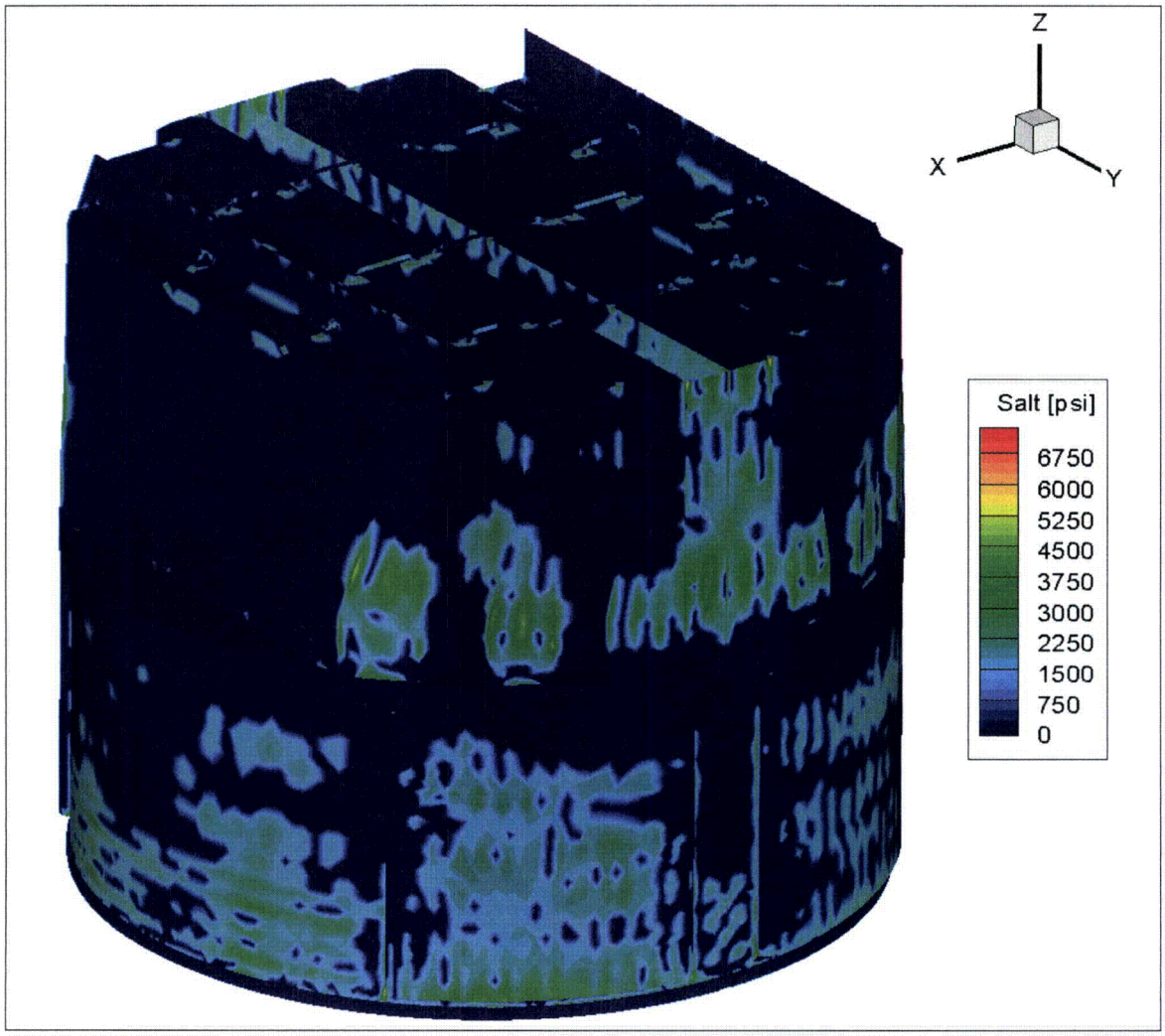

Figure 12d. Contour plot of alternating stress intensity, S_{alt}, for CLTP operation with frequency shifts. The recorded stress at a node is the maximum value taken over all frequency shifts. The maximum alternating stress intensity is 7,143 psi. First view.

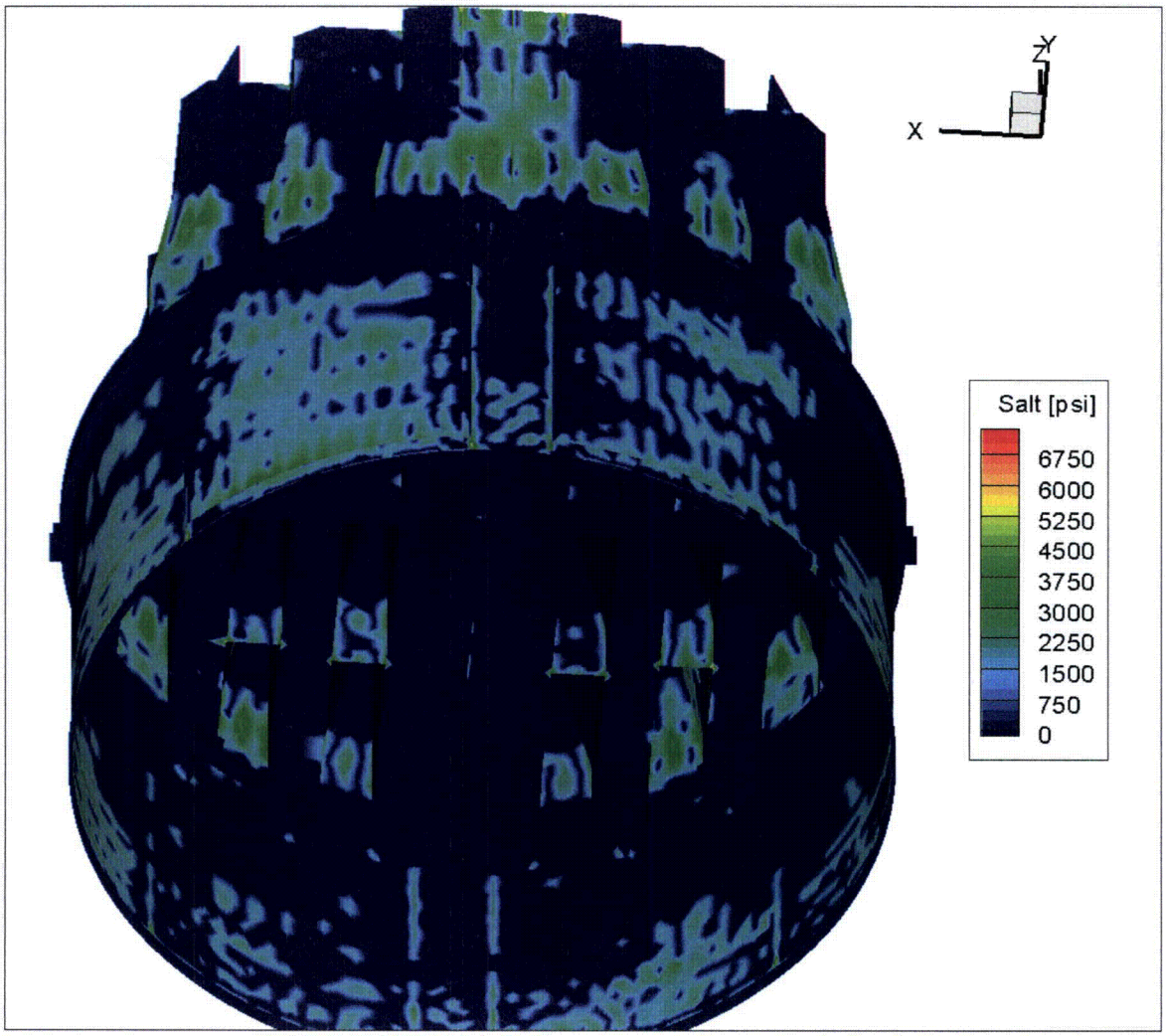

Figure 12e. Contour plot of alternating stress intensity, S_{alt}, for CLTP operation with frequency shifts. This second view from beneath reveals more of the high stress regions on hood supports.

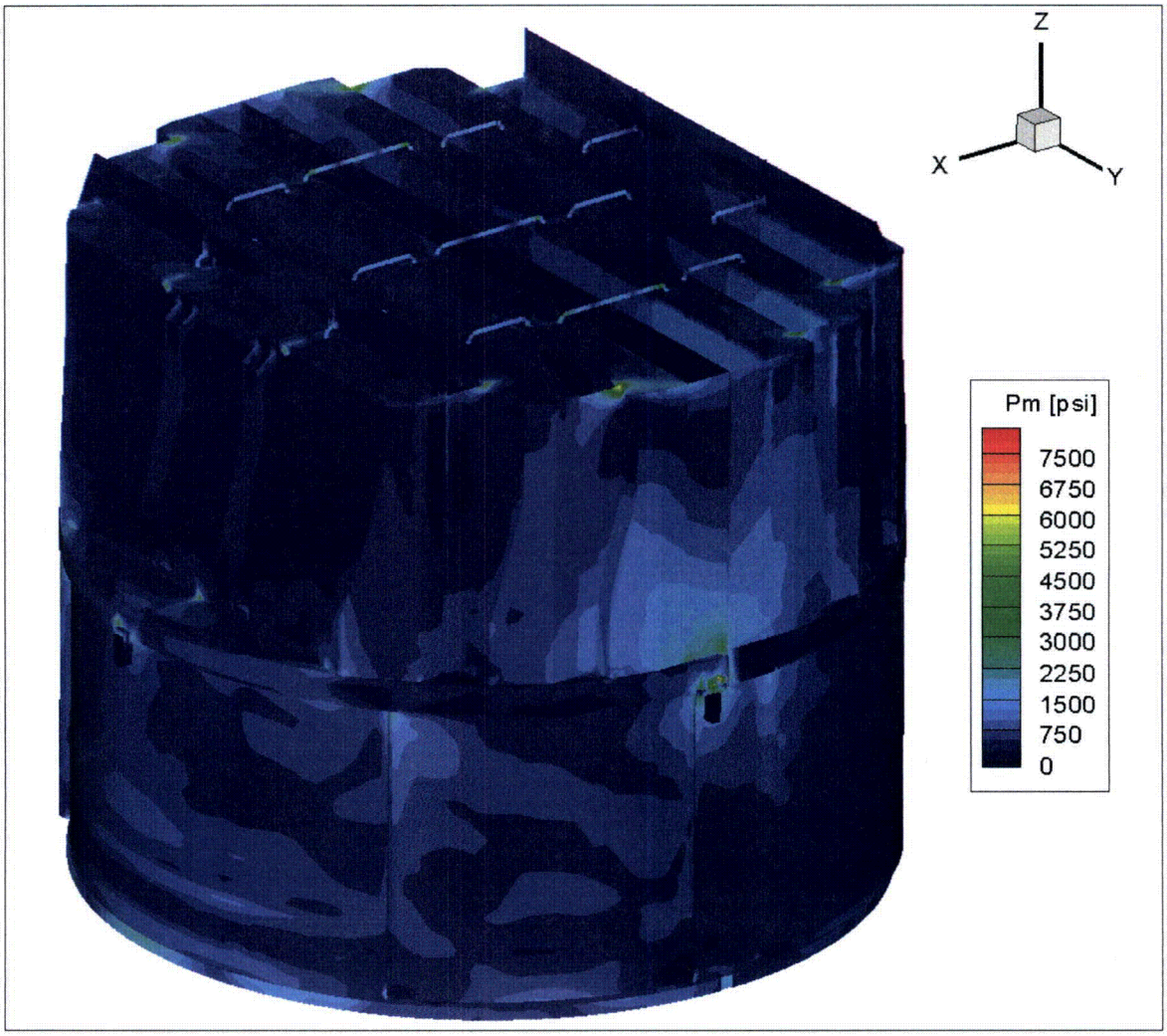

Figure 13a. Contour plot of maximum membrane stress intensity, Pm, for CLTP load with -10% frequency shift. The maximum stress intensity is 7,888 psi.

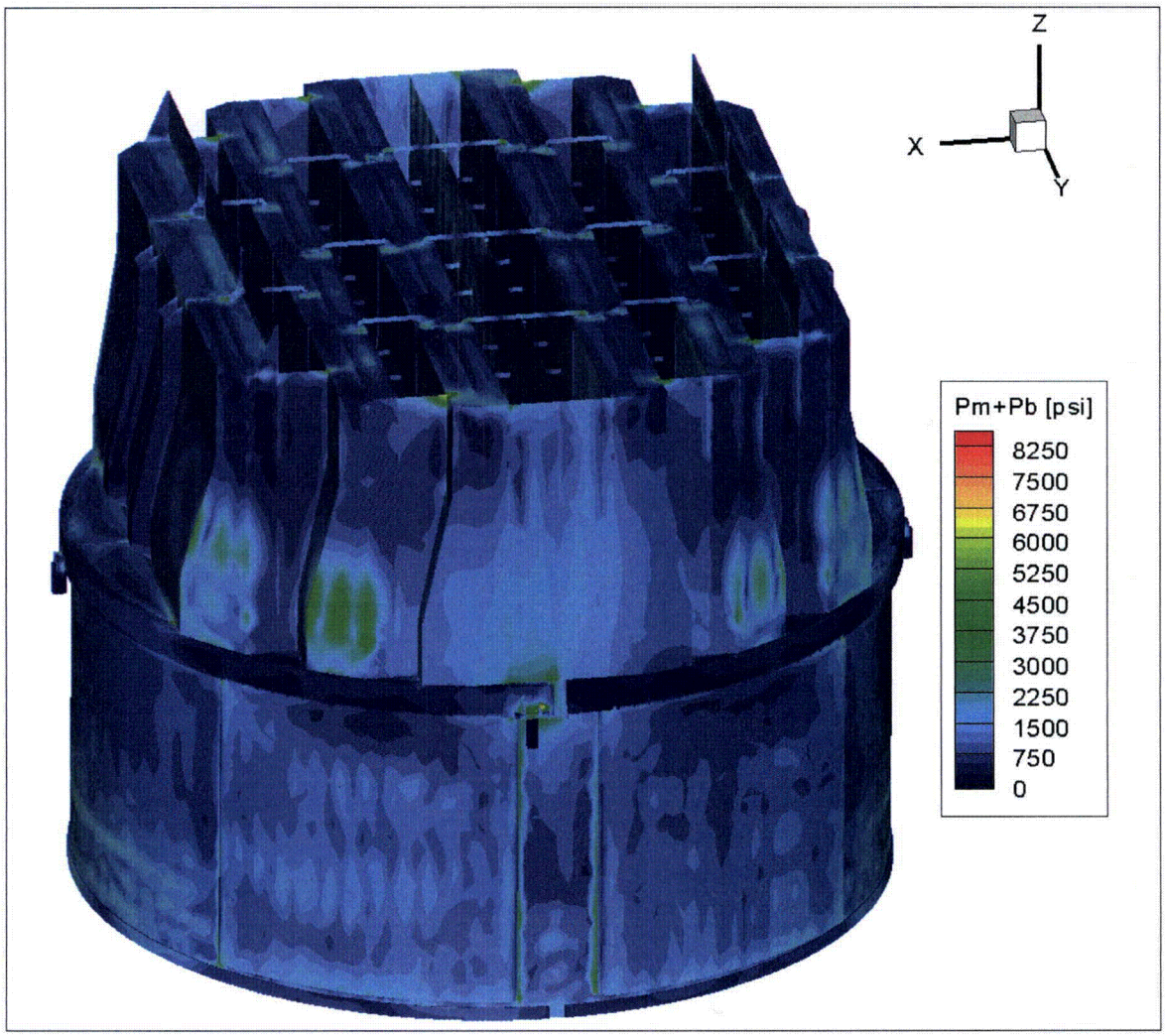

Figure 13b. Contour plot of maximum membrane+bending stress intensity, Pm+Pb, for CLTP load with -10% frequency shift. The maximum stress intensity is 8,368 psi.

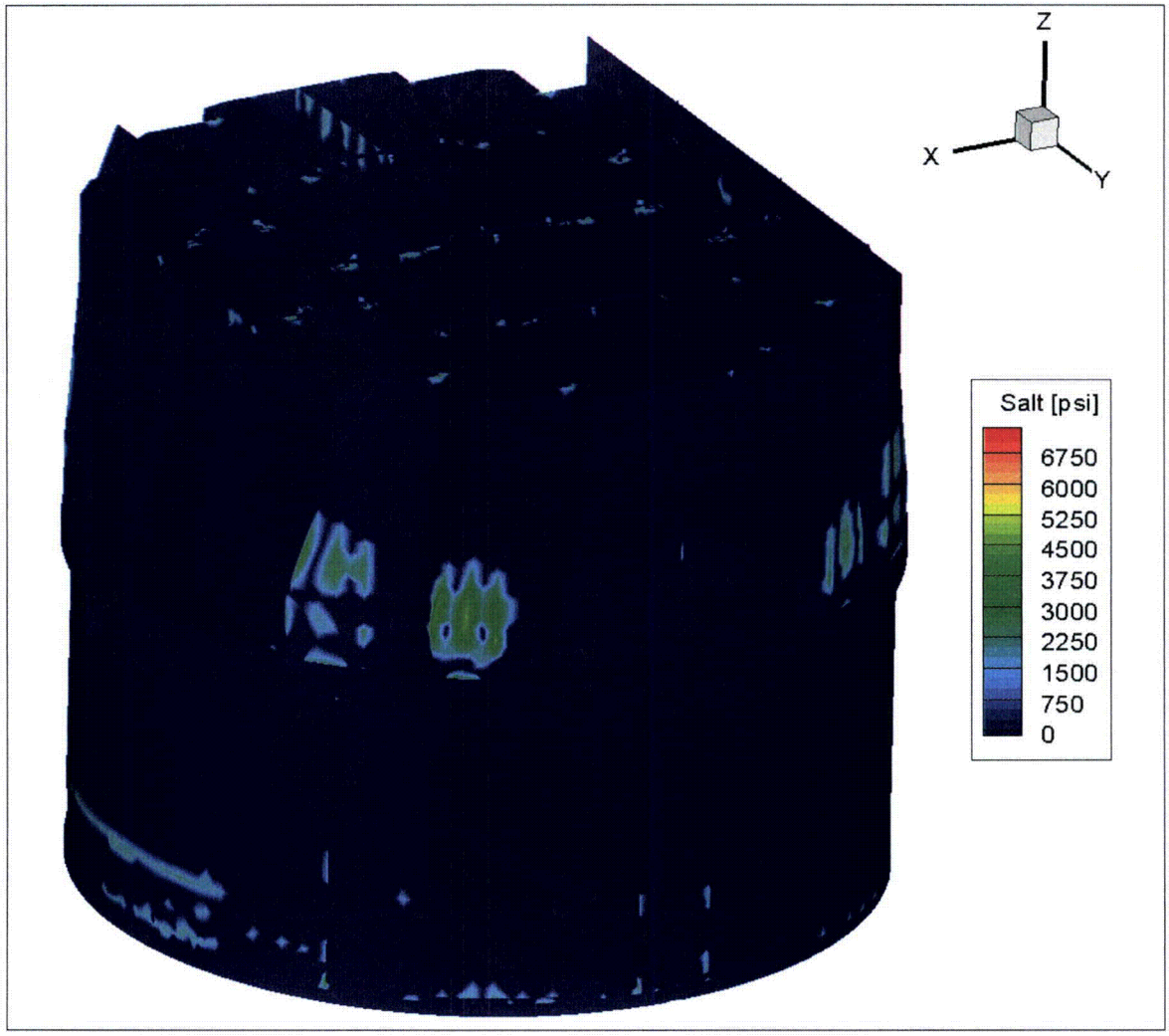

Figure 13c. Contour plot of alternating stress intensity, S_{alt}, for CLTP load with -10% frequency shift. The maximum alternating stress intensity is 7,143 psi. First view.

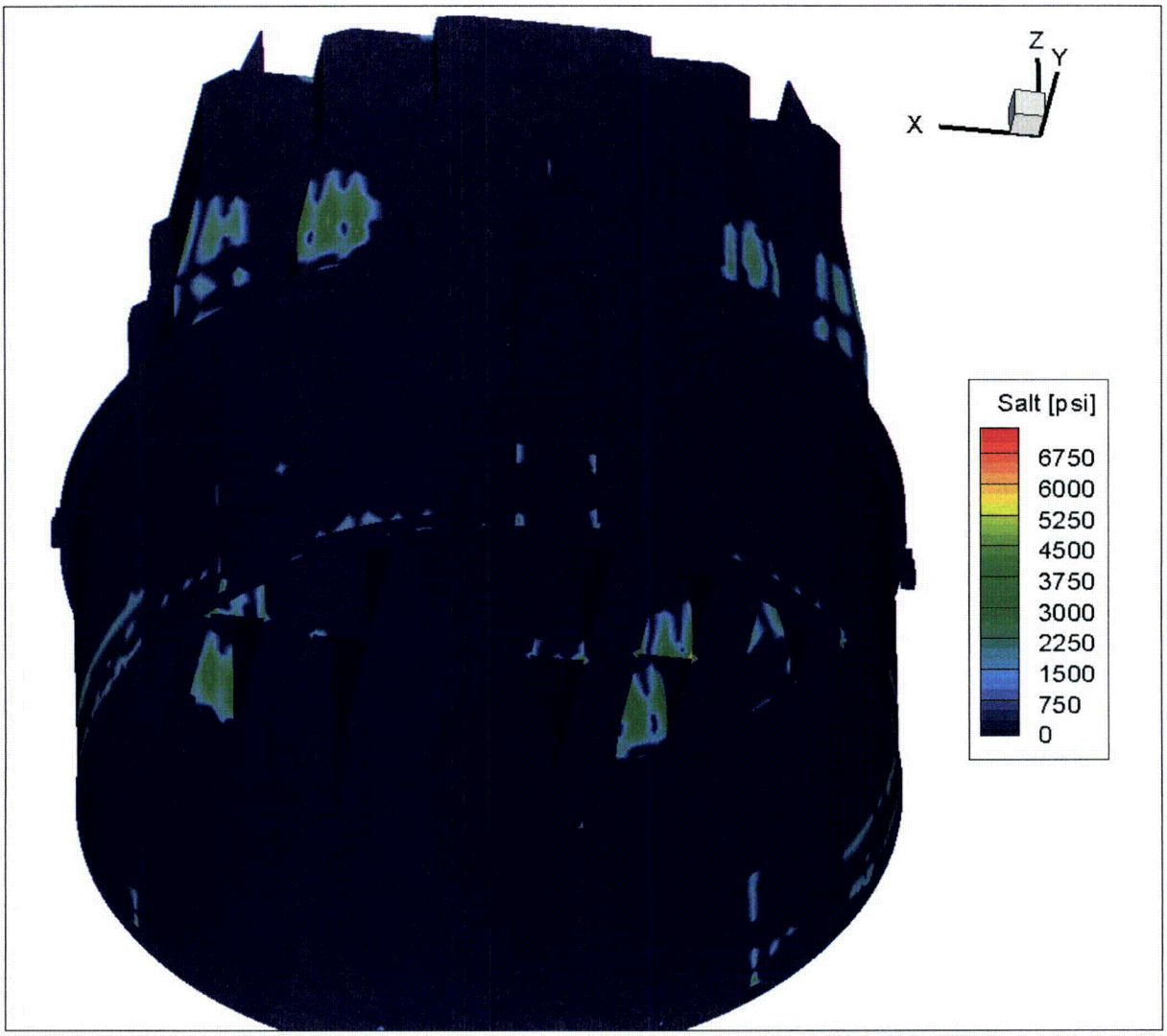

Figure 13d. Contour plot of alternating stress intensity, S_{alt}, for CLTP load with -10% frequency shift. Second view showing high stress locations on hood supports.

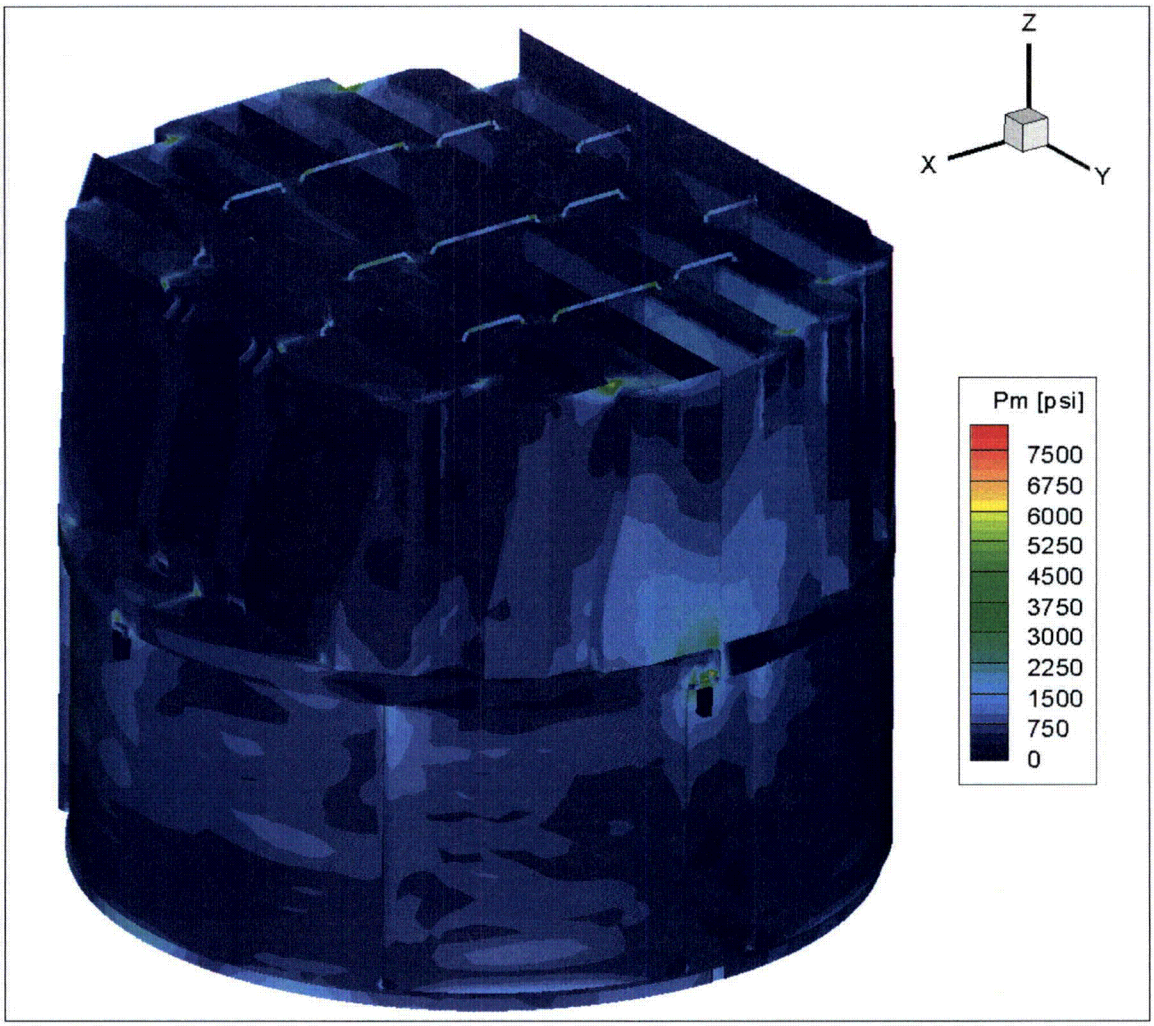

Figure 14a. Contour plot of maximum membrane stress intensity, Pm, for CLTP load with +10% frequency shift. The maximum stress intensity is 7,910 psi.

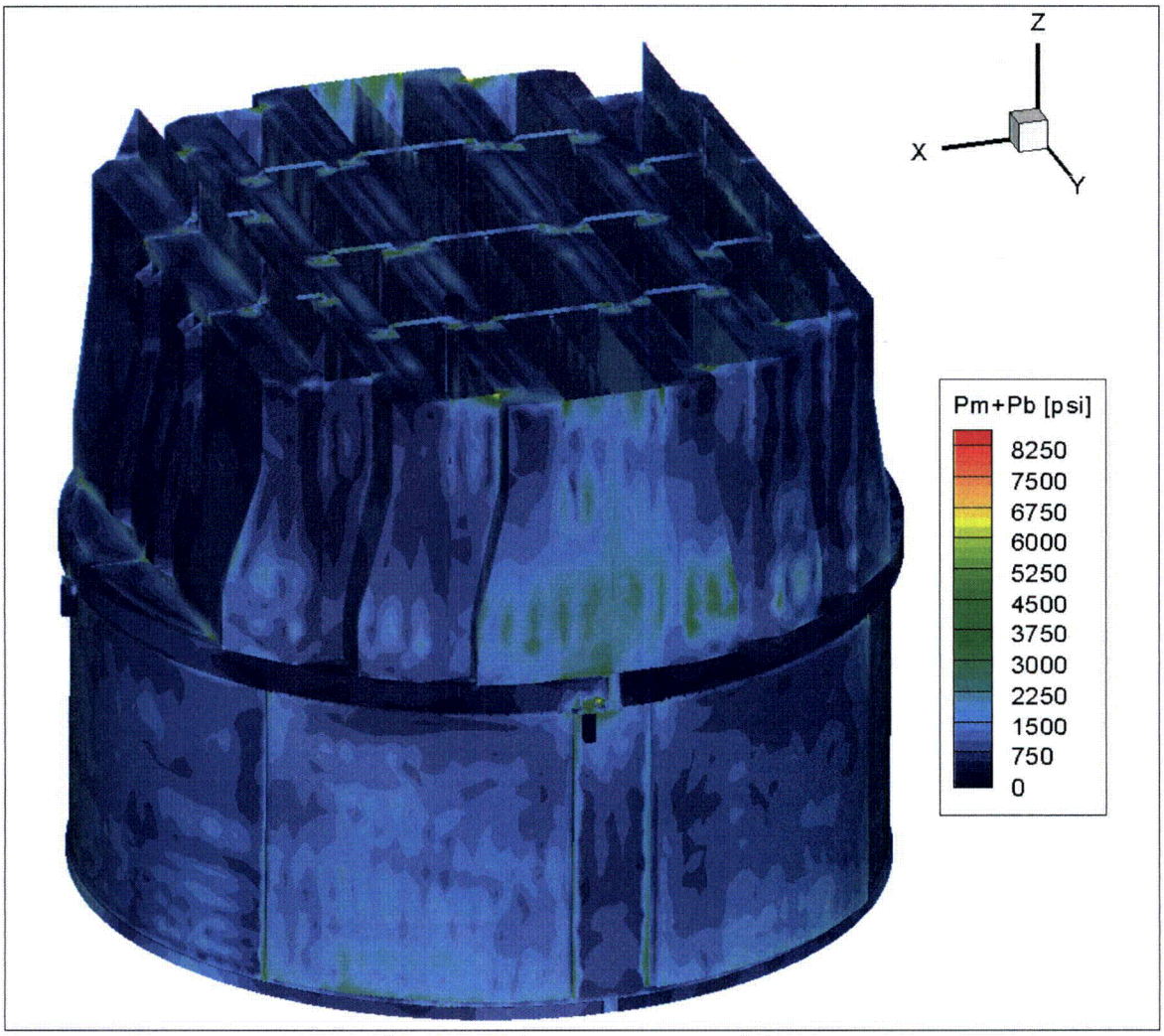

Figure 14b. Contour plot of maximum membrane+bending stress intensity, Pm+Pb, for CLTP load with +10% frequency shift. The maximum stress intensity is 8,444 psi.

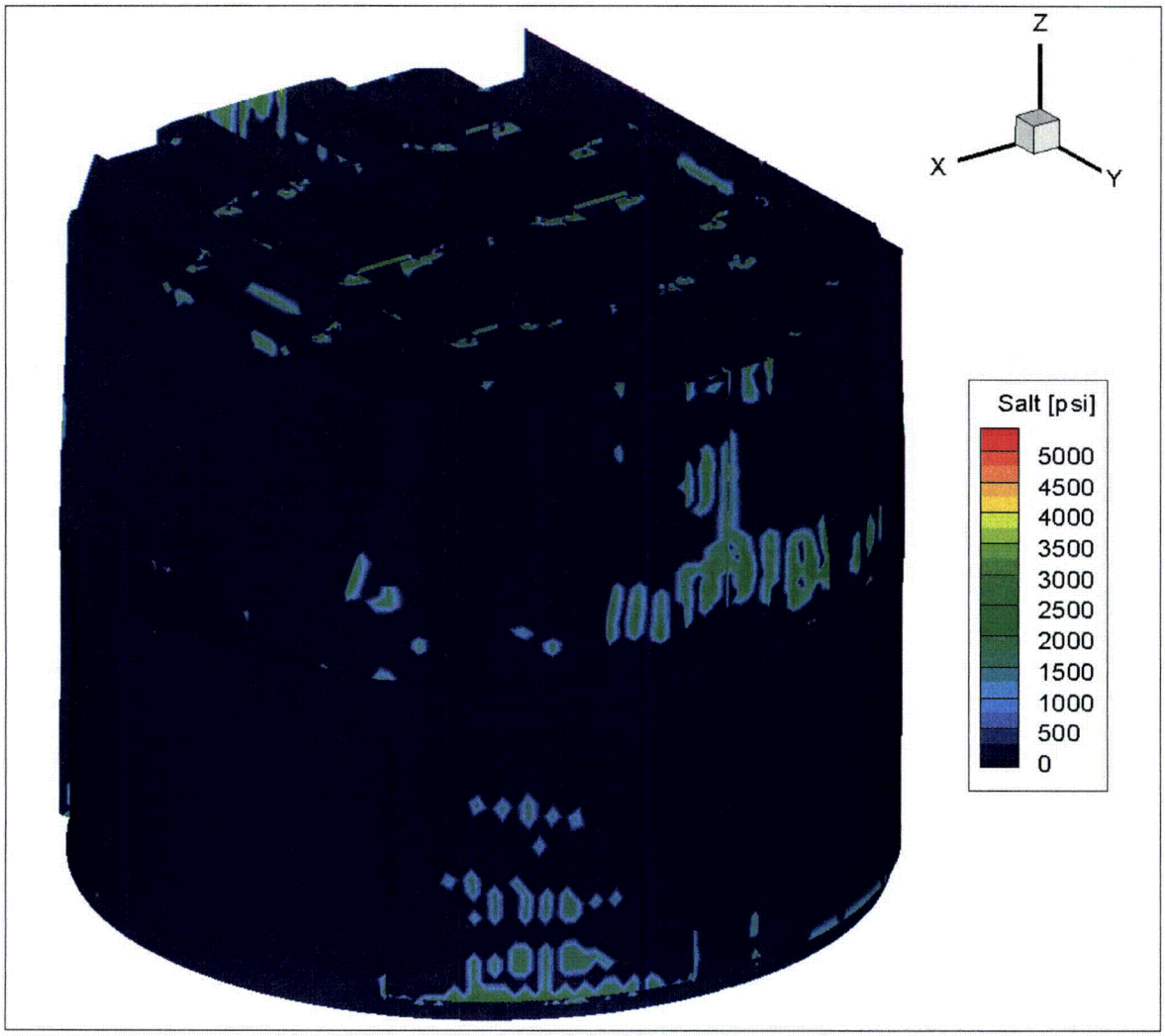

Figure 14c. Contour plot of alternating stress intensity, S_{alt}, for CLTP load with +10% frequency shift. The maximum alternating stress intensity is 5,166 psi.

5.2 Load Combinations and Allowable Stress Intensities

The stress ratios computed for CLTP at nominal frequency and with frequency shifting are listed in Table 8. The stress ratios are grouped according to type (SR-P for maximum membrane and membrane+bending stress, SR-a for alternating stress) and location (away from welds or on a weld).

For CLTP operation at nominal frequency the minimum stress ratio is identified as an alternating stress, SR-a=1.20, and occurs at the junction of middle hood, the hood support and the adjacent base plate. The minimum stress ratio due to maximum stress intensity, SR-P=1.25, occurs at the dryer supports connecting to the upper support ring. The next lowest stress ratios occurs where the drain channels join to the skirt. All of these locations lie on welds as summarized in Table 8a and the accompanying Figure 15.

The effects of frequency shifts can be conservatively accounted for by identifying the minimum stress ratio at every node, where the minimum is taken over all the frequency shifts considered (including the nominal or 0% shift case). The resulting stress ratios are then processed as before to identify the smallest stress ratios anywhere on the structure, categorized by stress type (maximum or alternating) and location (on or away from a weld). The results are summarized in Table 8b and show that the minimum stress ratio, SR-a=0.96, is identified with an alternating stress and occurs where middle hood, hood support, and base plate meet. This is the smallest stress ratio encountered anywhere on the structure for any frequency shift at the CLTP condition. The smallest stress ratio associated with a maximum stress is SR-P=1.25 and occurs on the steam dryer supports.

Because the worst case stress ratios (i.e., the minimum stress ratio over all frequency shifts) are most important for conservative structural assessment, the locations of *all* nodes having maximum stress ratios SR<2.0 are plotted in Figure 16e, and all nodes having alternating stress ratios SR-a<1.5 are plotted in Figure 16h-i. Note that all plotted stress ratios occur on welds since all stress ratios at non-welds are 2.17 or higher. These plots differ from the preceding ones where (see discussion in Section 5.3), the smallest stress ratio in a 10 inch region is identified and all other nodes in this region excluded from display and tabulation. In the current plots, this blanking is not performed so that a more complete picture of where stress ratios are low, is conveyed. These plots show that all stress ratios, SR-P<2.0 occur at: (i) the steam dryer supports; (ii) the closure plate/vane bank junctions; (iii) the drain channel/skirt welds; and (iv) the outer hood/cover plate junctions. All alternating stress ratios, SR-a<1.5 occur at: (i) the joints between the bottoms of the hood supports and adjacent components (vane banks, hoods and base or cover plates); (ii) the skirt/drain channel welds; (iii) the tops of the closure plates where they join to the vane banks and (iv) the vane bank end plates.

In summary, the general picture that emerges is that at CLTP loads the frequency shifts significantly affect the minimum stress ratios and reposition the high stress locations to different parts of the structure. These indicate that the dryer has a rich modal structure so that shifting load frequencies results in the excitation of different modes.

Table 8a. Locations with minimum stress ratios for CLTP conditions with no frequency shift. Stress ratios are grouped according to stress type (maximum – SR-P; or alternating – SR-a) and location (away from a weld or at a weld). Bold text indicates minimum stress ratio of any type on the structure. Locations are depicted in Figure 15.

Stress Ratio	Location	Weld	Location (in.)				Stress Intensity (psi)			Stress Ratio	
			x	y	z	node	Pm	Pm+Pb	S_{alt}	SR-P	SR-a
SR-P	1. middle closure plate	No	-34.4	-108.4	88.9	18211	5402	5506	1779	3.39	6.95
SR-a	1. lock gusset	No	78.3	31.4	91.6	75630	3593	4525	4484	5.09	2.76
	2. submerged drain channel		71.8	99.2	-100.5	20854	1933	3801	3527	7.22	3.51
SR-P	1. upper support ring/support	Yes	-5.8	-122.4	-6.5	7705	8046	8046	0	1.25	>4
"	2. inner hood/top cover plate/middle closure plate	"	-31.5	-108.4	88.9	76022	6292	6677	2376	1.60	2.89
"	3. submerged drain channel/skirt	"	-91.0	76.7	-100.5	77550	2071	8648	4584	1.75	1.50
"	4. outer hood/cover plate	"	-102.0	60.2	0.0	91589	1131	8531	1707	1.77	4.02
"	5. outer hood/hood support	"	-93.5	-28.7	86.9	89700	5299	5443	4117	1.90	1.67
SR-a	**1. middle hood/outer base plate/hood support**	**Yes**	**-70.8**	**-54.6**	**0.0**	**91667**	**4514**	**6337**	**5729**	**2.23**	**1.20**
"	2. submerged drain channel/skirt	"	91.0	-76.7	-100.5	84412	2145	8533	4718	1.77	1.46
"	3. outer hood/hood support remnant	"	-93.5	-28.7	86.9	89700	5299	5443	4117	1.90	1.67
"	4. middle base plate/hood support/vane bank	"	-55.0	-54.6	0.0	86676	1066	3895	3814	3.88	1.80
"	5. outer hood/outer end wall	"	-99.3	70.8	31.9	89063	377	3830	3709	3.94	1.85
"	6. tie bar/middle bank top cover plate	"	48.0	3.0	88.9	92355	753	4320	3601	3.49	1.91
"	7. tie bar/middle bank top cover plate	"	60.5	31.4	88.9	79136	505	4058	3600	3.72	1.91

See Table 7a for coordinates description.

Table 8b. Locations with minimum stress ratios for CLTP conditions with frequency shifts. Stress ratios at every node are recorded as the lowest stress ratio identified during the frequency shifts. Stress ratios are grouped according to stress type (maximum – SR-P; or alternating – SR-a) and location (away from a weld or at a weld). Bold text indicates minimum stress ratio of any type on the structure. Locations are depicted in Figure 16.

Stress Ratio	Location	Weld	% Freq. Shift	Location (in.)				Stress Intensity (psi)			Stress Ratio	
				x	y	z	node	Pm	Pm+Pb	S_{alt}	SR-P	SR-a
SR-P	1. middle closure plate	No	0	-34.4	-108.4	88.9	18211	5402	5506	1779	3.39	6.95
SR-a	1. lock gusset	No	-5	78.3	31.4	91.6	75630	3711	6160	5695	4.46	2.17
"	2. middle end wall	"	-10	62.5	103.7	19.2	58609	569	4664	4594	5.89	2.69
SR-P	1. upper support ring/support	Yes	+5	5.8	122.4	-6.5	7532	8047	8047	0	1.25	>4
"	2. submerged drain channel/skirt	"	-5	91.0	76.7	-100.5	85938	2832	10488	6518	1.44	1.05
"	3. inner hood/top cover plate/middle closure plate	"	0	-31.5	-108.4	88.9	76022	6292	7431	3151	1.60	2.18
"	4. top perforated plate/inner closure plate/top cover plate	"	+7.5	15.0	118.9	88.9	89175	2064	8937	6694	1.69	1.03
"	5. outer hood/cover plate	"	+7.5	-102.0	60.2	0.0	91589	1191	8868	2084	1.70	3.30
SR-a	**1. middle hood/outer base plate/hood support**	**Yes**	**-10**	**70.8**	**54.6**	**0.0**	**87364**	**4385**	**7643**	**7143**	**1.98**	**0.96**
"	2. inner hood/middle base plate/hood support	"	+7.5	39.8	59.8	0.0	91846	3700	7851	7027	1.92	0.98
"	3. top perforated plate/inner closure plate/inner side panel	"	+7.5	15.0	118.9	88.9	89175	2064	8937	6694	1.69	1.03
"	4. submerged drain channel/skirt	"	-5	-91.0	-76.7	-100.5	86016	2809	10059	6628	1.50	1.04
"	5. middle base plate/hood support/vane bank	"	-10	55.0	54.6	0.0	93714	1007	6410	6321	2.36	1.09

See Table 7a for coordinates description.

Table 8b (continued). Locations with minimum stress ratios for CLTP conditions with frequency shifts. Stress ratios at every node are recorded as the lowest stress ratio identified during the frequency shifts. Stress ratios are grouped according to stress type (maximum – SR-P; or alternating – SR-a) and location (away from a weld or at a weld).

Stress Ratio	Location	Weld	% Freq. Shift	Location (in.)				Stress Intensity (psi)			Stress Ratio	
				x	y	z	node	Pm	Pm+Pb	S_{alt}	SR-P	SR-a
SR-a	6. submerged drain channel/skirt	Yes	-7.5	11.5	118.4	-100.5	84494	2581	7039	6071	2.14	1.13
"	7. inner base plate/hood support/vane bank	"	+8.5	24.0	59.8	0.0	87231	1239	6223	6034	2.43	1.14
"	8. outer hood/outer end wall	"	-5	-99.3	70.8	31.9	89063	408	5841	5795	2.58	1.19
"	9. middle side panel/vane bank	"	-10	55.0	108.4	12.1	88569	774	5029	4869	3.00	1.41
"	10. inner closure plate weld strip/mid plate	"	+7.5	0.0	118.9	88.9	76522	661	5109	4867	2.95	1.41
"	11. vane bank/inner end wall/inner side plate	"	+7.5	-24.0	118.9	12.1	88270	893	5024	4717	3.00	1.46
"	12. outer hood/hood support remnant	"	-2.5	-93.5	-28.7	86.9	89700	5495	5808	4544	1.83	1.51

See Table 7a for coordinates description.

Table 8c. Locations with minimum stress ratios at CLTP conditions with -10% frequency shift. Stress ratios are grouped according to stress type (maximum – SR-P; or alternating – SR-a) and location (away from a weld or at a weld). Bold text indicates minimum stress ratio of any type on the structure. Locations are depicted in Figure 17. Stress ratios at non-weld locations are greater than 4.0.

Stress Ratio	Location	Weld	Location (in.)				Stress Intensity (psi)			Stress Ratio	
			x	y	z	node	Pm	Pm+Pb	S_{alt}	SR-P	SR-a
SR-P	1. middle closure plate	No	34.4	108.4	88.9	17687	5300	5373	1669	3.45	7.41
SR-a	1. middle end wall	No	62.5	103.7	19.2	58609	519	4664	4594	5.89	2.69
	2. hood support	"	62.9	54.6	0.0	19386	726	4216	4122	6.51	3.00
SR-P	1. upper support ring/support	Yes	5.8	122.4	-6.5	7532	7888	7888	0	1.28	>4
"	2. inner hood/top cover plate/middle closure plate	"	31.5	108.4	88.9	87571	6183	6399	2010	1.63	3.42
"	3. submerged drain channel/skirt	"	-91.0	-76.7	-100.5	86016	2180	8368	4747	1.80	1.45
"	4. outer hood/cover plate	"	-102.0	60.2	0.0	91589	1061	8241	0	1.83	>4
"	5. middle hood/outer base plate/hood support	"	-70.8	54.6	0.0	87549	3930	7801	6699	1.94	1.03
SR-a	**1. middle hood/outer base plate/hood support**	**Yes**	**70.8**	**54.6**	**0.0**	**87364**	**3654**	**7643**	**7143**	**1.98**	**0.96**
"	2. middle base plate/hood support/vane bank	"	55.0	54.6	0.0	93714	671	6410	6321	2.36	1.09
"	3. middle side panel/vane bank	"	55.0	108.4	12.1	88569	774	5029	4869	3.00	1.41
"	4. submerged drain channel/skirt	"	-91.0	-76.7	-100.5	86016	2180	8368	4747	1.80	1.45
"	5. middle hood/middle end wall	"	70.4	98.8	20.4	91492	714	4444	4224	3.40	1.63
"	6. hood support/vane bank	"	55.0	54.6	12.1	78102	349	4199	4165	3.60	1.65
"	7. inner hood/middle base plate/hood support	"	39.8	59.8	0.0	91846	3645	4969	4126	2.76	1.66
"	8. submerged drain channel/skirt	"	11.5	-118.4	-100.5	91879	1665	6312	3917	2.39	1.75

See Table 7a for coordinates description.

Table 8d. Locations with minimum stress ratios for at CLTP conditions with +10% frequency shift. Stress ratios are grouped according to stress type (maximum – SR-P; or alternating – SR-a) and location (away from a weld or at a weld). Bold text indicates minimum stress ratio of any type on the structure. Locations are depicted in Figure 18.

Stress Ratio	Location	Weld	Location (in.)				Stress Intensity (psi)			Stress Ratio	
			x	y	z	node	Pm	Pm+Pb	S_{alt}	SR-P	SR-a
SR-P	1. middle closure plate	No	34.4	108.4	88.9	17687	5116	5256	0	3.58	>4
SR-a	1. lock gusset	No	-78.3	-31.4	91.6	75607	3438	5201	5166	5.28	2.39
"	2. tie-bar	"	-9.0	-39.9	62.9	12952	3451	3451	3439	5.30	3.60
SR-P	1. upper support ring/support	Yes	5.8	122.4	-6.5	7532	7910	7910	0	1.27	>4
"	2. inner hood/top cover plate/middle closure plate	"	31.5	108.4	88.9	87571	5956	6876	2575	1.69	2.67
"	3. outer hood/cover plate	"	-102.0	60.2	0.0	91589	1157	8444	1750	1.79	3.93
SR-a	**1. inner side panel/top cover plate/inner closure plate**		**-15.0**	**-118.9**	**88.9**	**77828**	**1986**	**6723**	**4396**	**2.25**	**1.56**
"	2. tie bar/top cover plate	"	48.0	3.0	88.9	92355	1087	4561	3755	3.31	1.83
"	3. tie bar/middle bank top cover plate	"	60.5	31.4	88.9	79136	531	4246	3739	3.56	1.84
"	4. outer hood/cover plate	"	102.0	-60.8	0.0	90532	3778	6614	3639	2.28	1.89
"	5. vane bank/inner end wall/inner side panel		-24.0	118.9	12.1	88270	884	3806	3441	3.97	2.00

See Table 7a for coordinates description.

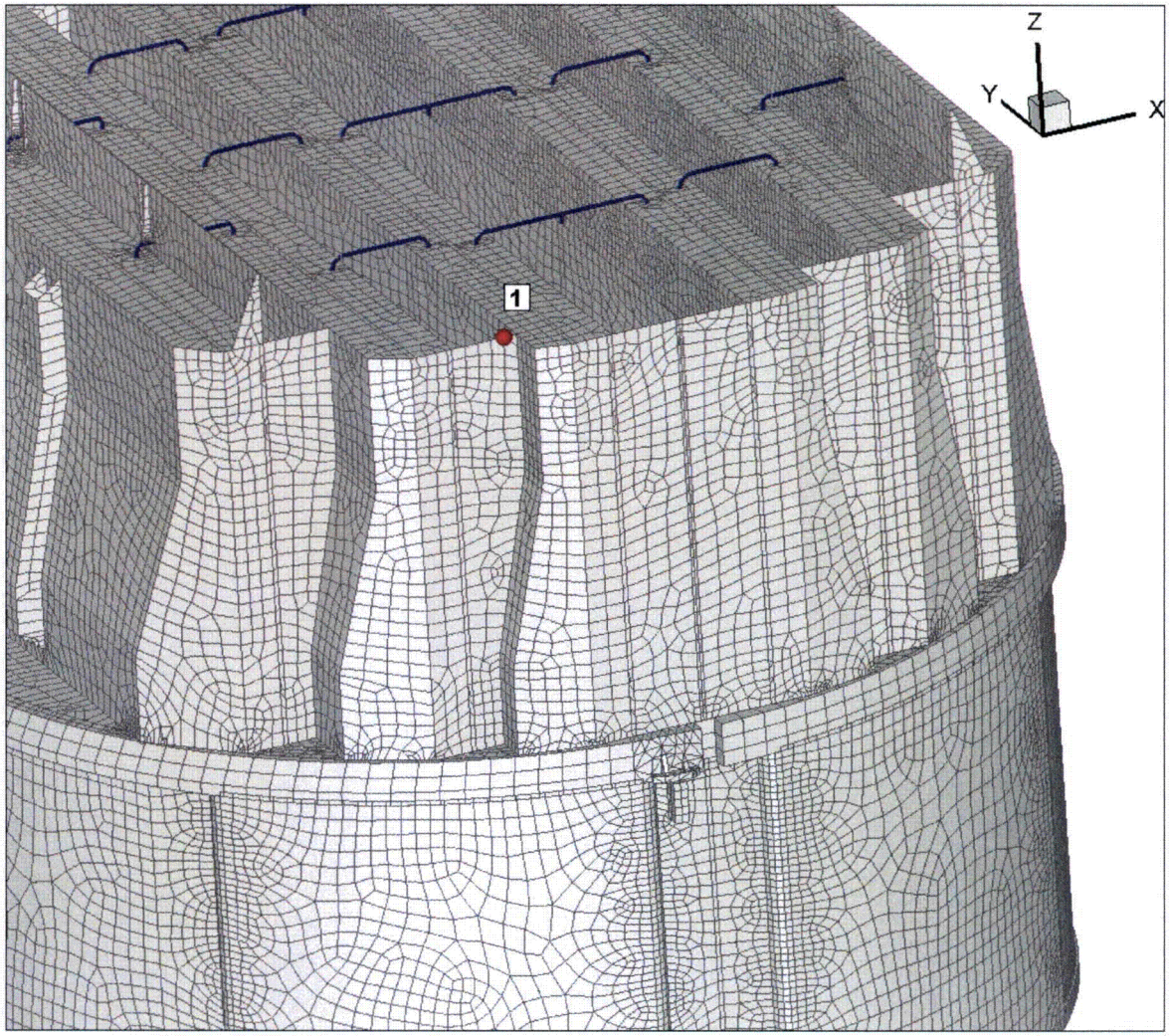

Figure 15a. Location of smallest maximum stress ratio, SR-P, at non-welds for nominal CLTP operation. Number refers to the enumerated locations for SR-P values at non-welds in Table 8a.

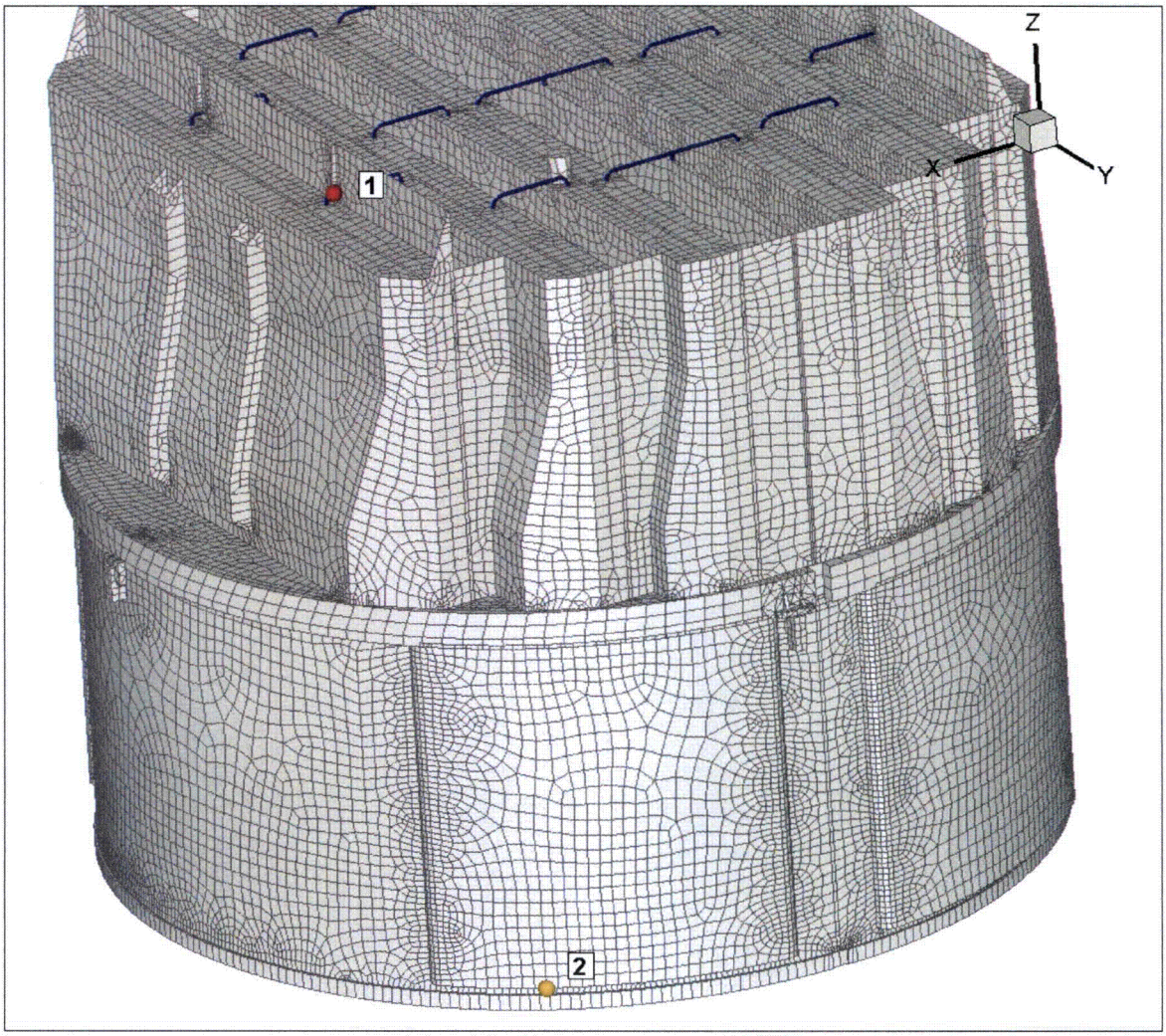

Figure 15b. Location of minimum alternating stress ratio, SR-a, at non-welds for nominal CLTP operation. Number refers to the enumerated locations for SR-a values at non-welds in Table 8a.

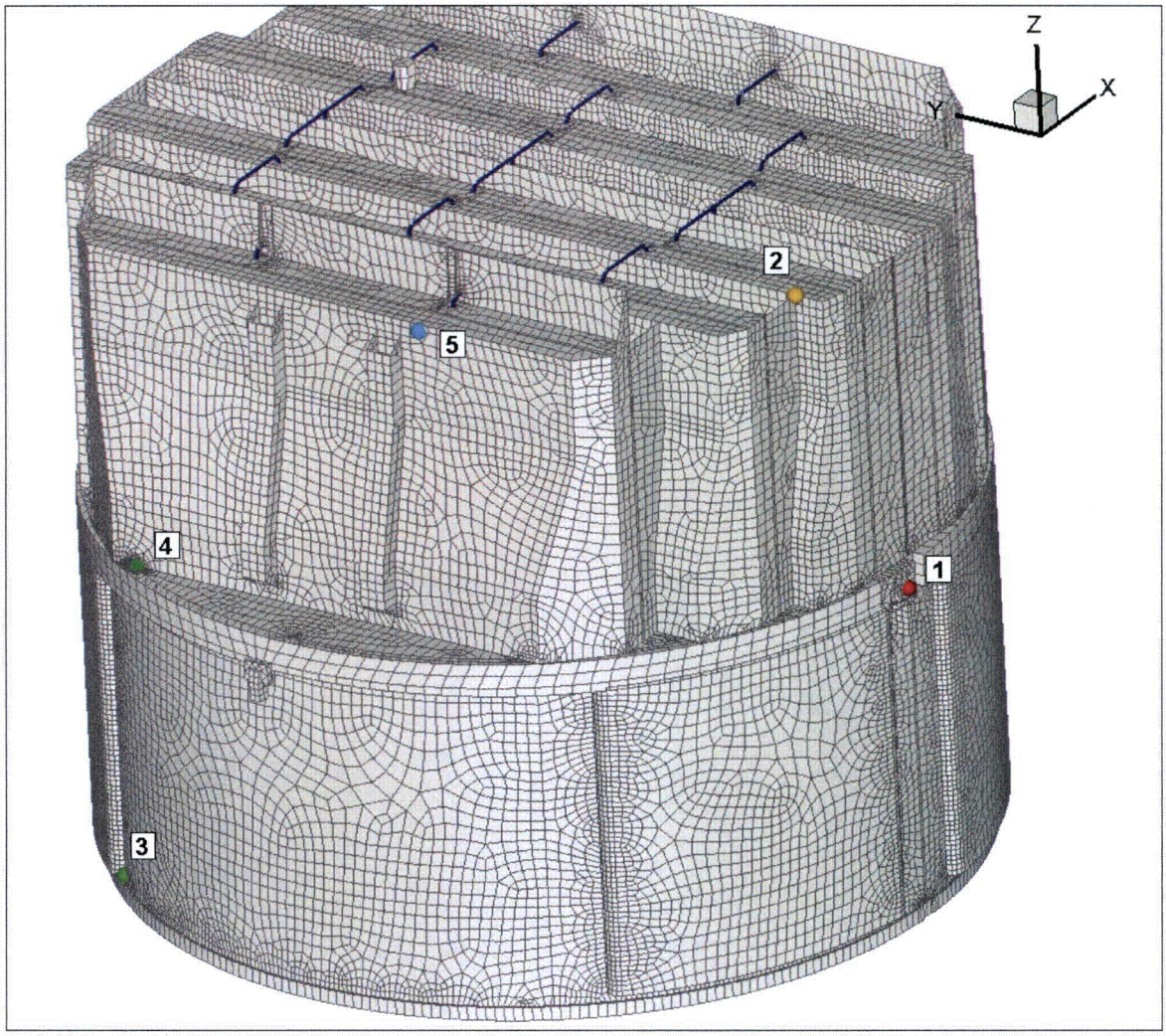

Figure 15c. Locations of smallest maximum stress ratios, SR-P, at welds for nominal CLTP operation. Numbers refer to the enumerated locations for SR-P values at welds in Table 8a.

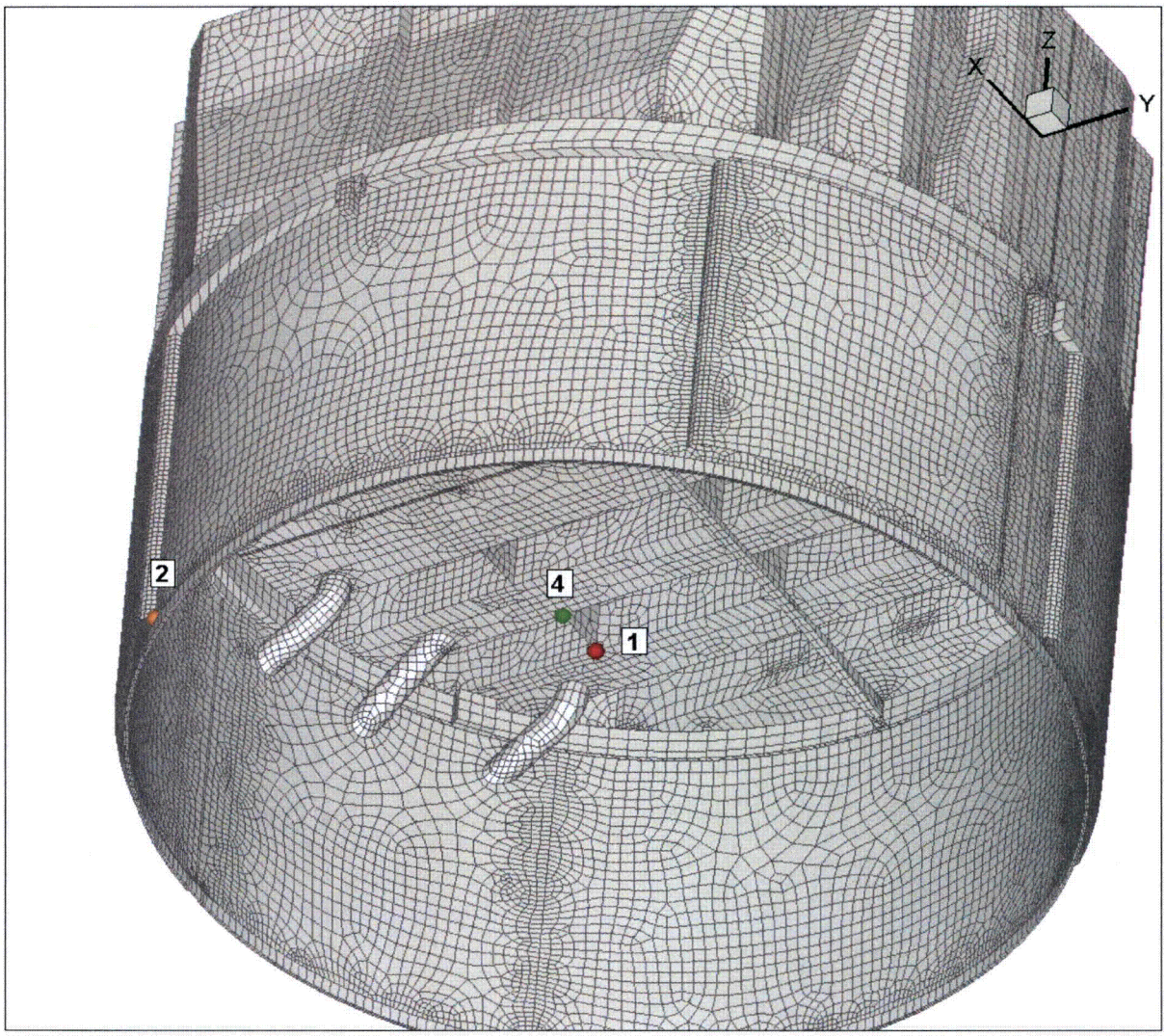

Figure 15d. Locations of minimum alternating stress ratios, SR-a, at welds for nominal CLTP operation. Numbers refer to the enumerated locations for SR-a values at welds in Table 8a. Locations 1, 2 and 4 are shown.

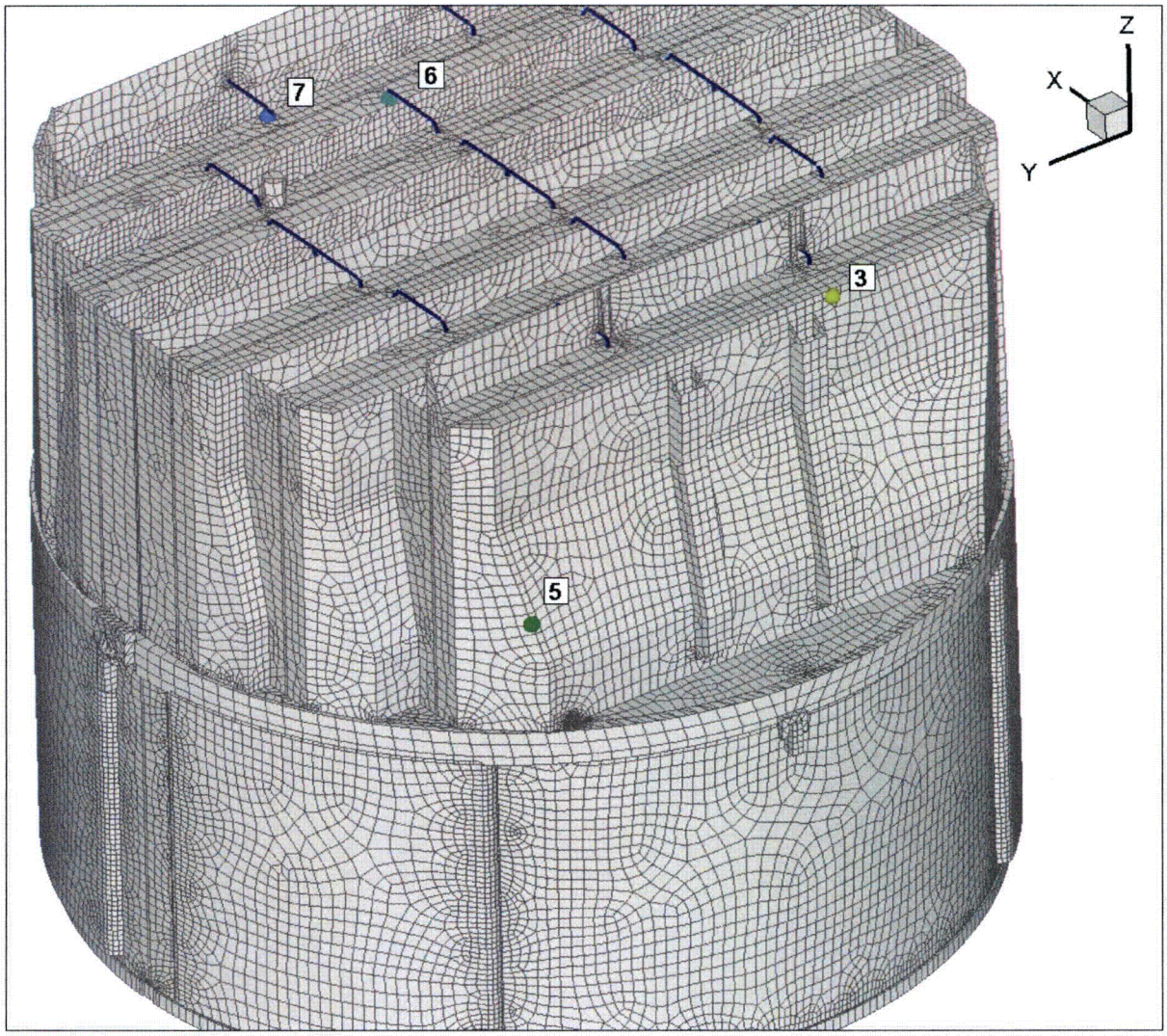

Figure 15e. Locations of minimum alternating stress ratios, SR-a, at welds for nominal CLTP operation. Numbers refer to the enumerated locations for SR-a values at welds in Table 8a. Locations 3 and 5-7 are shown.

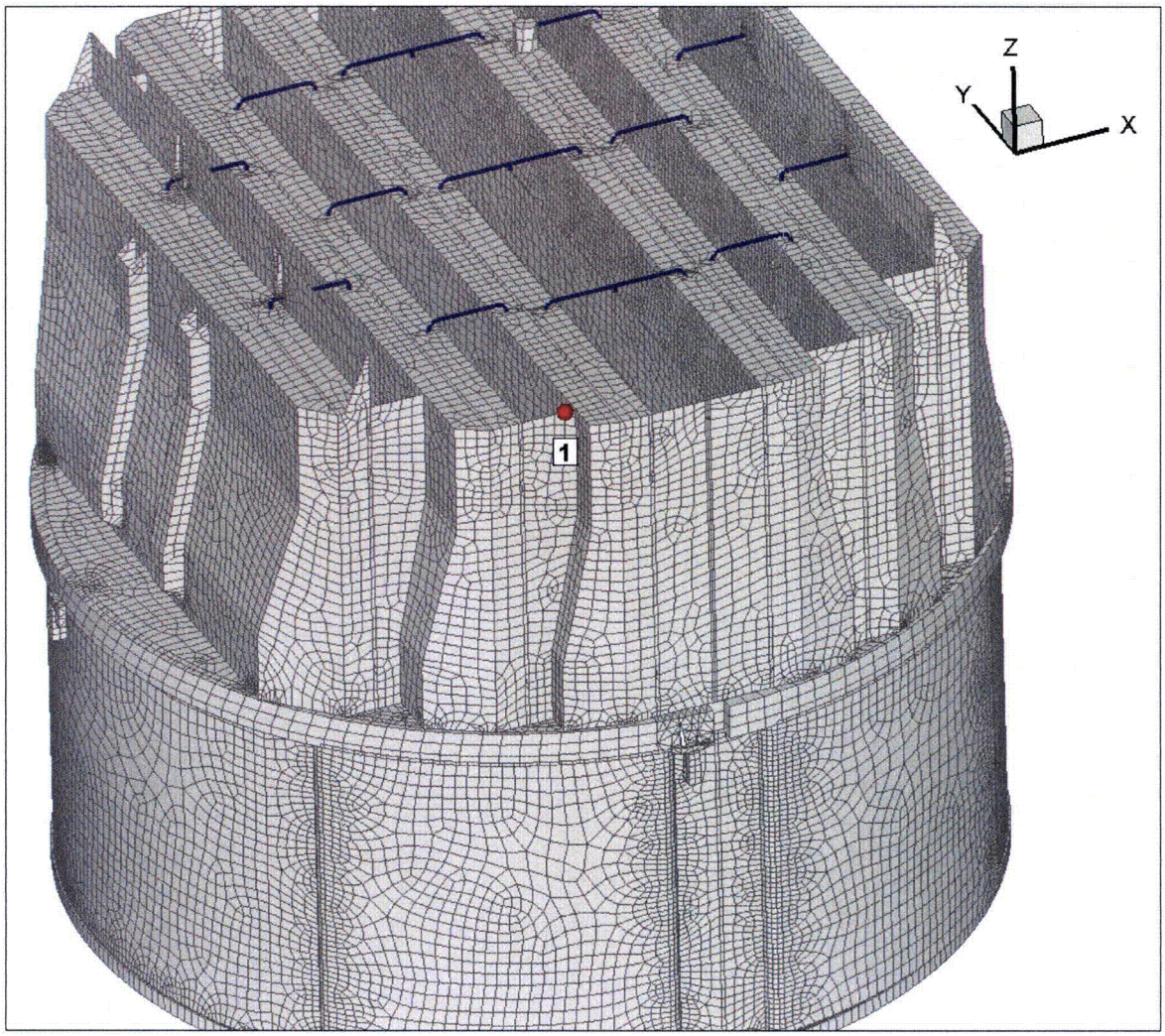

Figure 16a. Location of minimum stress ratio, SR-P, associated with maximum stress intensities at non-welds for CLTP operation with frequency shifts. The recorded stress ratio is the minimum value taken over all frequency shifts. The number refers to the enumerated location for SR-P values at non-welds in Table 8b.

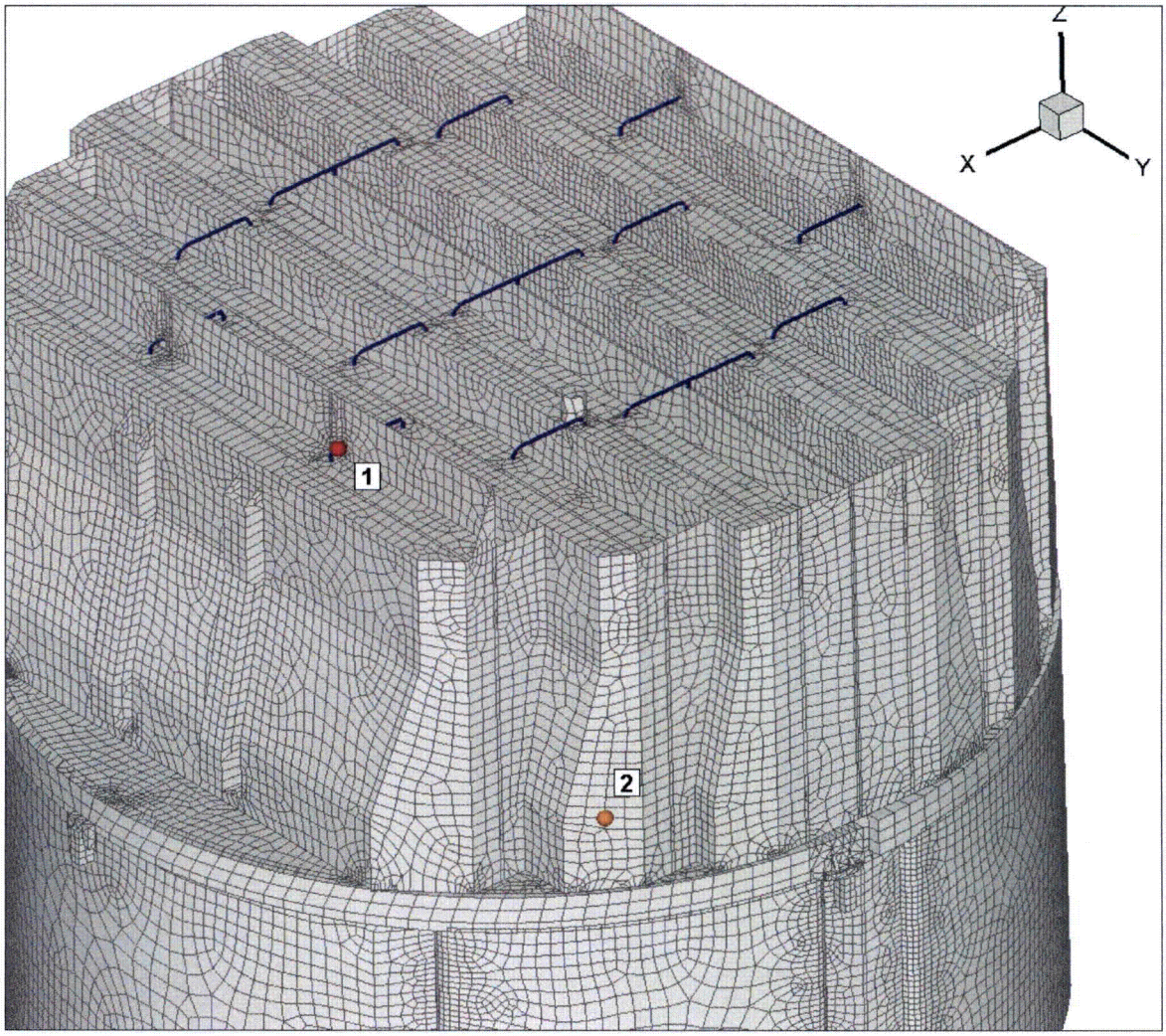

Figure 16b. Locations of minimum alternating stress ratios, SR-a, at non-welds for CLTP operation with frequency shifts. The recorded stress ratio at a node is the minimum value taken over all frequency shifts. Numbers refer to the enumerated locations for SR-a values at non-welds in Table 8b.

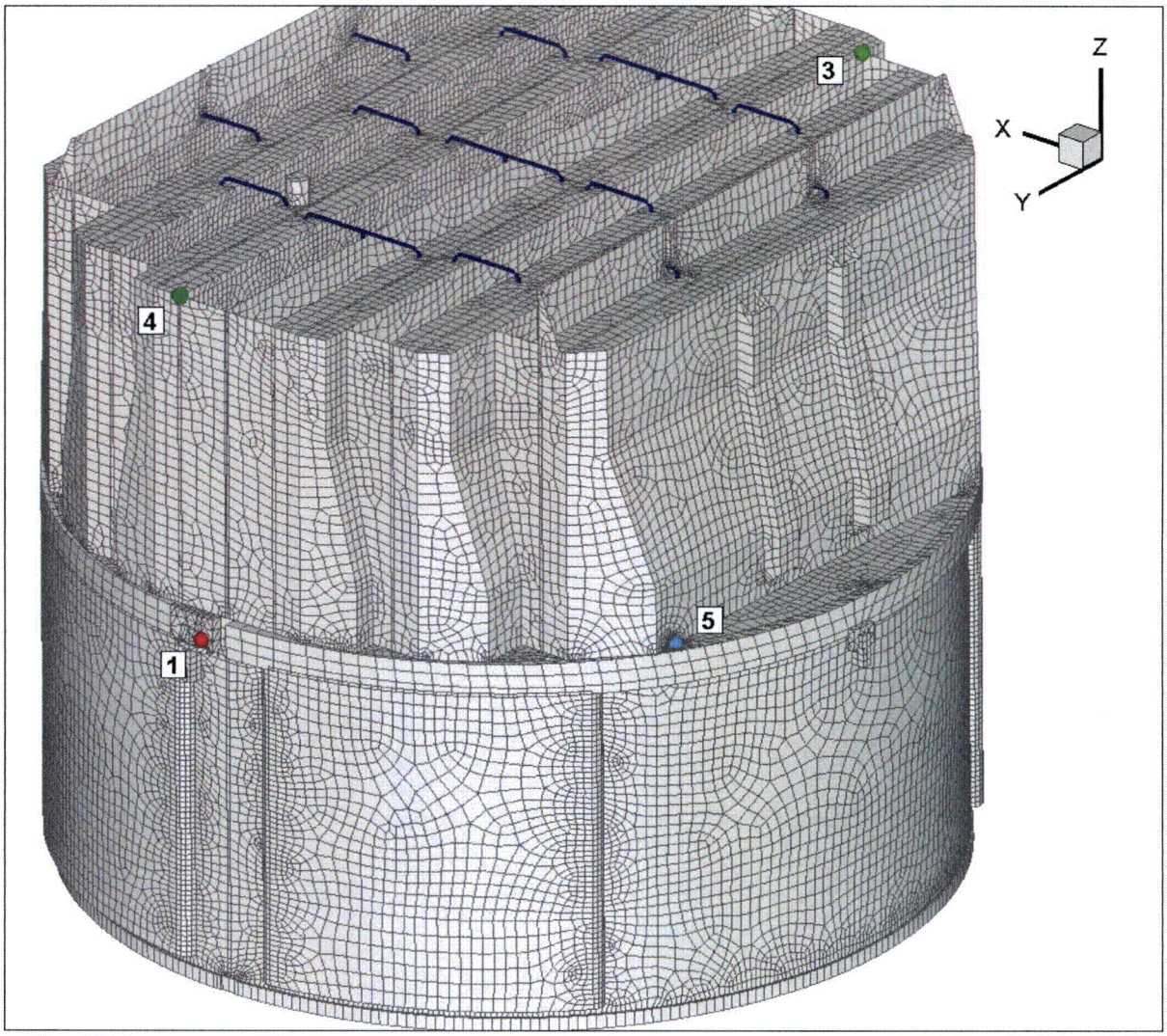

Figure 16c. Locations of minimum stress ratios, SR-P, associated with maximum stress intensities at welds for CLTP operation with frequency shifts. The recorded stress ratio at a node is the minimum value taken over all frequency shifts. Numbers refer to the enumerated locations for SR-P values at welds in Table 8b. This view shows locations 1 and 3-5.

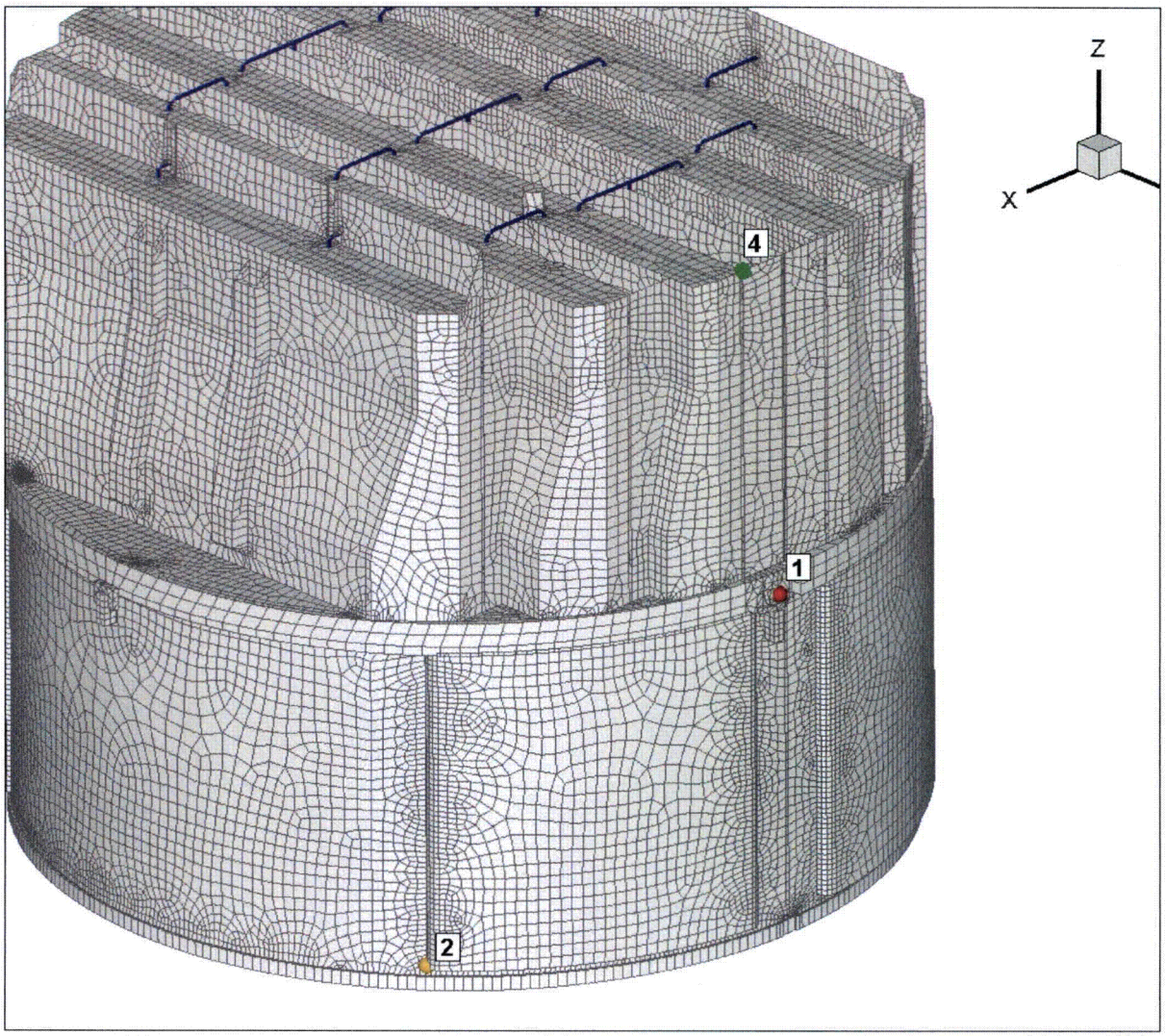

Figure 16d. Locations of minimum stress ratios, SR-P, associated with maximum stress intensities at welds for CLTP operation with frequency shifts. The recorded stress ratio at a node is the minimum value taken over all frequency shifts. Numbers refer to the enumerated locations for SR-P values at welds in Table 8b. This view shows locations 1, 2 and 4.

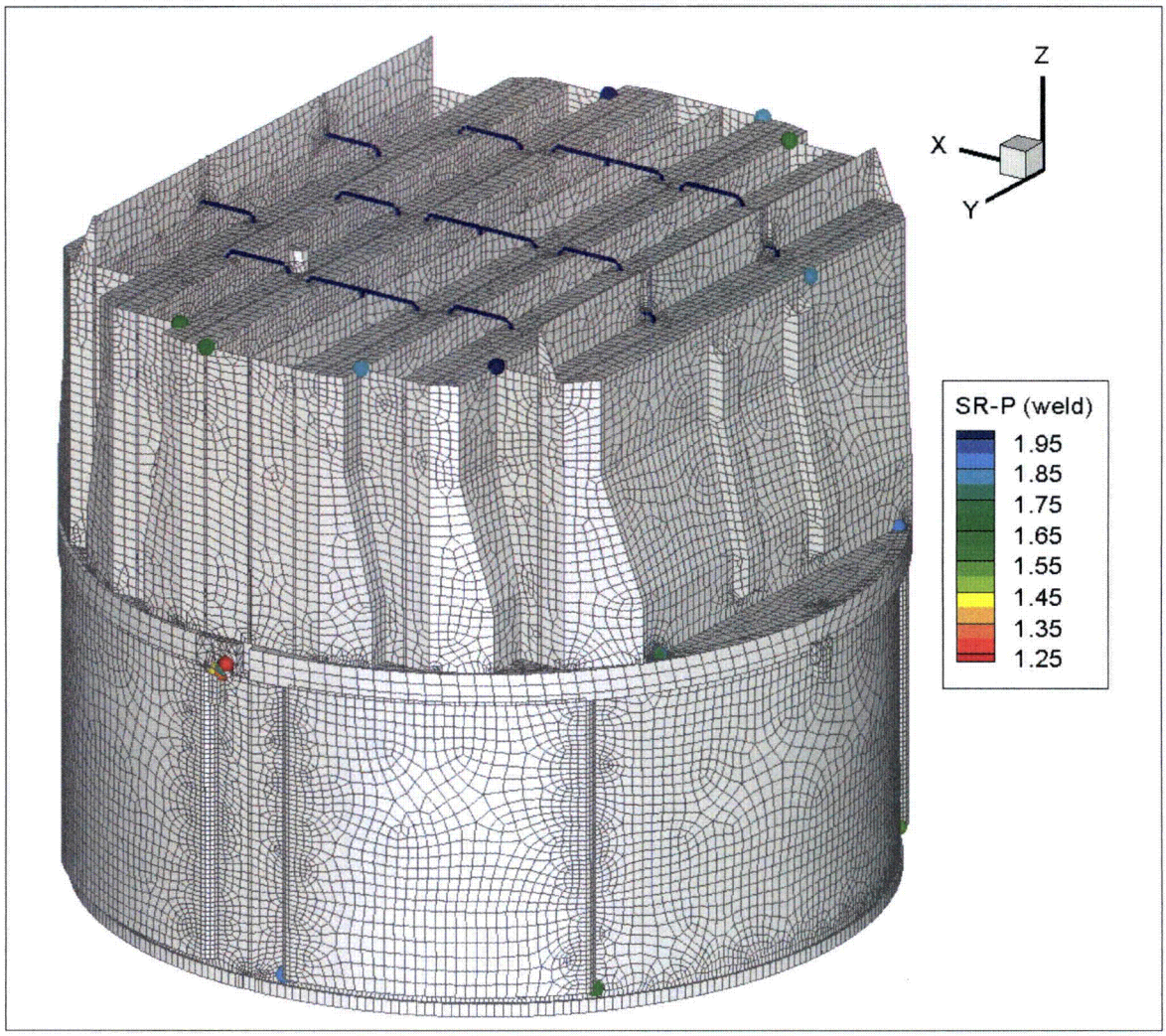

Figure 16e. Locations of minimum stress ratios, SR-P, associated with maximum stress intensities at welds for CLTP operation with frequency shifts. The recorded stress ratio at a node is the minimum value taken over all frequency shifts. This view displays *all* nodes with SR-a<2.0.

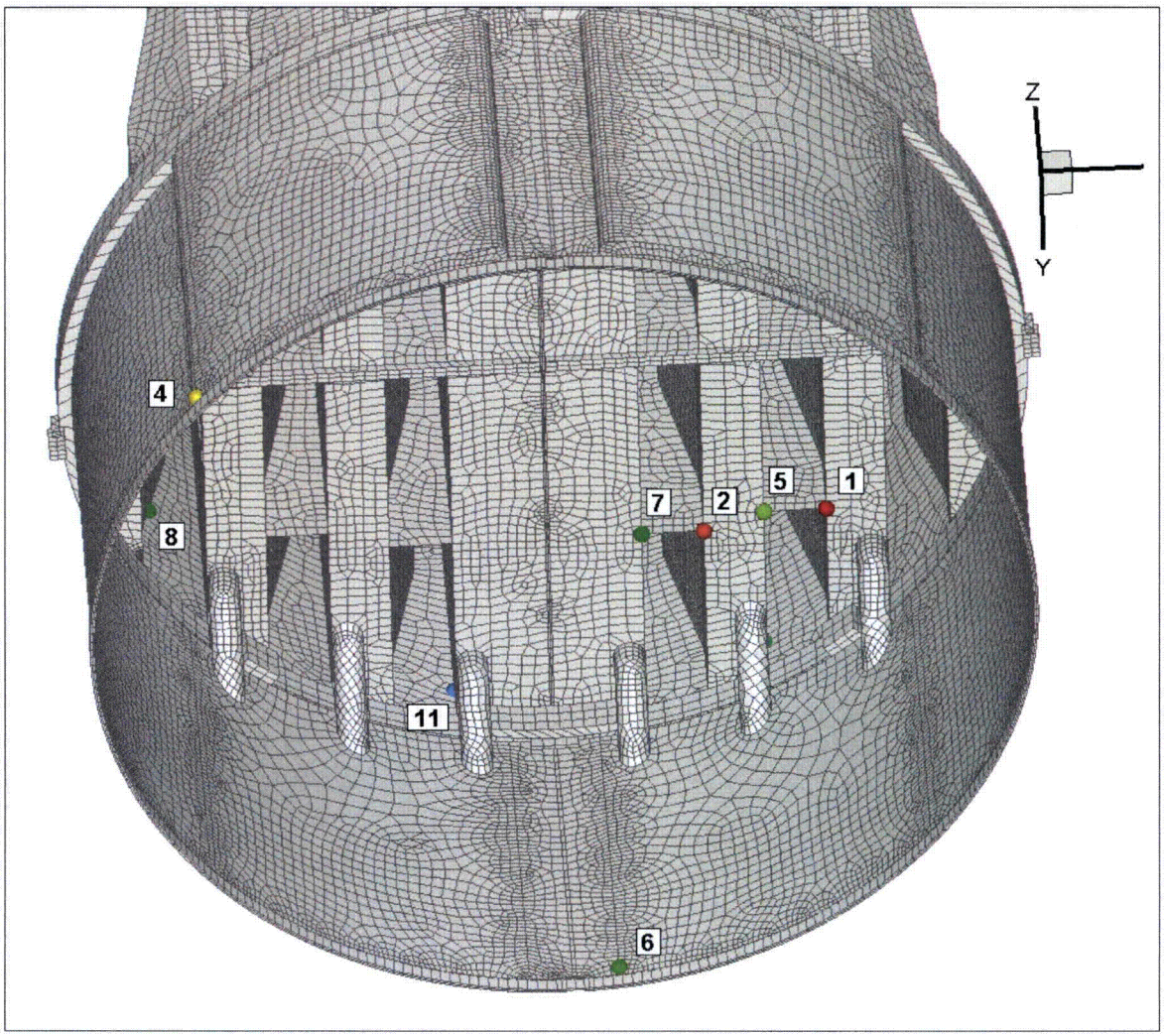

Figure 16f. Locations of minimum alternating stress ratios, SR-a, at welds for CLTP operation with frequency shifts. The recorded stress ratio at a node is the minimum value taken over all frequency shifts. Numbers refer to the enumerated locations for SR-a values at welds in Table 8b. First view showing enumerated locations 1, 2, 4-8 and 11.

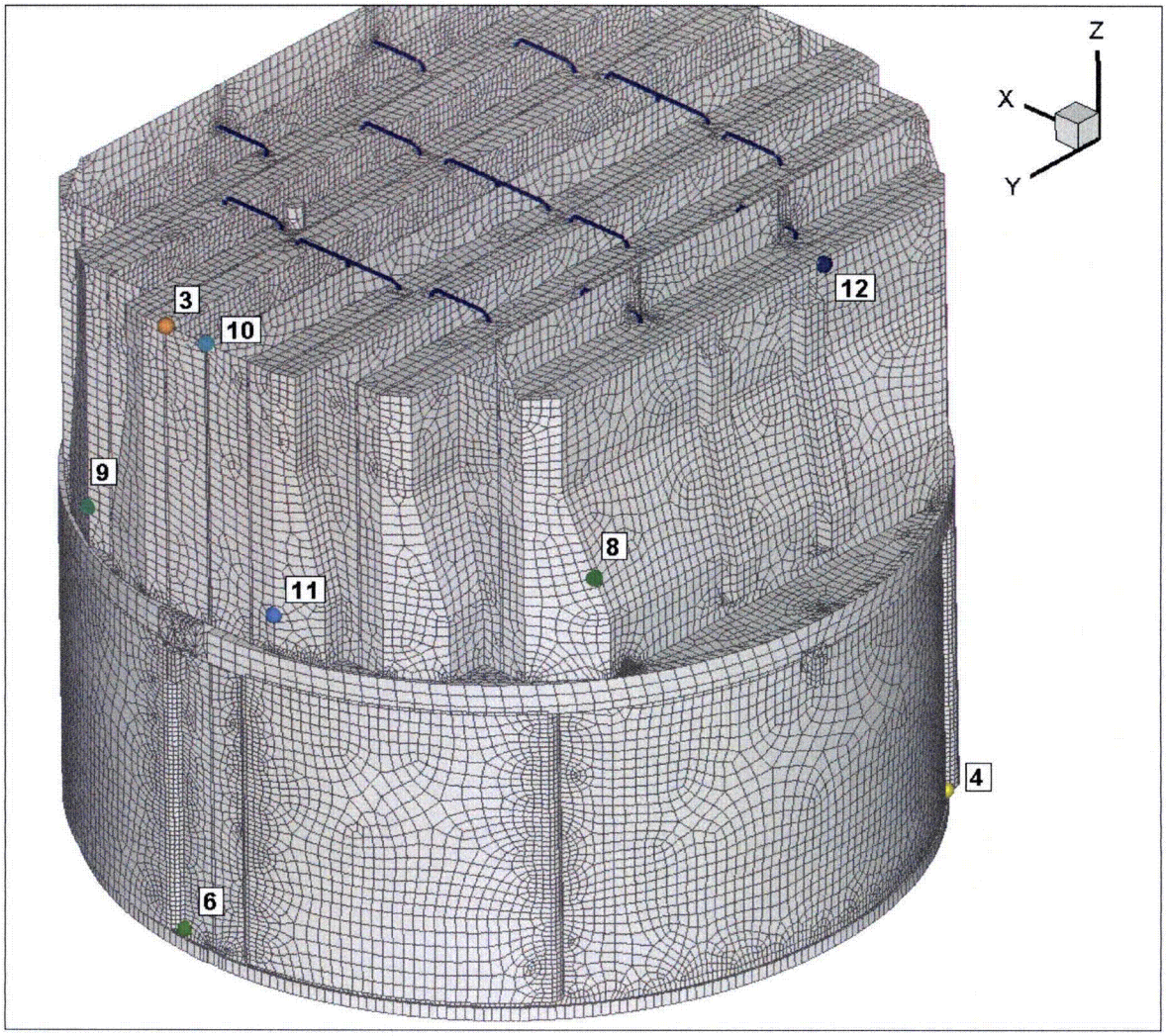

Figure 16g. Locations of minimum alternating stress ratios, SR-a, at welds for CLTP operation with frequency shifts. The recorded stress ratio at a node is the minimum value taken over all frequency shifts. Numbers refer to the enumerated locations for SR-a values at welds in Table 8b. Second view showing locations 3, 4, 6 and 8-12.

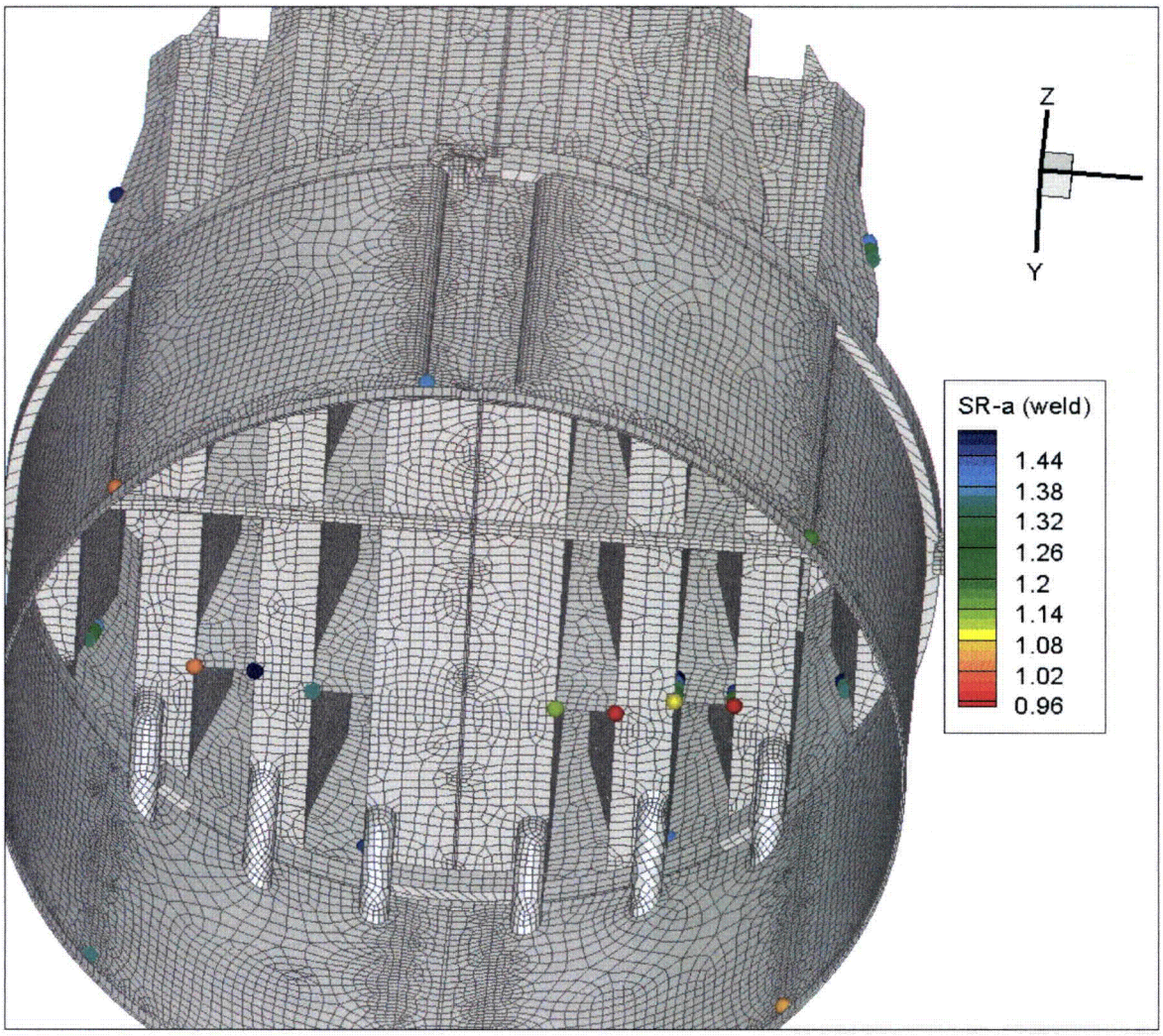

Figure 16h. Locations of minimum alternating stress ratios, SR-a, at welds for CLTP operation with frequency shifts. The recorded stress ratio at a node is the minimum value taken over all frequency shifts. This figure shows *all* nodes with SR-a<1.5. View 1 (from bottom).

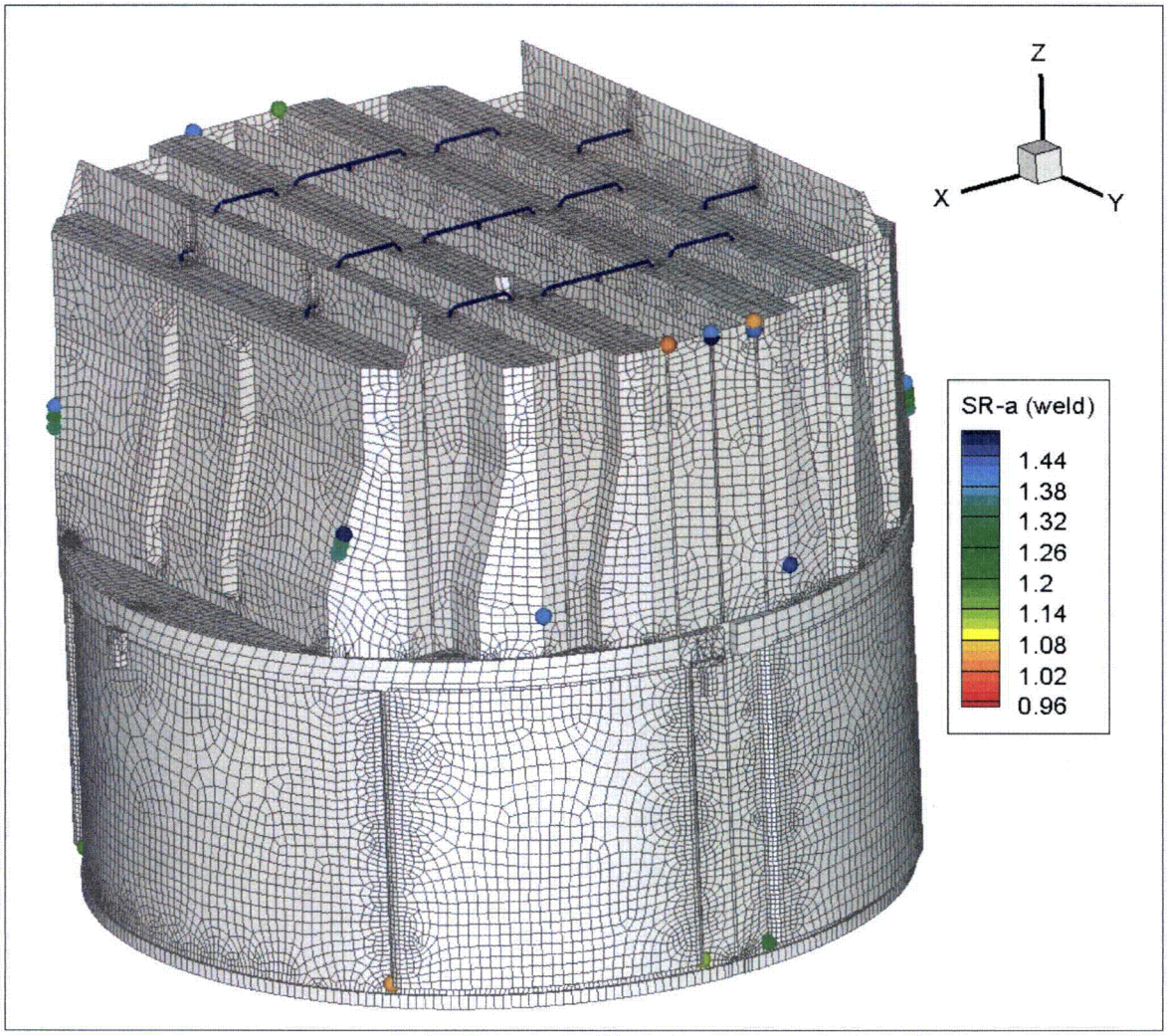

Figure 16i. Locations of minimum alternating stress ratios, SR-a, at welds for CLTP operation with frequency shifts. The recorded stress ratio at a node is the minimum value taken over all frequency shifts. This figure shows *all* nodes with SR-a<1.5. View 2.

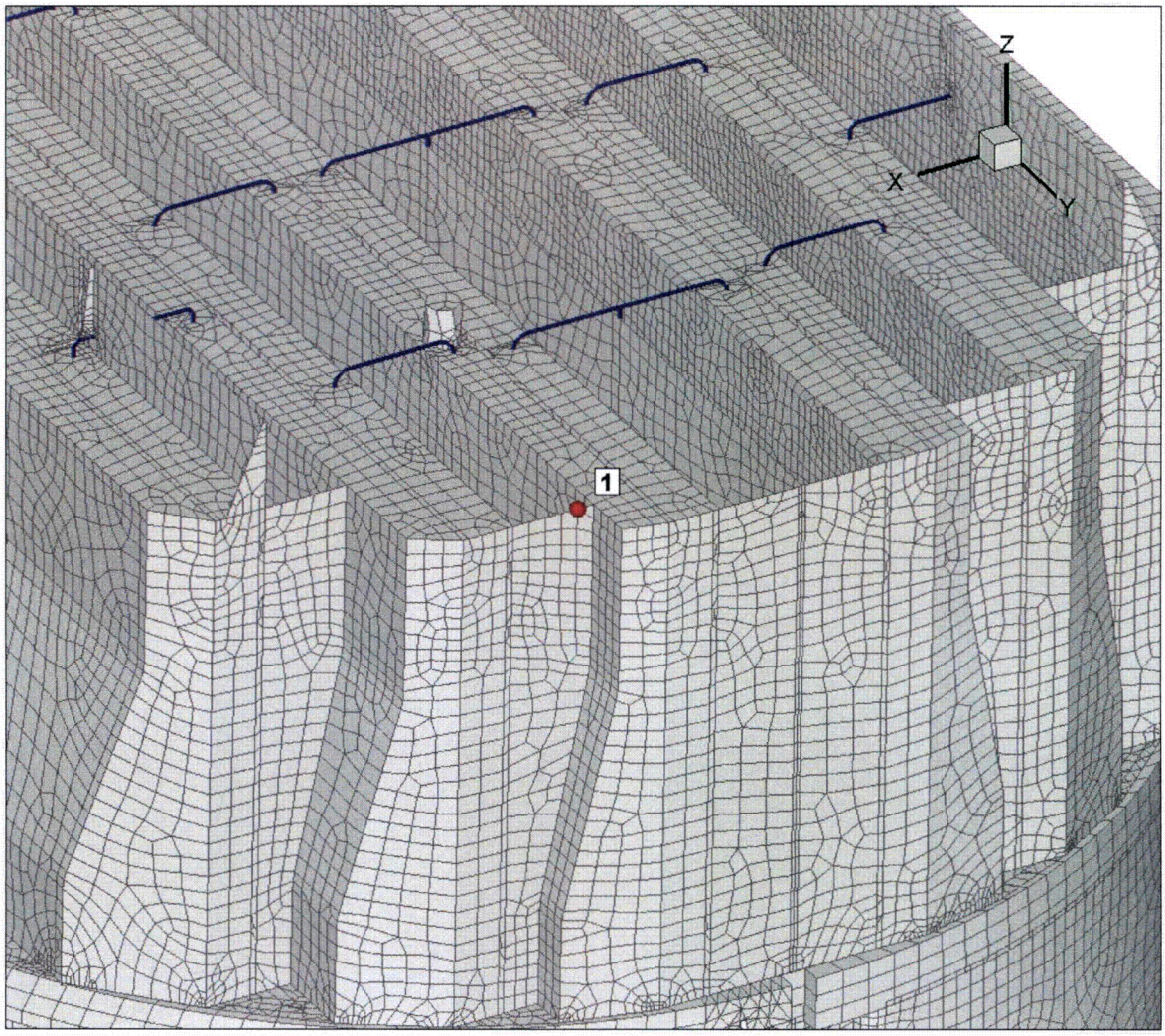

Figure 17a. Location of minimum stress ratio, SR-P, associated with maximum stress intensities at non-welds for CLTP operation with -10% frequency shift. Numbers refer to the enumerated locations for SR-P values at non-welds in Table 8c.

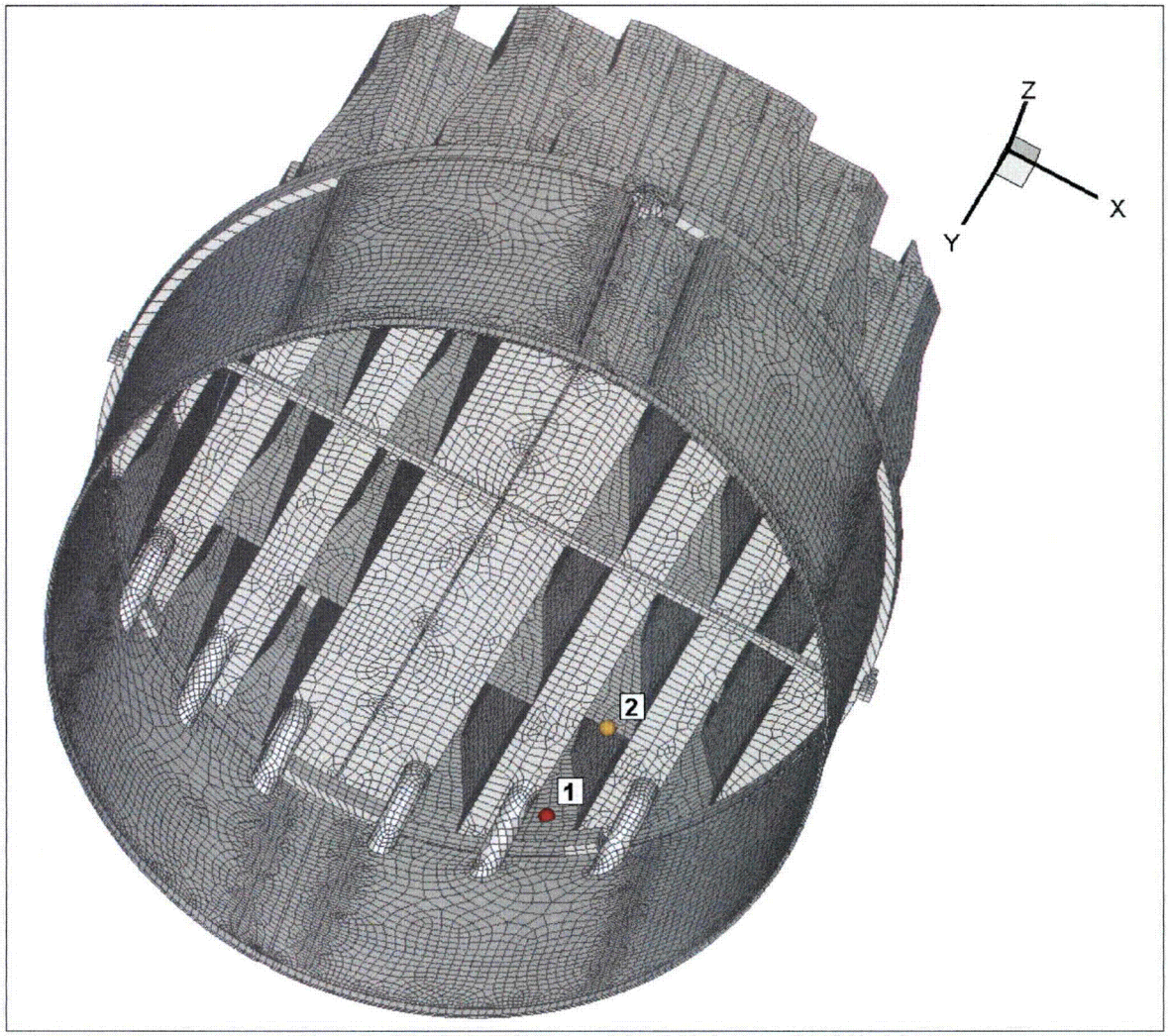

Figure 17b. Locations of minimum alternating stress ratios, SR-a, at non-welds for CLTP operation with -10% frequency shift. Numbers refer to the enumerated locations for SR-a values at non-welds in Table 8c.

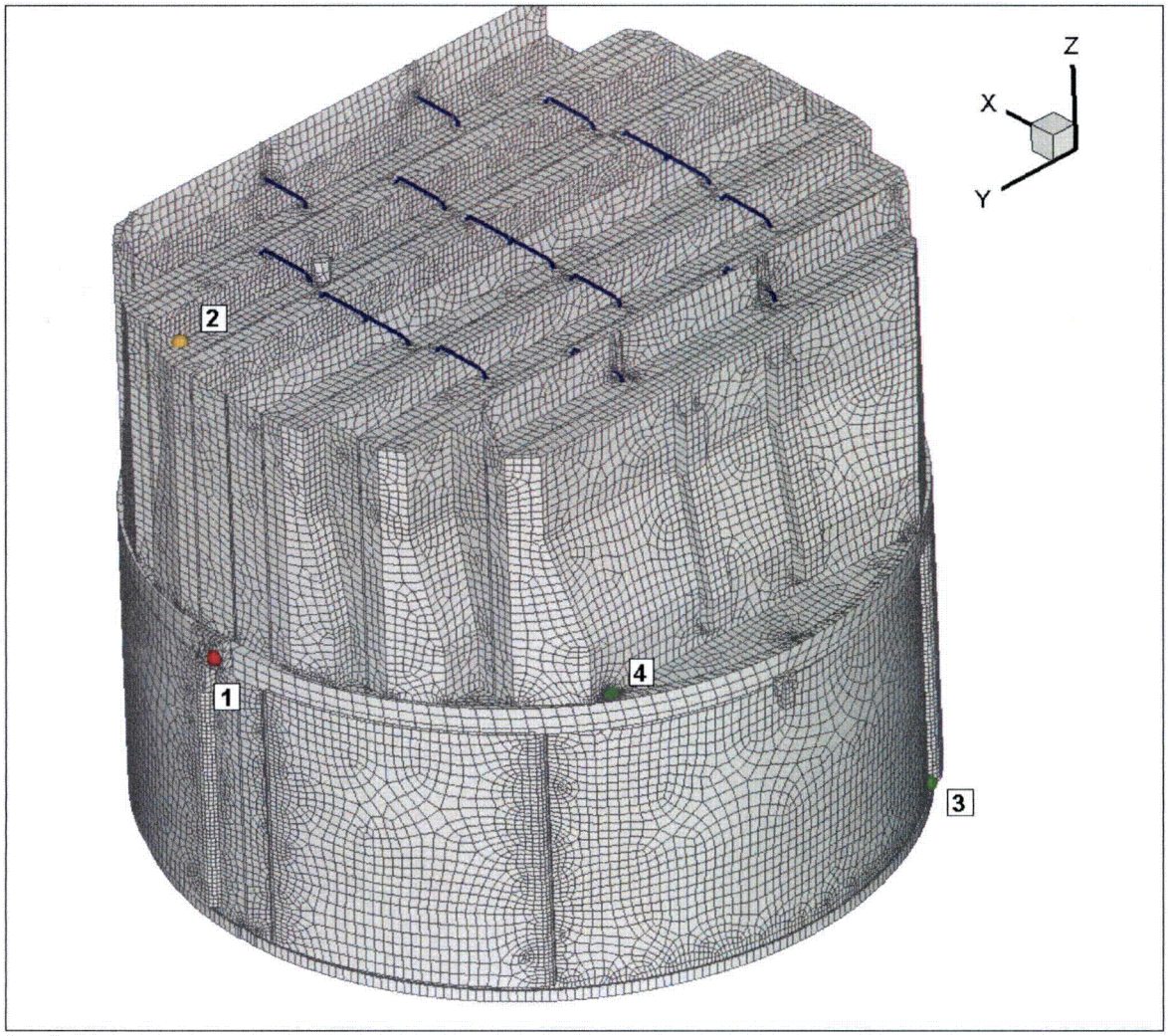

Figure 17c. Locations of minimum stress ratios, SR-P, associated with maximum stress intensities at welds for CLTP operation with -10% frequency shift. Numbers refer to the enumerated locations for SR-P values at welds in Table 8c. View 1 showing locations 1-4.

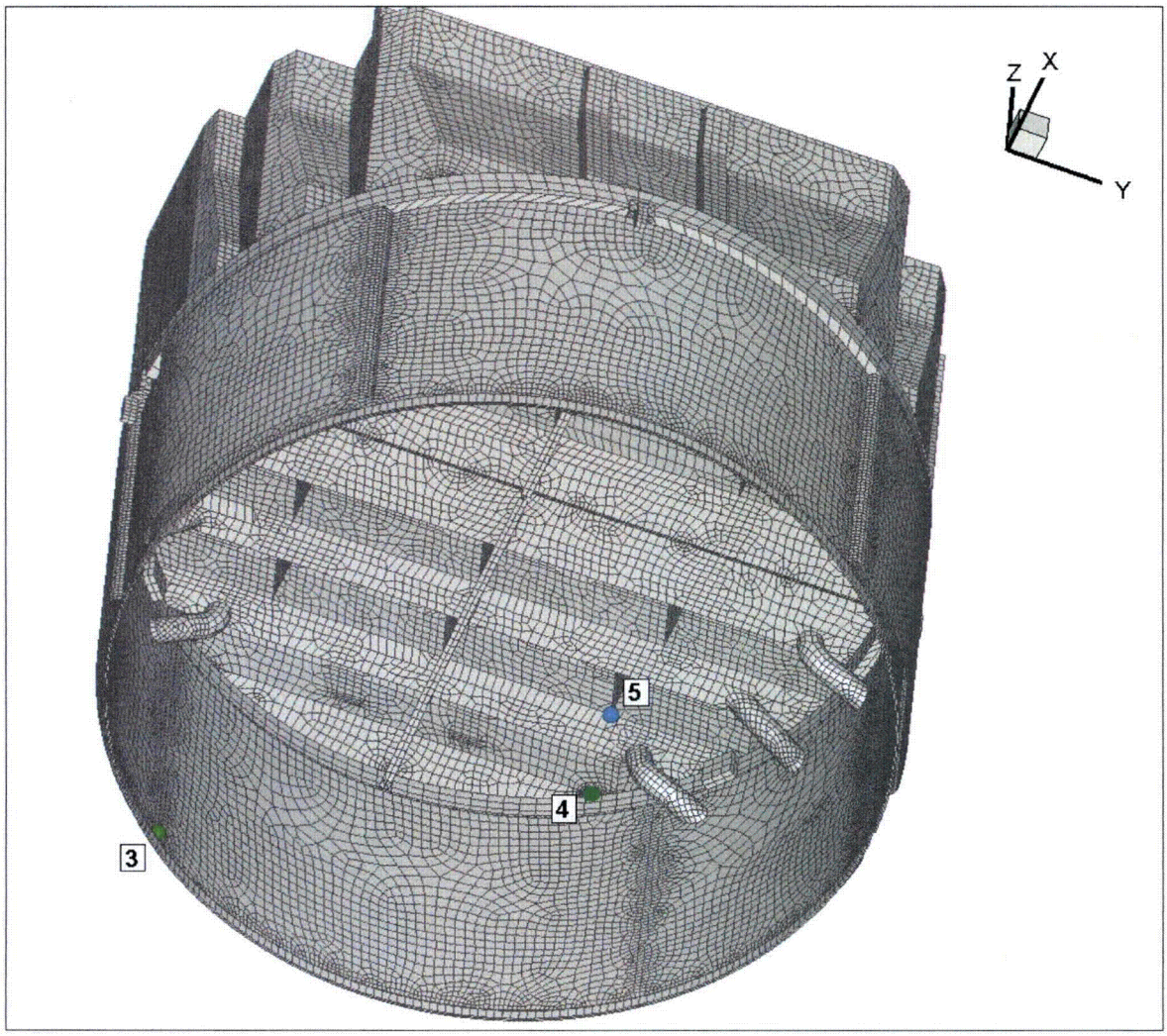

Figure 17d. Locations of minimum stress ratios, SR-P, associated with maximum stress intensities at welds for CLTP operation with -10% frequency shift. Numbers refer to the enumerated locations for SR-P values at welds in Table 8c. View 2 showing locations 3-5.

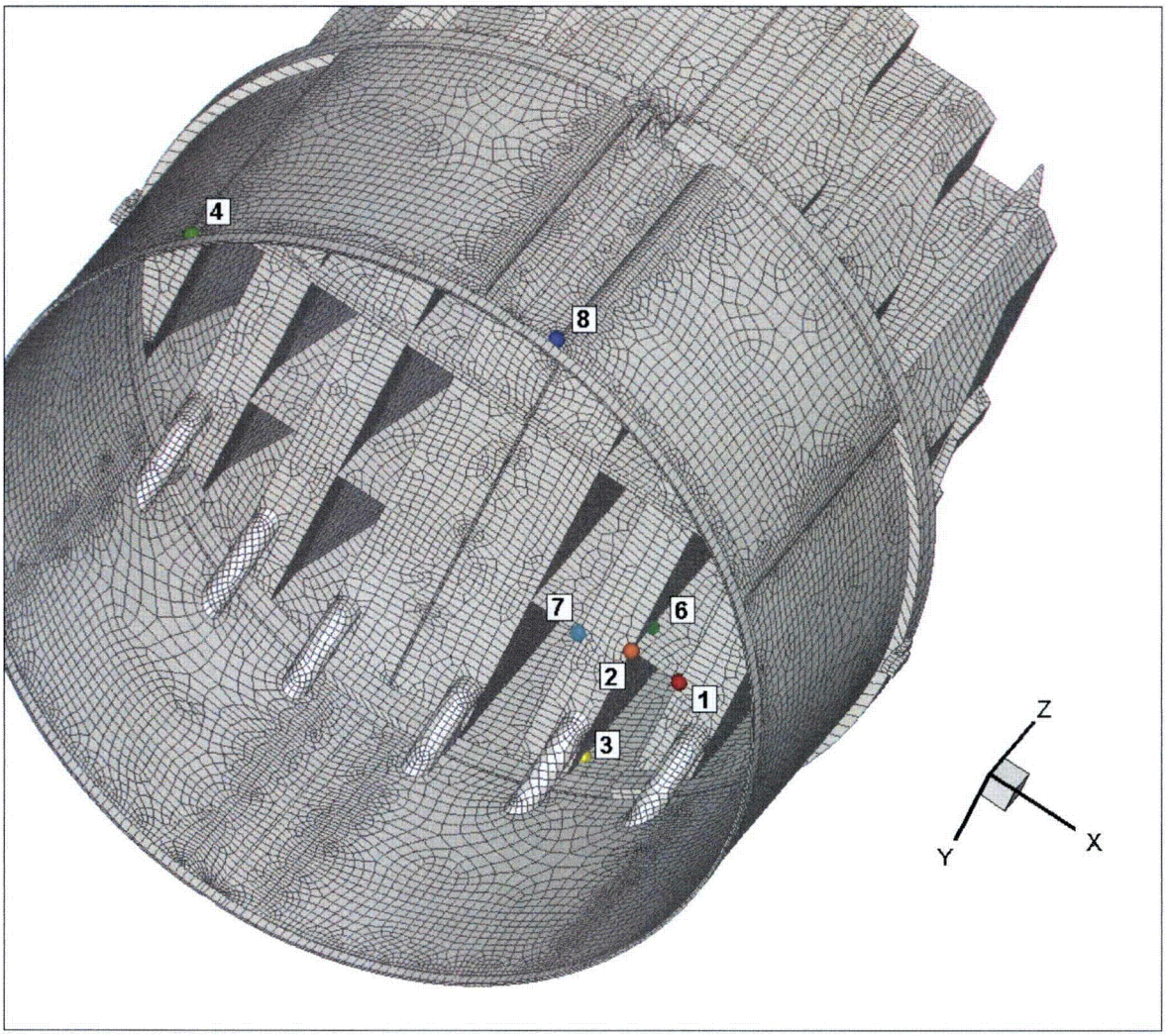

Figure 17d. Locations of minimum alternating stress ratios, SR-a, at welds for CLTP operation with -10% frequency shift. Numbers refer to the enumerated locations for SR-a values at welds in Table 8c. This view shows locations 1- 4 and 6-8.

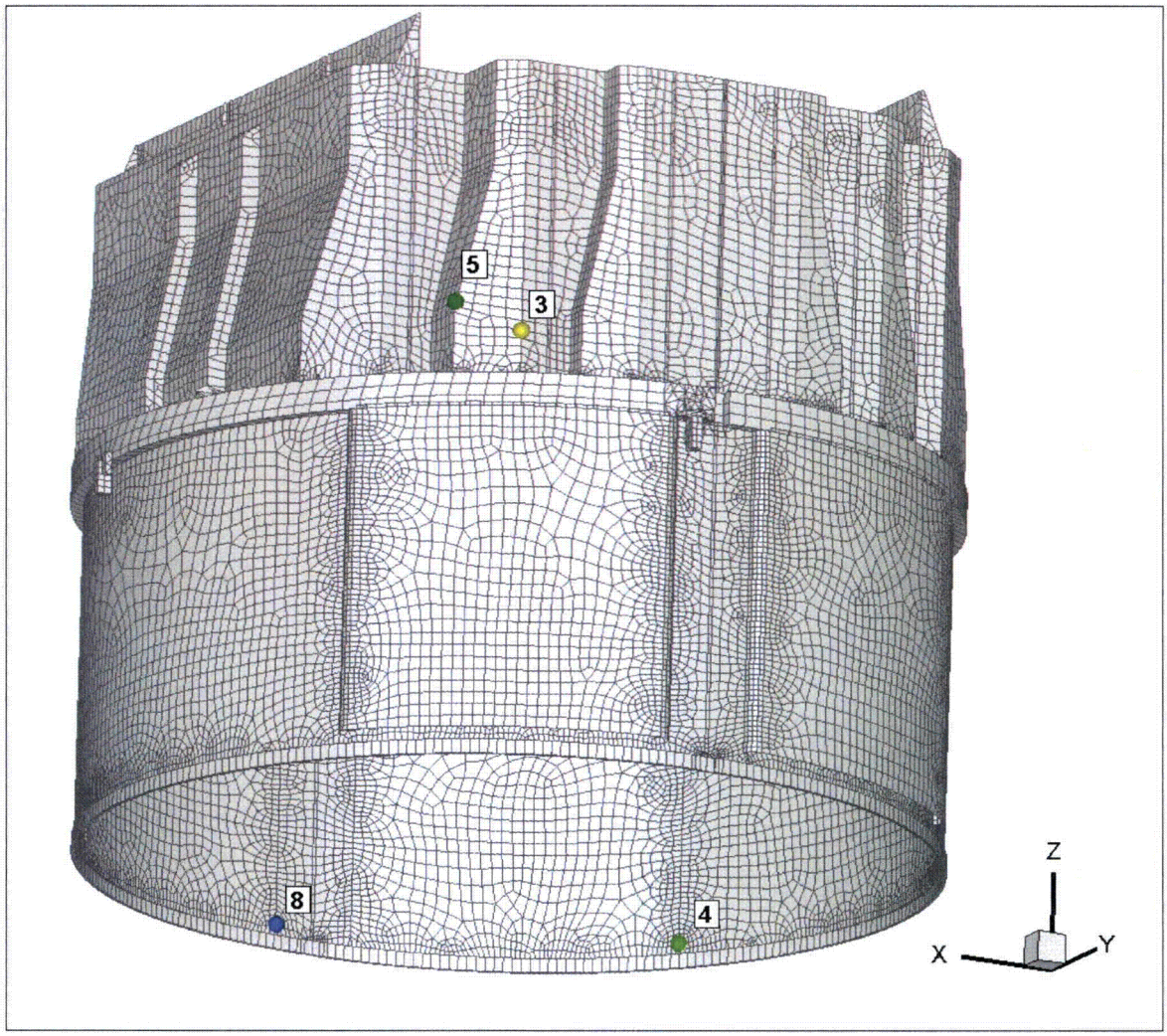

Figure 17e. Locations of minimum alternating stress ratios, SR-a, at welds for CLTP operation with -10% frequency shift. Numbers refer to the enumerated locations for SR-a values at welds in Table 8c. This second view shows locations 3-5 and 8.

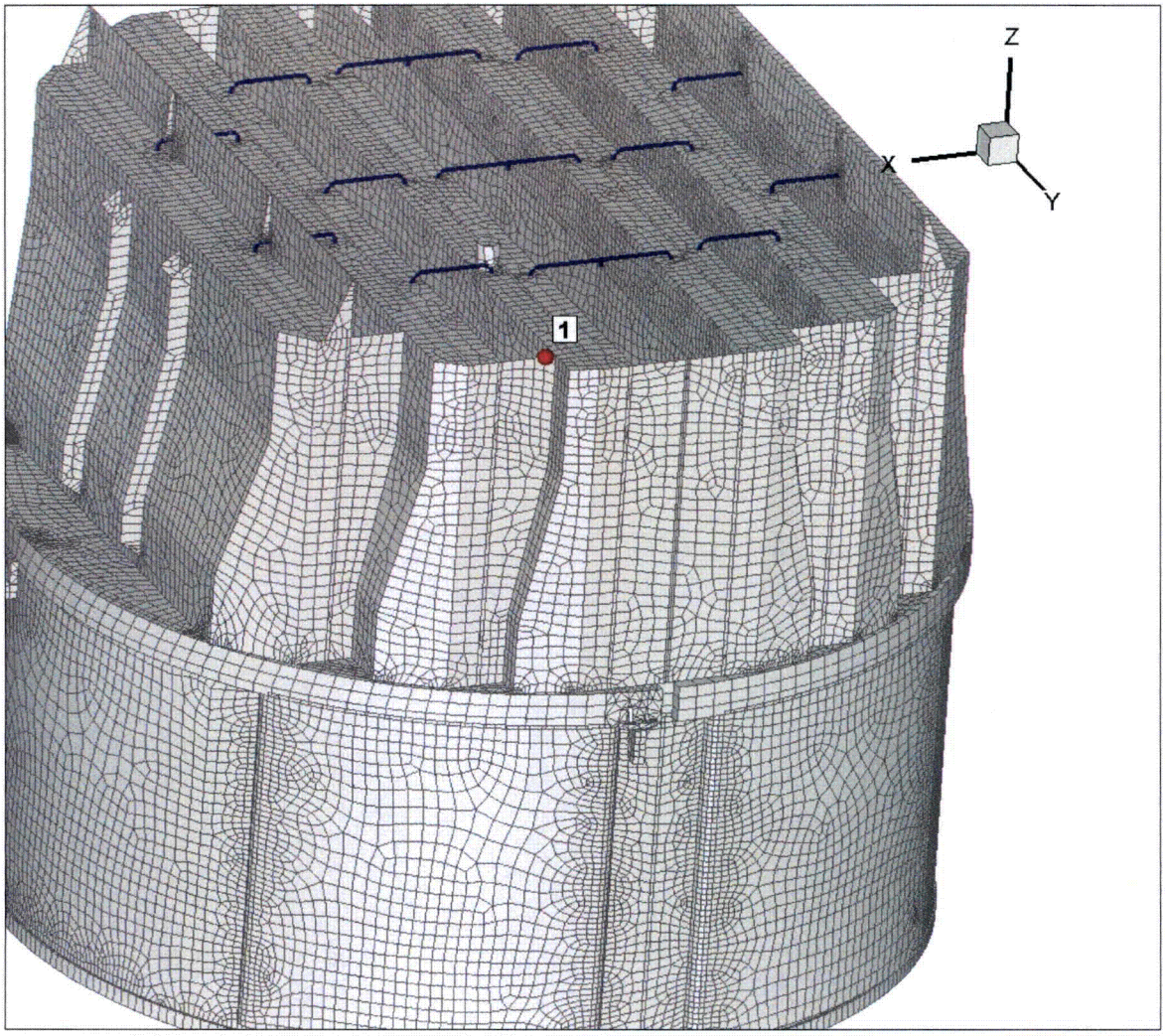

Figure 18a. Locations of minimum stress ratios, SR-P, associated with maximum stress intensities at non-welds for CLTP operation with +10% frequency shift. Numbers refer to the enumerated locations for SR-P values at non-welds in Table 8d.

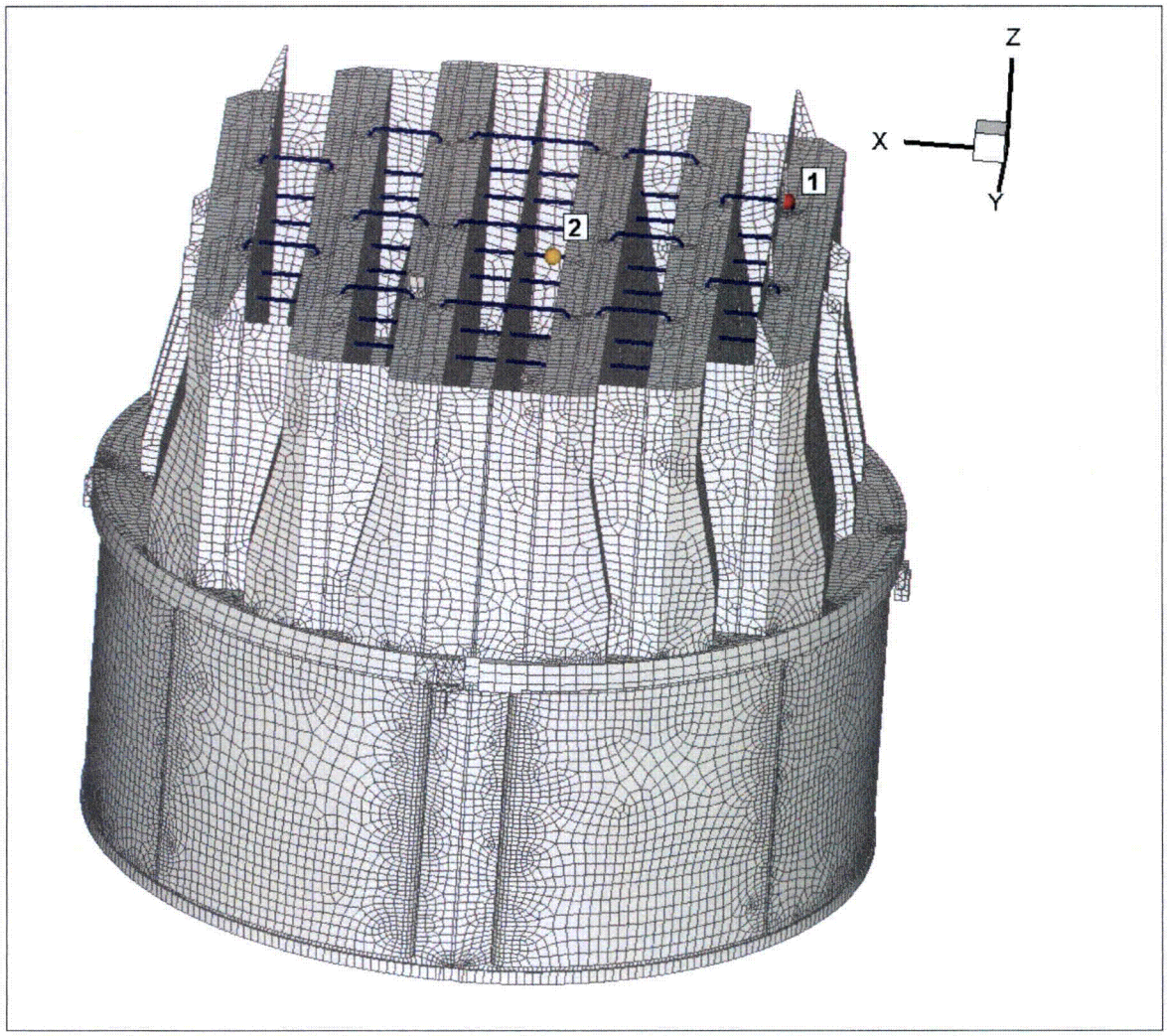

Figure 18b. Locations of minimum alternating stress ratios, SR-a, at non-welds for CLTP operation with +10% frequency shift. Numbers refer to the enumerated locations for SR-a values at non-welds in Table 8d.

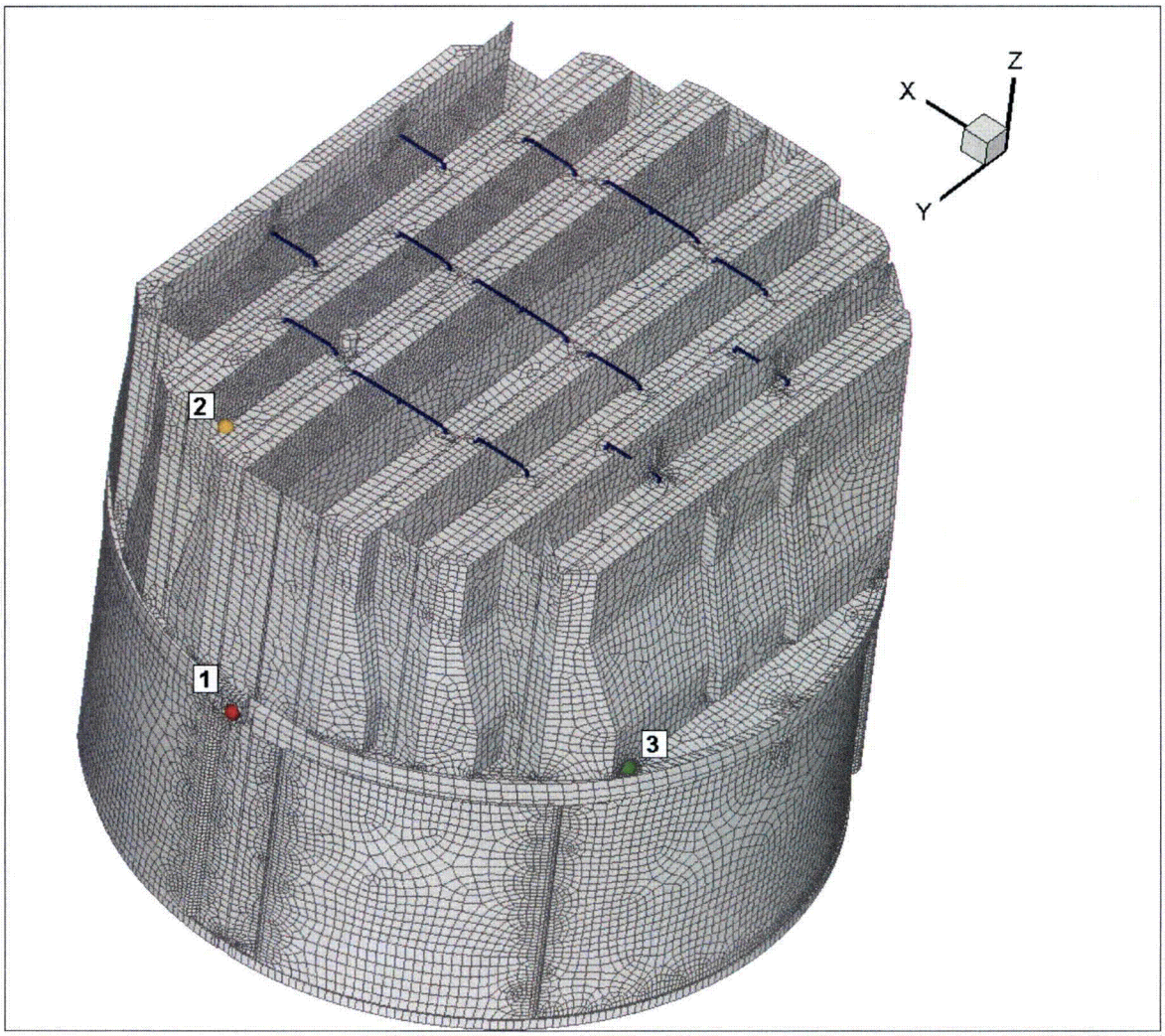

Figure 18c. Locations of minimum stress ratios, SR-P, associated with maximum stress intensities at welds for CLTP operation with +10% frequency shift. Numbers refer to the enumerated locations for SR-P values at welds in Table 8d.

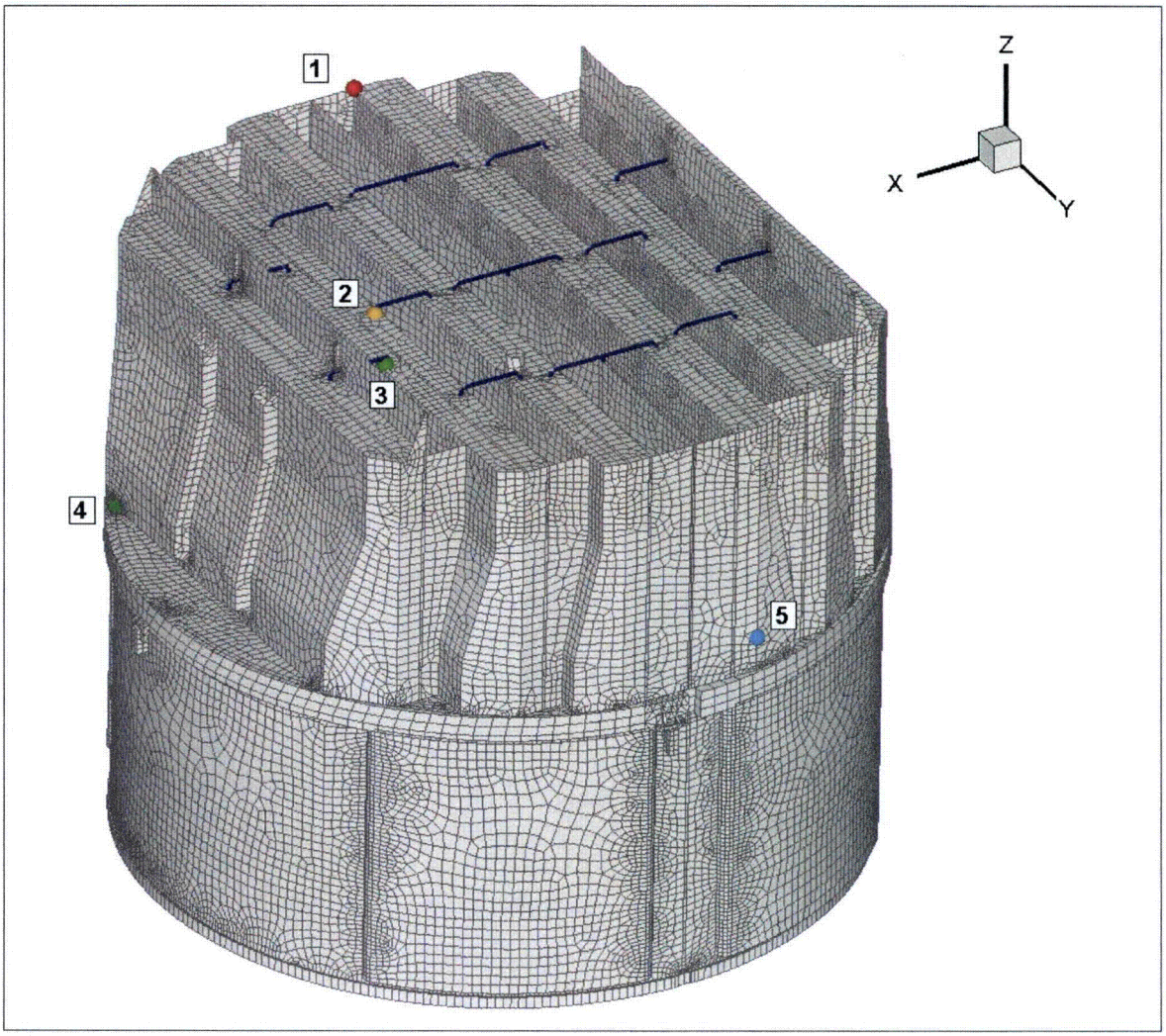

Figure 18d. Locations of minimum alternating stress ratios, SR-a, at welds for CLTP operation with +10% frequency shift. Numbers refer to the enumerated locations for SR-a values at welds in Table 8d.

5.3 Frequency Content and Filtering of the Stress Signals

As indicated previously, both the loads and stress signals contain a strong 218 Hz component that can be identified with the blanked-off standpipes in the system. This can be seen by examining the accumulative PSDs for the two nodes that gave the lowest alternating stress ratios at nominal (zero frequency shift) CLTP operation according to Table 8a. The accumulative PSDs are computed directly from the Fourier coefficients as

$$\Sigma(\omega_n) = \sqrt{\sum_{k=1}^{n} \left|\tilde{\sigma}(\omega_k)\right|^2}$$

where $\tilde{\sigma}(\omega_k)$ is the complex stress harmonic at frequency, ω_k. Accumulative PSD plots are useful for determining the frequency components and frequency ranges that make the largest contributions to the fluctuating stress. Unlike PSD plots, no "binning" or smoothing of frequency components is needed to obtain smooth curves. Steep step-like rises in $\Sigma(\omega)$ indicate the presence of a strong component at a discrete frequency whereas gradual increases in the curve imply significant content over a broader frequency range. From Parsival's theorem, equality between $\Sigma(\omega_N)$ (where N is the total number of frequency components) and the RMS of the stress signal in the time domain is established.

The selected nodes are:

Node 91667 - located on the junction of the middle hood/hood support/outer base plate junction. The associated PSDs are shown in Figure 19.

Node 84412 - located on the welded drain channel/skirt junction. The associated PSDs are shown in Figure 20.

Both plots show a pronounced rise at 218 Hz. For node 91667 this is clearly the dominant component and, given the sharp rise in $\Sigma(\omega)$ at this frequency, the component is narrow band. Closer examination of the signal shows a major rise at 218.84 Hz and a lesser one at 219.84 Hz. The corresponding time response shows a 1 Hz beating phenomenon due to the close proximity of the two components. For node 84412 the contribution of the 218 Hz component is smaller and the total response is dominated by a gradual rise between 30-50 Hz.

In order to examine how the stresses change when the 218 Hz signal is removed (e.g., via insertion of plugs at the terminations of the eight unused standpipes in main steam lines A and D; the four unused standpipes in main steam lines B and C are located on the dead-headed branches and do not contribute to the 218 Hz signal [17]), the pressure signals in each MSL were filtered by a simple Gaussian notch filter centered at 218 Hz according to:

[[[3]]]

where f is the frequency, and the stress intensities and stress ratios re-evaluated.

These are reported in Table 9 for: (i) nominal CLTP operation; and (ii) as the minimum (worst case) stress ratios taken over all frequency shifts. It is clear that the elimination of this signal results in a significant reduction in alternating stresses and corresponding increase in alternating stress ratios. Comparing the minimum stress ratio over all frequency shifts before (SR-a=0.96 in Table 8b) and after filtering (SR-a=2.00 in Table 9b) of the 218 Hz signal shows that worst case stresses are reduced by a factor of 2.08. The worst case maximum stress ratios on the other hand remain virtually unchanged at SR-P=1.26. This reflects the dominance of the static component to the maximum stress at the support locations.

Since acoustic loads scale roughly with the square of the steam flow, it is reasonable to anticipate that under EPU conditions (where steam flow increases by 16%) the stresses would increase to by approximately $(116\%)^2=1.35$. Under this assumption the minimum alternating stress ratio would reduce from 2.0 to 2/1.35=1.48, which given that the applied loads already account for all end-to-end biases and uncertainties, still contains sufficient margin for sustained EPU operation.

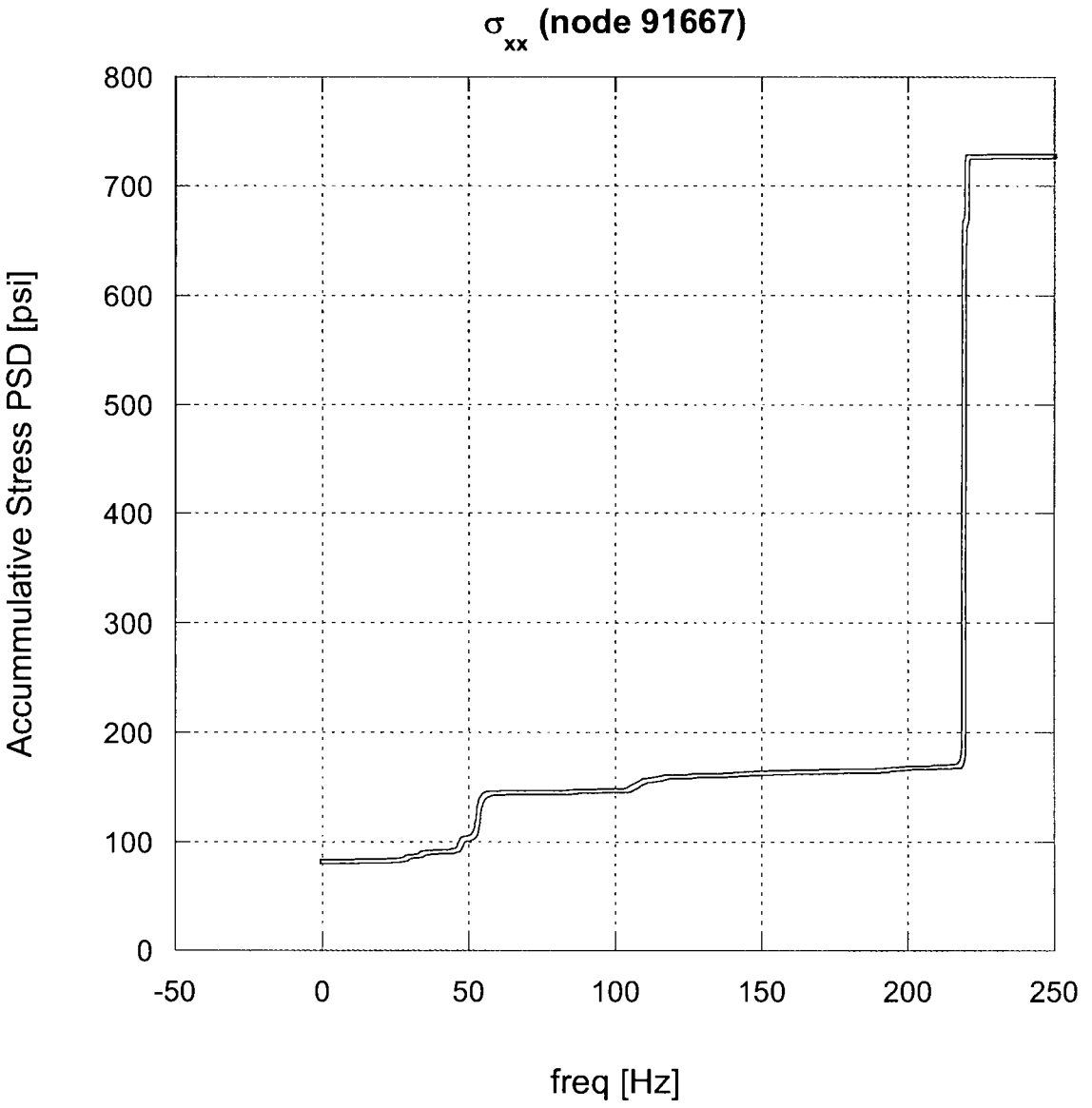

Figure 19. Accumulative PSD of the σ_{xx} stress response at node 91667 for nominal CLTP operation.

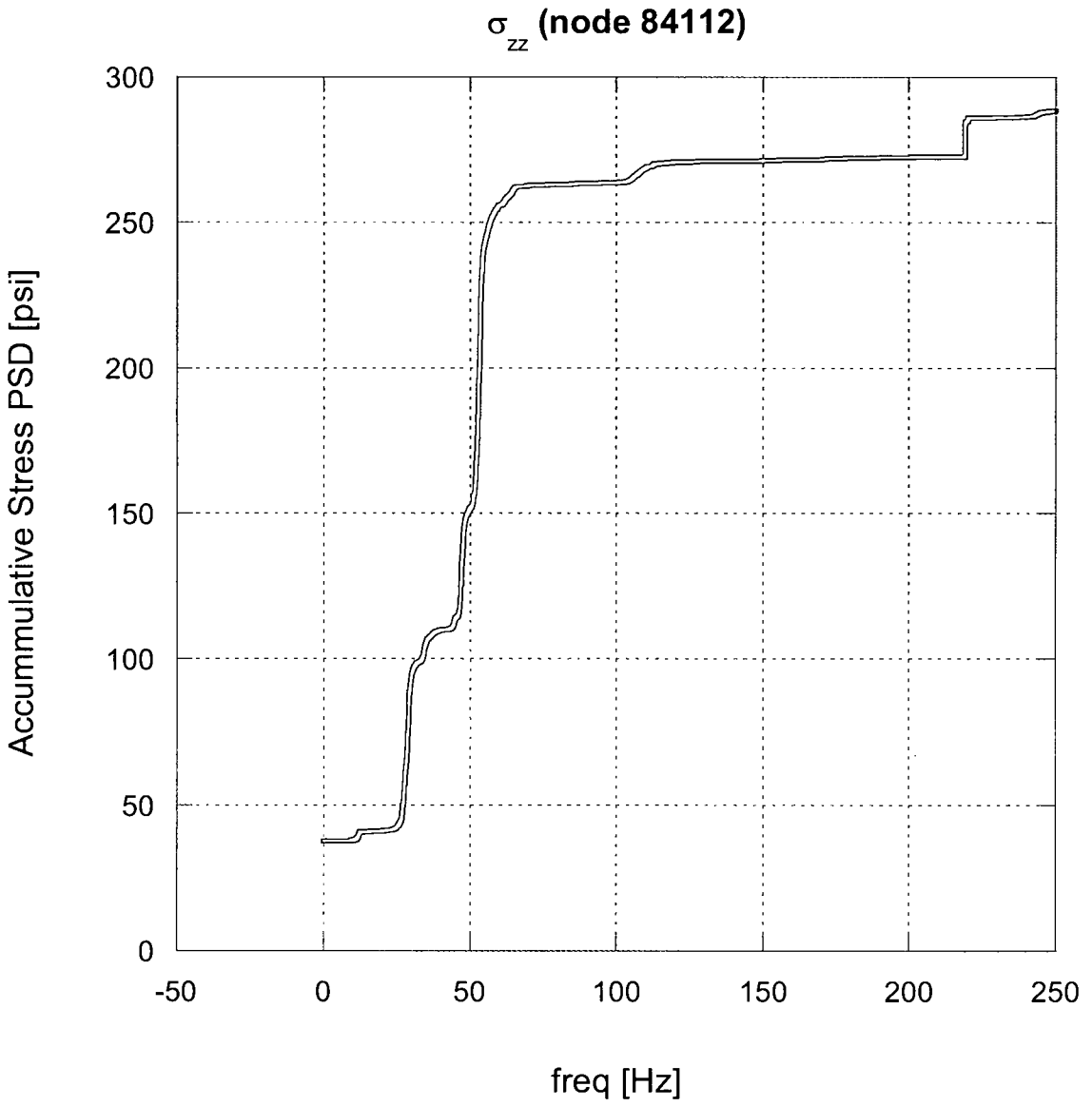

Figure 20. Accumulative PSD of the σ_{zz} stress response at node 84112 for nominal CLTP operation.

Table 9a. Locations with minimum stress ratios for CLTP conditions with no frequency shift using loads with 218 Hz component filtered. Stress ratios are grouped according to stress type (maximum – SR-P; or alternating – SR-a) and location (away from a weld or at a weld). Bold text indicates minimum stress ratio of any type on the structure.

Stress Ratio	Location	Weld	Location (in.)				Stress Intensity (psi)			Stress Ratio	
			x	y	z	node	Pm	Pm+Pb	S_{alt}	SR-P	SR-a
SR-P	1. T-cross-section stiffener	No	-99.3	0.0	0.0	74585	4811	4839	<1500	3.80	>4
SR-a	1. lock gusset	No	-78.3	31.4	91.6	75587	2620	4191	3388	6.55	3.65
SR-P	**1. upper support ring/support**	**Yes**	**5.8**	**122.4**	**-6.5**	**7532**	**7946**	**7946**	**<1500**	**1.27**	**>4**
"	2. outer hood/cover plate	"	-102.0	60.2	0.0	91589	1029	7796	<1500	1.94	>4
"	3. inner hood/top cover plate/middle closure plate	"	-31.5	-108.4	88.9	76022	5184	5326	<1500	1.94	>4
"	4. submerged drain channel/skirt	"	-91.0	76.7	-100.5	77550	1009	6268	2207	2.41	3.11
SR-a	1. inner hood top cover plate/tie bar	Yes	-29.5	3.0	88.9	76452	551	3457	2921	4.37	2.35
"	2. top cover plate/tie bar	"	-81.5	-30.2	88.9	78139	594	3213	2791	4.70	2.46
"	3. middle hood top cover plate/tie bar	"	60.5	31.4	88.9	79136	448	3325	2786	4.54	2.47
"	4. top cover plate/tie bar	"	48.0	3.0	88.9	92355	500	3343	2767	4.52	2.48

See Table 7a for coordinates description.

Table 9b. Locations with minimum stress ratios for CLTP conditions with frequency shifts using loads with 218 Hz component filtered. Stress ratios at every node are recorded as the lowest stress ratio identified during the frequency shifts. Stress ratios are grouped according to stress type (maximum – SR-P; or alternating – SR-a) and location (away from a weld or at a weld). Bold text indicates minimum stress ratio of any type on the structure.

Stress Ratio	Location	Weld	% Freq. Shift	Location (in.)				Stress Intensity (psi)			Stress Ratio	
				x	y	z	node	Pm	Pm+Pb	S_{alt}	SR-P	SR-a
SR-P	1. T-cross-section stiffener	No	+10	-99.3	0.0	0.0	74585	4927	4951	0	3.71	>4
SR-a	1. lock gusset	No	+10	-78.3	31.4	91.6	75587	3525	5148	4377	5.19	2.82
"	2. skirt	"	+7.5	-57.8	-104.0	-103.8	13744	294	3465	3348	7.92	3.69
SR-P	1. upper support ring/support	Yes	+5	5.8	122.4	-6.5	7532	8013	8013	0	1.26	>4
"	2. outer hood/cover plate	"	+10	-102.0	60.2	0.0	91589	1066	8175	0	1.85	>4
"	3. inner hood/top cover plate/middle closure plate	"	+5	-31.5	-108.4	88.9	76022	5303	5457	0	1.90	>4
"	4. submerged drain channel/skirt	"	+10	91.0	-76.7	-100.5	84412	1441	6481	2688	2.33	2.56
"												
SR-a	1. inner hood top cover plate/tie bar		+10	-29.5	3.0	88.9	76452	551	4088	3440	3.69	2.00
"	2. top cover plate/tie bar		+10	48.0	3.0	88.9	92355	554	4102	3343	3.68	2.05
"	3. middle hood top cover plate/tie bar		+10	60.5	31.4	88.9	79136	502	3586	3227	4.21	2.13
"	4. top cover plate/tie bar		-10	81.5	30.2	88.9	79121	566	3654	2954	4.13	2.33

See Table 7a for coordinates description.

6. Conclusions

A frequency-based steam dryer stress analysis has been used to calculate high stress locations and calculated / allowable stress ratios for the Browns Ferry Unit 1 steam dryer at CLTP load conditions using plant measurement data. A detailed description of the frequency-based methodology and the finite element model for the BFN1 steam dryer is presented. The CLTP loads obtained in a separate acoustic circuit model [2], including end-to-end bias and uncertainty [3], were applied to a finite element model of the steam dryer consisting mainly of the ANSYS Shell 63 elements, brick continuum elements, and beam elements. The resulting stress histories were analyzed to obtain maximum and alternating stresses at all nodes for comparison against allowable levels. These results are tabulated in Table 8 of this report. The minimum stress ratio at nominal operation is 1.20 and the minimum stress ratio taken over all frequency shifts is 0.96. In both cases the minimum stress ratio corresponds to an alternating stress.

Examination of the stress response reveals a strong 218 Hz component which is attributable to acoustics in the dead-headed safety valve standpipes. The structural response is largely explained by the excitation of structural modes in the vicinity of this frequency. Elimination of this signal by plugging these unused standpipes results in a significant stress reduction. The minimum alternating stress ratio is increased to SR-a=2.00 which qualifies the steam dryer with substantial margin for EPU conditions.

On the basis of these CLTP plant loads, the dynamic analysis of the steam dryer shows that the combined acoustic, hydrodynamic, and gravity loads produce the following minimum stress ratios:

Frequency Shift	Minimum Stress Ratio (no filtering)		Minimum Stress Ratio (218 Hz signal removed)	
	Max. Stress, SR-P	Alternating Stress, SR-a	Max. Stress, SR-P	Alternating Stress, SR-a
0% (nominal)	1.25	1.20	1.27	2.35
-10%	1.28	0.96	1.28	2.33
-7.5%	1.30	1.13	1.30	2.66
-5%	1.28	1.04	1.30	2.45
-2.5%	1.28	1.17	1.29	2.45
+2.5%	1.26	1.61	1.29	2.08
+5%	1.25	1.50	1.26	2.38
+7.5%	1.27	0.98	1.27	2.20
+10%	1.27	1.56	1.28	2.00
All shifts	1.25 - 1.30	0.96 – 1.61	1.26 - 1.30	2.00 – 2.66

7. References

1 Continuum Dynamics, Inc. (2005). "Methodology to Determine Unsteady Pressure Loading on Components in Reactor Steam Domes (Rev. 6)." C.D.I. Report No. 04-09 (Proprietary).

2. Continuum Dynamics, Inc. (2007). "Acoustic and Low Frequency Hydrodynamic Loads at CLTP Power Level on Browns Ferry Nuclear Unit 2 Steam Dryer to 250 Hz (Rev. 0)." C.D.I. Report No. 07-10P (Proprietary)

3. Continuum Dynamics, Inc. (2007). "Methodology to Predict Full Scale Steam Dryer Loads from In-Plant Measurements, with the Inclusion of a Low Frequency Hydrodynamic Contribution," C.D.I. Report No. 07-09P (Proprietary).

4. Structural Integrity Associates, Inc. (2006). "Main Steam Line 100% CLTP Strain Data Transmission." SIA Letter Report No. GSZ-06-017.2.

5. ANSYS Release 10.0. URL http://www.ansys.com. Documentation: ANSYS 10.0 Complete User's Manual Set

6. Press, W. H., S. A. Teukolsky, et al. (1992). *Numerical Recipes*, Cambridge University Press.

7. O'Donnell W.J. (1973). "Effective Elastic Constants For the Bending of Thin Perforated Plates With Triangular and Square Penetration Patterns," ASME Journal of Engineering for Industry, Vol. 95, pp. 121-128.

8. Idel'chik, I E. and Fried, E. (1989). *Flow Resistance, a Design Guide for Engineers*, Taylor & Francis, Washington D.C., p 260.

9. DeSanto, D.F. (1981). "Added Mass and Hydrodynamic Damping of Perforated Plates Vibrating in Water," Journal of Pressure Vessel Technology, Vol. 103, p. 176-182.

10. Continuum Dynamics, Inc. (2007). "Dynamics of BWR Steam Dryer Components," C.D.I. Report No. 07-11P

11. U.S. Nuclear Regulatory Commission, (2007). Regulatory Guide 1.20 "Comprehensive Vibration Assessment Program for Reactor Internals During Preoperational and Initial Startup Testing," March 2007.

12. WRC Bulletin 432 (1998). "Fatigue Strength Reduction and Stress Concentration Factors For Welds In Pressure Vessels and Piping," WRC, NY, p.32

13. Pilkey W.D. (1997). *Peterson's Stress Concentration Factors*, 2nd ed., John Wiley, NY, p.139.

14. Lawrence F.V., Ho N.-J., Mazumdar P.K. (1981). "Predicting the Fatigue Resistance of Welds," Ann. Rev. Mater. Sci., vol. 11, pp. 401-425.

15. General Electric (GE) Nuclear Energy (2003). Supplement 1 to Service Information Letter (SIL) 644, "BWR/3 Steam Dryer Failure," September 5, 2003.

16. Tecplot 10 (2004). URL: http://www.tecplot.com. Documentation: *Tecplot* User's Manual Version 10 Tecplot, Inc. Bellevue, Washington October.

17. Nelson G. (2006). "BFN Frequencies by GCN.xls" file received by email 31 October 2006.

18. Flugge, W. (ed.) (1962). *Handbook of Engineering Mechanics*, McGraw-Hill, p.61-62.

19. Blevins R. (1979). "Formulas for Natural Frequency and Mode Shape," van Nostrand-Reinhold Co., p. 261

20. ASME (2004). ASME Boiler and Pressure Vessel Code, Section III, Article A-8000, Stresses in Perforated Flat Plates.

Appendix A. Comparison of ANSYS Frequency Predictions Against Analytical Formulas for Flat Plates

The computed modal masses affect the response amplitude, and while these masses can be computed using the ANSYS finite element (FE) software, there are no modal mass measurements or analytical solutions they can be compared against. One recourse for assessing bias errors and uncertainties is to consider a geometrically simple structure (e.g., a flat plate) for which analytical solutions for the modal amplitudes, masses, and responses are available. Predictions of these properties using an ANSYS FE model having the same elements and connections present in the steam dryer model can then be compared against these analytical results thus allowing one to estimate the errors in frequency as a function of response frequency.

Modal analysis was performed for: (i) a simply supported plate of dimensions comparable to the vane bank side panel; and (ii) a clamped rectangular plate with dimensions comparable to the section of the middle hood that experienced the lowest alternating stress ratios at SMT EPU conditions with +10% frequency shift. In all cases, the mesh has spatial resolution similar to that used in the steam dryer model and the same element type SHELL63 is employed. For the simply supported plate, simple analytical solutions are available for any aspect ratio. For the clamped plate case, tabulated frequency predictions are available only at selected aspect ratios. Thus, for this case dimensions were chosen to correlate most closely with the steam dryer dimensions while adhering to one of the tabulated aspect ratios.

The material properties used in the finite element model were: Young's modulus, E=25.55 10^6 psi; density, ρ=0.284 lbm/in^3 and Poisson's ratio, ν=0.3. Modal frequencies are readily obtained in ANSYS. Modal masses are more difficult to extract due to underlying assumptions regarding the normalization of modes and the absence of analytical modal mass information. However, since any error in the modal mass will be reflected in the computed frequencies (the modal frequencies depend on the generalized stiffness for the mode and the associated modal mass), the errors in modal frequencies are a good estimate of the errors in modal masses. The comparisons between ANSYS and analytical modal frequency predictions follow below.

Simply Supported Plate

Analytical eigenfrequencies for simply supported plates are given by [18]:

$$f_{mn} = \frac{\pi}{2}\sqrt{\frac{D}{\rho h}}\left(\frac{m^2}{a^2}+\frac{n^2}{b^2}\right)$$

where $D = \frac{Eh^3}{12(1-\nu^2)}$, E is the Young's modulus, ρ is the density, h is the plate thickness, a and b denote the plate dimensions, and m and n are modal numbers. For the model of the vane bank side panel, h = 0.375", a = 8.5" and b = 88.4375". Then: D = 13940.6 Nm, and the lowest frequencies and relative errors are (note: m and n are mode numbers):

Table A1. Comparison of analytical and ANSYS predictions of natural frequencies for simply-supported plate.

m	n	Analytical frequency, Hz	ANSYS frequency, Hz	Rel. Error (%)
1	1	464.1	462.4	-0.37
1	2	476.8	474.8	-0.42
1	3	498.1	495.5	-0.52
1	4	527.8	524.4	-0.64

Thus the errors in computed frequencies are less than 1% and are due to mesh resolution.

Clamped Plate

The middle hood is modeled with plate of thickness h=0.125" and side lengths, a=17.92" and b = 44.8". This corresponds to the section of plate immediately adjacent to the location of high stress in the SMT calculation at EPU with +10% frequency shift. At this aspect ratio, b/a=2.5, the analytical eigenfrequencies are given by [19]:

$$f_{ij} = \frac{\lambda_{ij}^2}{2\pi b^2}\sqrt{\frac{D}{\rho h}}$$

where D = 516.32 Nm and the coefficients λ_{ij}^2, the lowest frequencies and relative errors are shown in the table below.

Table A2. Comparison of analytical and ANSYS predictions of natural frequencies for clamped plate.

i	j	λ_{ij}^2	Analytical frequency, Hz	ANSYS frequency, Hz	Rel. Error (%)
1	1	147.8	82.69	82.98	0.35
1	2	173.9	97.29	96.01	-1.32
1	3	221.5	123.92	121.14	-2.03
1	4	291.9	163.3	158.73	-2.8

The mesh used to calculate plate eigenfrequencies and the mesh on the steam dryer model are shown below.

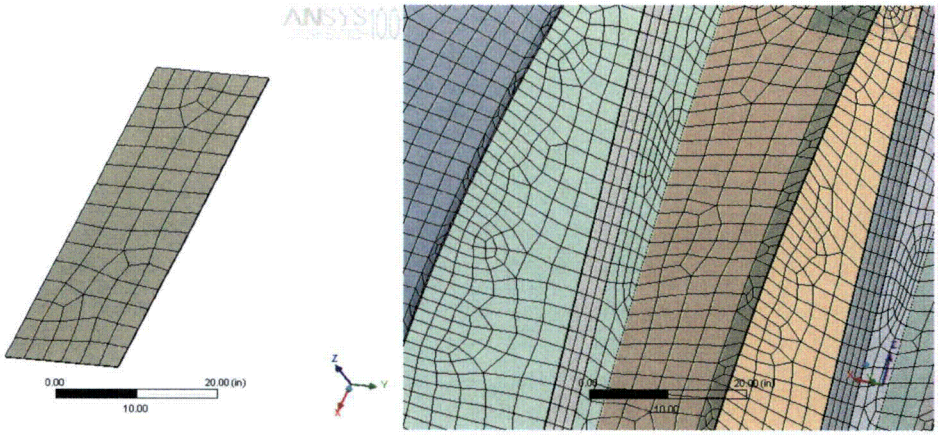

Left – mesh on the flat plate model for eigenvalue comparison calculations; right – mesh on the actual steam dryer FE model. The size of elements in both models is kept similar.

Appendix B. Comparison of Transient and Frequency-Based Simulations for the Browns Ferry Unit 1 Dryer

[[

[3]]]

[[

[3]]]

[[

[3]]]

[[

[3]]]

Figure 21a. [[

[3]]]

[[

[3]]]

Figure 21b. [[

[3]]]

[[

[3]]]

Figure 22a. [[
[3]]]

[[

[3]]]

Figure 22b. [[[3]]]

[[

[3]]]

Figure 22c. [[
[3]]]

[[

[3]]]

Figure 22d. [[
[3]]]

Appendix C. Structural Modeling of Perforated Plates

Modeling the perforated plates in the steam dryer assembly explicitly is computationally prohibitive and an alternative approach is adopted where the plates are characterized by modified material properties adjusted to match the key static and dynamic behavior. This Appendix summarizes the modeling method employed and its verification against measurements.

The perforated plates used in the steam dryer assembly are very thin, i.e. the ratio of thickness and pitch of perforation is less than unity so that the effective properties provided in ASME B&PVC, [20], for thick perforated plates cannot be used. Therefore, to model the steam dryer we have adopted the effective material properties reported by O'Donnell in [7] which directly apply to the bending of thin plates. In his work the effective properties are calculated by equating an average stress field over the periodicity cell in a perforated plate. Thus, for a given static loading the solid plate with the effective or modified material properties will yield a similar stress field as the perforated plate with original material properties. Comparisons are made against the values provided in ASME Code [20], as well as to experimental data where good agreement is obtained.

In order to apply these results to the steam dryer analysis the staggered 45° perforation was approximated with an equilateral staggered 60° perforation. The difference was judged insignificant for modeling purposes. The effective properties were therefore inferred from Fig. 8 (Young's modulus) and Fig. 9 (Poisson ratio) of [7].

Verification

[[

[3]]]

[[

[3]]]

Figure 23. [[

[3]]]

[[

[3]]]

Figure 24. [[[3]]]